UNIVERSITY OF CALIFORNIA
RIVERSIDE

Expanding the Current Imaging Toolkit With Novel Fluorescent Protein Based Biosensors

A Dissertation submitted in partial satisfaction
of the requirements for the degree of

Doctor of Philosophy

in

Environmental Toxicology

by

Yichong Fan

September 2017

Dissertation Committee:
Dr. Huiwang Ai, Chairperson
Dr. Yinsheng Wang
Dr. Xin Ge

The Dissertation of Yichong Fan is approved:

_____

_____

_____

Committee Chairperson

University of California, Riverside

ACKNOWLEDGEMENTS

This dissertation has used paragraphs, sentences, figures and tables from three published articles by Yichong Fan and Dr. Huiwang Ai. Published articles are listed below:

1. Yichong Fan, Zhijie Chen, Huiwang Ai. 2015. Monitoring redox dynamics in living cells with a redox-sensitive red fluorescent protein. Analytical Chemistry. 87: 2802-2810.
2. Yichong Fan, Huiwang Ai. 2016. Development of redox-sensitive red fluorescent proteins for imaging redox dynamics in cellular compartments. Analytical and Bioanalytical Chemistry. 408: 2901-2911.
3. Yichong Fan, Merna Makar, Michael X. Wang, Huiwang Ai. 2017. Monitoring thioredoxin redox with a genetically encoded red fluorescent biosensor. Nature Chemical Biology. DOI: 10.1038/NCHEMBIO. 2417.

To my husband, Mr. Linxiao Geng;

To my mother, Ms. Liying Wang;

To my advisor, Dr. Huiwang Ai.

ABSTRACT OF THE DISSERTATION

Expanding the Current Imaging Toolkit With Novel Fluorescent Protein Based Biosensors

by

Yichong Fan

Doctor of Philosophy, Graduate Program in Environmental Toxicology
University of California, Riverside, September 2017
Dr. Huiwang Ai, Chairperson

The objective of my Ph.D. study is to develop novel genetically encoded fluorescent biosensors to image and dissect biological signaling pathways in the context of live cells. I utilized protein engineering techniques to convert fluorescent proteins into fluorescent biosensors that can actively respond to specific, spatiotemporally organized cellular changes.

In this thesis, we expanded the fluorescent protein toolkit by engineering one of the first red fluorescent probes—rxRFP1—for sensing general redox states in the live cells. To further extend the usage of this sensor in various subcellular domains, such as mitochondria, endoplasmic reticulum, and the cell nucleus, we developed a group of rxRFP1 mutants showing different midpoint redox potentials for studying compartmentalized redox dynamics under various pathophysiological conditions. We also developed the first genetically encoded fluorescent biosensor for thioredoxin (Trx) redox by engineering a redox relay between the active-site cysteines of human Trx1 and rxRFP1. We utilized the resultant biosensor—TrxRFP1—to selectively monitor the

perturbations of Trx redox in various mammalian cell lines. We further combined TrxRFP1 with a green fluorescent Grx1-roGFP2 biosensor to simultaneously monitor the dynamics of the two major cellular antioxidant systems, Trx and glutathione, in live cells in response to chemically and physiologically relevant stimuli.

We exploit another strategy which introduces reactive functional groups into circular permutated fluorescent proteins (cpFPs) using a genetic code expansion technology. Through a powerful directed protein evolution process, we were able to modulate the reactivity and chemoselectivity of an introduced *p*-boronophenylalanine (*p*BoF) in a cpRFP scaffold, resulting in fluorescent probes selectively responsive to hydrogen peroxide (H_2O_2) and peroxynitrite ($ONOO^-$). Furthermore, by using boronic acid and short peptides as synergistic recognition motifs, we were able to engineer a series of reversible probes for nucleotides and carbohydrates showing surprisingly high specificity and large dynamic ranges. We have successfully utilized this new family of fluorescent probes to visualize various cellular activities.

TABLE OF CONTENTS

LIST OF FIGURES

LIST OF TABLES

Chapter 1: Introduction

1.1 Critical roles of cellular redox signaling

1.1.1 Reactive Oxygen Species and Oxidative Stress

Reactive oxygen species (ROS), such as superoxide anion ($O_2^{\bullet -}$), hydrogen peroxide (H_2O_2), hydroxyl radical (•OH), consist of non-radical and radical oxygen species formed through partial reduction of oxygen.[1] ROS are continuously produced in cells as byproducts of aerobic metabolism, primarily in mitochondria, and may also rise through interactions with exogenous sources such as xenobiotic compound. ROS are well recognized for playing a dual role as deleterious and beneficial species.[2,3] ROS is appreciated as critical signaling molecules involved in a wide range of physiology such as cell proliferation and survival. In particular, in recent years hydrogen peroxide has become recognized as an important regulator of eukaryotic signal transduction. It can be generated in response to various stimuli, such as integrins, growth factor and cytokines, by simulating the activation of NADPH oxidases. Hydrogen peroxide is also believed to be involved in regulating diverse biological activities such as immune cell activation and vascular remodeling in mammals.[3] It can also activate signaling pathways to stimulate cell proliferation, differentiation, migration and apoptosis.[2]

However the continues efflux of ROS can result in accumulative oxidative damage to cellular components and alter cellular functions. Due to their high reactivity and short-lived half time, ROS are prone to cause rapid damage to biomolecules such as DNA, protein and lipid, and are thereby also potentially mutagenic, toxic, or carcinogenic. Such

oxidative damages are implicated in various disease states such as neurodegeneration, cancer, diabetes, and aging.[2,5,6]

1.1.2 Antioxidant System

Continues exposure to various types of oxidative stress has led the cell and the entire organism to develop sophisticated defense mechanisms, both enzymatic and nonenzymatic, to counterbalance the lethal effects of ROS.[7] Among various defense mechanisms, antioxidant system is extremely important due to its direct removal of pro-oxidants. The antioxidant system contains two major groups: antioxidant enzymes and low molecular weight antioxidants. The enzymatic antioxidants are SODs, catalase, and glutathione peroxidase. As the primary ROS produced from a variety of sources, superoxide can be dismutated by SOD, which is of primary importance for cells. Hydrogen peroxide is produced by the action of SODs or oxidases, such as xanthine oxidase, and is reduced to water by catalase and the glutathione peroxidase. In addition, disposure of H_2O_2 is also closely associated with thiol-containing enzymes, namely, thioredoxins (Trx1 and Trx2), thioredoxin reductase, thioredoxin peroxidase, and glutaredoxin. Reduced Trx is a general protein disulfide reductant, and the activities of Trx are found to be related to redox regulation of the transcription factor and inflammable responses in immune systems. Nonenzymatic antioxidants include vitamins (vitamins C and E), β-carotene, uric acid, and glutathione (GSH), which is a tripeptide (L-g-glutamyl-L-cysteinyl-Lglycine) that comprise a thiol group. Regulation of cellular redox states through various antioxidant systems is critical for cell viability, activation, proliferation and organ function.[8,9]

1.1.3 The Needs for Novel Redox Probes

Despite considerate effort and interest, the relationship between oxidants, oxidative stress and diseases have remained largely elusive. Obviously, the fundamental progresses rely on the development of high-precision tools that allow the quantitative, specific and dynamic measurements of redox processes in cells or organism.

Conventional redox measurements such as enzymatic assays, HPLC, or gel mobility provides valuable information on the levels of a specific redox couple in question. Successful examples are measurements of glutathione, ascorbate, NADPH, and thioredoxin, with their redox potential estimated accurately, and oxidized and reduced forms quantified separately. However, the major problem associated with such redox measurements is that they require disruption of cells. Oxidation artifacts can be created through cellular disruption and tissue extraction thus compromising the accuracy of results. Moreover, cell disruption precludes reversible dynamic measurements and limits spatial-resolution for subcellular compartments in spite of their reproducibility. Another widespread method for redox measurements is using fluorescent dyes although most molecules are characterized by irreversibility and partial nonspecific behavior. A widely used example is utilizing non-fluorescent 2',7'-dihydrodichlorofluorescein (H2DCF) to label cells for H_2O_2 detection, producing fluorescent 2',7'-dichlorofluorescein (DCF).[10] However, oxidation of H_2DCF can occur in the absence of H_2O_2 and can be stimulated by intracellular peroxidases and cytochrome c. More improved and advanced chemical probes are being developed. Christopher Chang and colleagues synthesized specific and

reversible probes that enable dynamic and quantitative measurements of intracellular H_2O_2.[11,12,13] Chemical probes thus are prone to more important roles in the future.

1.2 Redox-sensitive fluorescent proteins

1.2.1 Probes with Disulfide Bonds Engineered into GFP β-barrel

Although considerable progress is being made in the development of chemical probes, there are still major limitations that draw our attentions, such as reversibility, subcellular targeting and quantitation.[12] Many of these limitations were overcome by the development of the first genetically encoded redox fluorescent probe, which allows dynamic quantitation of a dithiol-disulfide equilibration in live cells.[14-17] Within one decade, tremendous fundamental new insight has been gained driven by the rapid development of fluorescent protein redox sensors. Fluorescent proteins are resistant to proteases and stable under physiological pH conditions thus making them an excellent scaffold for physiologically suitable biosensors to study redox biology. Winter and co-workers reported the first fluorescent protein-based redox probes, rxYFP,[15] in 2001 by introducing a pair of cysteines into the β-barrel surface of a yellow fluorescent protein (YFP). A reversible disulfide bridge could form upon oxidized state, causing a fluorescence decrease compared to that in the reduced state. Remington et al. introduced similar cysteine disulfide to green fluorescent protein (GFP) creating a series of redox-sensitive GFPs (roGFPs) that show ratiometric fluorogenic behavior.[16] Recently, Fan and co-workers reported rxRFPs,[17] a family of red fluorescent protein-based redox probes, by introducing cysteines to the N- and C- termini of a circular permutated red FP (cpRFP). Emerging as advanced and promising tools, fluorescent protein sensors offer great

opportunities for understanding redox activities in live cells or *in vivo*, and revitalized the field of redox research towards more quantitative and dynamic approaches.

Wild-type green fluorescent protein was originally isolated from the jellyfish *Aequorea victoria* by Osamu Shimomura.[18] It is a 27 kDa soluble protein made of 238 amino acids that further form an 11-stranded β-barrel structure wrapping around a central α-helix.[19] The chromophore contains three amino acids that undergo post-translational modification and is completely protected from it surrounding medium. wtGFP chromophore is made through intramolecular cyclization of S65/Y66/G67 and subsequent oxidation leads to formation of a conjugated system of π-electrons that essentially is capable of absorbing and emitting visible light.[20] The wild-type GFP has two excitation peaks representing different protonation states of phenol group on Y66 position within the chromophore and through excited state proton transfer excitation of both states leads to emission of green light with similar wavelength. More importantly, the unique dual excitation behavior of wt-GFP makes it an excellent scaffold to exploit ratiometric sensors.

In general, the equilibration of chromophore protonation states can be shifted through interactions with its surrounding residues and thus can be affected by subtle changes in protein structure and composition.[21] Besides, another way to manipulate fluorescent protein emission is to alter chromphore stacking interactions. An example is the generation of a yellow fluorescent protein (YFP) by an additional T203Y mutation. The resulted π-electron stacking between the chromophore and the aromatic side chain of

Y203 leads to a red-shifted GFP derivative.[21,22] Such strategies can be exploited in developing fluorescent protein-based biosensors.

Ostergaard and colleagues developed the first redox-sensitive fluorescent protein rxYFP by introducing a pair of cysteines into YFP at N149C/S202C.[15] The two residues are capable of forming an intramolecular disulfide bridge in response to the presence of oxidant and dislocation of Y203 was expected to occur thus forcing YFP into a slightly different position. Such conformational change gives rxYFP a 2.2-fold redox-dependent fluorescence reduction. The midpoint redox potential of rxYFP was determined to be -261 mV, which is within the physiological range redox-active cysteines. rxYFP still exhibits similar excitation at 514 nm and emission at 512 nm as wtYFP. As a non-invasive, redox-sensitive reporter, rxYFP greatly revitalized the field of redox biology by expanding the current toolbox and provided capabilities to study redox processes in living cells and organisms.

Likewise, Hanson and colleagues inserted two cysteines into S147 and Q204, which are in close proximity to positions mutated in rxYFP, based on wtGFP or EGFP, respectively. A series of redox-sensitive GFPs (roGFP1 and roGFP2) were created with advantageous excitation ratiometric response.[23] Because of S65T mutation, the chromophore of reduced roGFP2 is preferentially deprotonated, while upon oxidation the chromophore is preferentially protonated, thus losing predominant excitability at 488 and gaining excitability at 405nm. Structural changes were also observed on crystallized reduced and oxidized roGFP2, which likely confirmed the chromophore protonation shift induced by disulfide formation.[14] The midpoint potential of roGFPs have been

determined to be -291 mV for roGFP1 and -280 mV for roGFP2. Their dynamic range is significantly increase compared with rxYFP because of their ratiometric property. With excitation at 390 nm and 480 nm, roGFP2 has a dynamic range of about 12.[24] Ratiometric response of roGFPs also overcomes the disadvantages of single excitation wavelength probes, by avoiding absolute fluorescence values that may get influenced by protein expression level, bleaching, illumination intensity, etc.

1.2.2 A Circular Permutated Topology to Develop Redox-sensitive RFP

Although rxYFP and roGFPs have been broadly utilized in a variety of biological redox studies and fundamental new insights have been gained, they all emit green light of similar wavelength. Simultaneous measurements in multiple subcellular compartments, although highly needed, is technically not available. In addition, light used to excite rxYFP and roGFP can also unavoidably excite endogenous molecules, such as NADH/NADPH, thus leading to autofluorescence. Thus, it will be beneficial to develop differentially colored redox probes, especially red-shifted fluorescent probes. Recently, Fan and colleagues developed one of the first redox-sensitive red fluorescent proteins—rxRFP1—by introducing cysteine residues to the N- and C- termini of a circular permutated RFP (cpRFP). Circular permutated fluorescent proteins, containing more accessible chromophore than those of native fluorescent proteins, have been exploited to derive a large variety of single fluorescent protein-based biosensors. An example is a Ca^{2+} biosensor, R-GECO1,[25] derived by fusing a vertebrate calmodulin (CaM) and CaM-binding region of chicken myosin light chain kinase (M13) to the N- and C- termini of cp-mApple. A cpRFP scaffold identified from R-GECO1 was capable

of maintaining its intrinsic fluorescence and utilized as the template for adding reversible disulfide bridge.[17] The resultant redox-sensitive RFP, rxRFP1, has the midpoint potential determined to be -281 mV and it was highly responsive to redox changes, with a 4-fold fluorescence enhancement in the oxidized state compared to that in the reduced state. The successful development of rxRFP not only provides a different strategy to introduce disulfide switches into fluorescent proteins, it has also expanded the genetically encoded redox toolkits with new capabilities.

1.2.3 Variants of Redox Probes with Altered Properties

A collection of redox-sensitive fluorescent proteins based on rxYFP, roGFPs and rxYFP1 have been developed to match different needs and applications. Fusing them with subcellular localization sequences allows precise targeting of these probes into various subcellular domains. Since individual cellular compartment have quite different basal redox states, an important task is to create probes with modified midpoint potential and measuring ranges. For instance, in order to detect deflections from the steady state in both directions, it is important to apply probes whose midpoint potential match the steady state redox potential of the environment under study. The first generation of redox-sensitive FPs is suitable to be used in reducing compartments, such as cytosol and the mitochondrial matrix, considering their relatively low midpoint potential (-260 mV or below). However, in the lumen of endoplasmic reticulum (ER), rxYFP, roGFP1 and roGFP2 were confirmed to be fully oxidized, indicating a redox potential higher than -240 mV in the ER. Thus, the use of these probes is limited when utilized in oxidizing compartment due to the high thermodynamic stability of the introduced disulfide bond.

In order to create redox probes that are better suited for study of relatively oxidizing cellular compartments, the thermodynamic stability of disulfide in these probes needs to be substantially lowered to allow more reactive thiols. The pKa of the two cysteines in rxYFP and roGFPs are calculated to be between 8.9 and 9.5, which leads to mostly protonated thiols and hence low reactivity.[28] Introduction of basic residues in proximity to the cysteines can lead to stabilization of the thiolate form and increasing the reactivity of thiols. Such approaches have been successfully used to obtain a promising family of variants, roGFP-iX, by insertion of one positively charged residue close to the two participating cysteins.[28] Similarly, single point mutation was introduced into rxRFP1 in close proximity to C261, a group of rxRFP1 variants showing different midpoint potentials were developed. The altered properties of these probes allow the study of compartmentalized redox dynamics and expanded the fluorescent protein toolkit with novel research tools.

1.2.4. Advantages of Redox-sensitive Fluorescent Protein Probes

Beyond the ability to target redox-sensitive fluorescent proteins to different subcellular compartments for redox measurements, the biggest advantage of such probes over conventional fluorescent dyes is that they provide reversibility of the oxidation process and thus allowing the monitoring of redox dynamics in live cells. For instance, in basal state rxRFP1 is maintained as a partially oxidized form in HEK 293 T cells, and was responsive to both cell-permeable oxidant aldrithiol-2 (200 μM) and reductant DTT (10 mM).[17] Moreover, a chemically induced intracellular redox changes was observed by treating rxRFP1-expressing HEK 293T cells with 2-AAPA, a glutathione reductase

inhibitor. 2-AAPA is expected to increase [GSSG] and decrease [GSH] in cells, shifting the cells to a more oxidizing state with the fluorescence of rxRFP1 gradually increased.

However, the applicability of these conventional redox-sensitive FPs is limited by slow equilibration with the glutathione systems. Since complete intracellular probe equilibration with glutathione system can take tens of minutes in cells, they are best suited to detect redox changes that are sufficiently long-lived to allow the probe to equilibrate. Nevertheless, in many physiological setting such as after growth factor stimulation,[29] the oxidative changes are transient and weak that conventional redox-sensitive FPs failed to show any responses. Most recently, fusion proteins of redox-sensitive FPs and redox enzymes have been explored for their potential use as redox probes. The rationale behind this approach is by covalently coupling a redox enzyme to redox-sensitive FPs, a redox relay may be formed through electron transfer. The redox enzyme will lend specificity and facilitate rapid equilibration with a defined cellular redox pair. To create a probe for glutathione (GSSG/GSH) pair, human Grx1 and roGFP2 were chosen as fusion partners and resulted Grx1-roGFP2 is exploited to enforce continuous rapid equilibration between two redox pairs: $roGFP2_{red}/roGFP2_{ox}$ and 2GSH/GSSG.[30] Grx1-roGFP2 is also expected to have a very high specificity for 2GSH/GSSG redox pair without interacting with Trx system. Importantly, Grx-mediated protein oxidation may also help to understand the phenomenon of H_2O_2-baed signaling on whether H_2O_2 can oxidize redox-regulated proteins despite competition by abundant cellular scavenger systems. Grx1-roGFP2 probe successfully exemplifies that H_2O_2 can facilitate regulatory protein thiol oxidation through the GSSG intermediate.

Effort has previously been made to fuse rxYFP or roGFPs to Trx1, but failed to yield any effective biosensor likely due to the steric hindrance that prevents a proper alignment of thiols in Trx and rxYFP or roGFPs for appropriate disulfide exchange. Recently, Fan and colleagues developed the first genetically encoded biosensor for probing redox changes of the Trx system, by engineering a redox relay between the active-site cysteines of Trx1 and rxRFP1. Different from the strategy to insert disulfide switch onto the surface of roGFP, rxRFP's disulfide bridge is designed from the outset of FP thus making it more accessible to the Trx active site. The resultant probe—TrxRFP1—has successfully been utilized in various mammalian cell lines to monitor perturbations of Trx redox induced by both chemical and physiological stimuli.

1.2.5 Other Genetically Encoded Redox Probes

Chimeric fusion strategy was also explored to develop specific probes for H_2O_2 or other peroxides. Recently, a peroxidase-based protein oxidation has been identified in yeast. Although it has been proposed that the oxidation of target protein may be facilitated by H_2O_2-scavenging peroxidase, this newly found protein oxidation relay, namely the oxidation of the transcription factor Yap1 by the peroxidase Orp1, is still highly interesting. Gutscher and colleagues showed that this oxidation relay phenomenon of Orp1 is not just restricted to Yap1, Orp1 also mediated quantitative oxidation of roGFP2 by H_2O_2, thus converting physiological H_2O_2 signals into measureable fluorescent signals in living cells.[31] Their work established a peroxidase-roGFP relay as novel design strategy for genetically encoded redox probes.

All genetically encoded redox probes discussed so far are based on redox-sensitive fluorescent proteins. However, strategies to develop redox probes from non-redox-sensitive FPs were also approved applicable. One principle is to exploit conformational change of a FP in response to altered redox states. A successful example of such approach is the development of HyPer, a specific indicator for intracellular H_2O_2.[32] A cpYFP is inserted into a H_2O_2 -active sensing domain (OxyR) and by reacting with H_2O_2 to form a intramolecular disulfide bridge on OxyR, a substantial conformational change of cpYFP takes place. HyPer was shown to detect nanomolar H_2O_2 *in vitro* and micromolar H_2O_2 when expressed in cells. More importantly, HyPer also allowed the detection of transient and week oxidative changes induced by growth factors. Another approach to provide a fluorescent signal associated with redox-dependent conformational changes is fluorescence resonance energy transfer (FRET). In general, this strategy requires a redox-active peptide or protein domain to be inserted between a FRET donor-acceptor pair. One of the few existing FRET redox probes explored to insert a cysteine pair-containing peptide between ECFP and YFP,[33] although its specificity was doubted and FRET efficiency needed to be further improved.

1.3 Future directions and challenges

The future understanding and study of redox processes in the context of whole organisms depends on out ability to acquire quantitative tools with high spatio-temporal resolution. Considering that redox-sensitive FPs provide a scaffold that is amendable to improvement and reconstruction, numerous opportunities for creating novel probes with altered properties and specificities can be envisaged. For instance, redox probes with

limited emission light range allows only one or a few redox parameters to be monitored at a time. To deliver goals on simultaneous monitoring of multiple physiological parameters, redox probes that are differentially colored are in highly need. Following initial discovery of GFP and dsRed, right now there are more than 150 distinct fluorescent proteins identified with colors expanding the whole visible spectrum. The large number of spectral varieties FPs was generated through mutagenesis, it can be envisaged that through such protein engineering approach, infinite possibilities for further modifications of the current probes can be achieved. For deep imaging of animal tissues, the "optical window" is favored by 650-1,100 nm, thus making far-red or near infrared fluorescent protein highly preferable for redox monitoring within living tissues.

Although novel redox probes, such as Grx1-roGFP2 and TrxRFP1, are already highly responsive to specific redox changes and equilibrate on a second-to-minute time scale, it may be possible to further shorten the response time of redox relay-based probes, potentially allowing the detection of highly transient reflections on shorter time scales. Attempts can be made to further optimize the chimeric fusion constructs, in terms of linker length or otherwise, to conceive kinetically enhanced versions.

More possible construct based on redox-sensitive FPs can be deployed in the design of novel probes. First of all, redox relays clearly offer opportunities for more redox probes allowing specificity and sensitivity. The fact that Orp1 mediates electron transfer between H_2O_2 and roGFP2 suggests that other peroxidases may also be applied by the same principle.[34] In this regard, an attractive goal is to design a genetically encoded probe for monitoring cellular lipid peroxidation. Another important goal for future redox probe

development is to further expand the toolkit to detect more defined redox pairs or reactive oxygen and nitrogen species. For instance, a probe for the redox pair AA/DHA[36] or one that allows real-time detection of nitric oxide (NO^-) are both high on the wish list.

Genetically encoded redox probes emerge as extremely advanced and useful tools for biological redox studies Together with fluorescence imaging techniques,[36] genetically encoded redox probes allow the dynamic detection of defined redox processes in singles cells or even at subcellular level. They also provide huge potential for high throughput screening (HTS) to identify novel drugs affecting specific redox processes. With the rapidly increasing number of applications, genetically encoded redox probes allow new insights into cellular redox system and more exciting times are awaiting us in the field of redox biology.

Reference:

1. Bartosz, G. Biochem. Reactive oxygen species: destroyers or messengers? Pharmacol. 2009, 77, 1303−1315.

2. Gius D, Spitz DR. Redox signaling in cancer biology. Antioxid Redox Signal. 2006;8(7/8):1249–52.

3. Stone JR, Yang S. Hydrogen peroxide: a signaling messenger. Antioxid Redox Signal. 2006;8(3/4):243–70.

4. Nikolaidis, M. G.; Kyparos, A.; Spanou, C.; Paschalis, V.; Theodorou, A. A.; Vrabas, I. S. Redox biology of exercise: an integrative and comparative consideration of some overlooked issues. J. Exp. Biol. 2012, 215, 1615−1625.

5. Madamanchi, N.R. & Runge, M.S. Redox signaling in cardiovascular health and disease. *Free Radic Biol Med* **61**, 473-501 (2013).

6. Sesti, F., Liu, S. & Cai, S.Q. Oxidation of potassium channels by ROS: a general mechanism of aging and neurodegeneration? *Trends Cell Biol* **20**, 45-51 (2010).

7. Halliwell, B. Reactive species and antioxidants. Plant Physiol. 2006, 141, 312−322.

8. Lu, J. & Holmgren, A. The thioredoxin antioxidant system. *Free Radic Biol Med* **66**, 75-87 (2014).

9. Klomsiri, C.; Karplus, P. A.; Poole, L. B. Cysteine-based redox switches in enzymes. Antioxid. Redox Signal. 2011, 14, 1065−1077.

10. Rota C, Chignell CF, and Mason RP. Evidence for free radical formation during the oxidation of 2'-7'-dichlorofluorescin to the fluorescent dye 2'-7'-dichlorofluorescein by horseradish peroxidase: possible implications for oxidative stress measurements. Free Radic Biol Med 27: 873–881, 1999.

11. Miller EW, Albers AE, Pralle A, Isacoff EY, and Chang CJ. Boronate-based fluorescent probes for imaging cellular hydrogen peroxide. J Am Chem Soc 127: 16652–16659, 2005.

12. Miller EW and Chang CJ. Fluorescent probes for nitric oxide and hydrogen peroxide in cell signaling. Curr Opin Chem Biol 11: 620–625, 2007.

13. Chang MCY, Pralle A, Isacoff EY, and Chang CJ. A selective, cell-permeable optical probe for hydrogen peroxide in living cells. J Am Chem Soc 126: 15392–15393, 2004.

14. Dooley CT, Dore TM, Hanson GT, Jackson WC, Remington SJ, and Tsien RY. Imaging dynamic redox changes in mammalian cells with green fluorescent protein indicators. J Biol Chem 279: 22284–22293, 2004.

15. Ostergaard H, Henriksen A, Hansen FG, and Winther JR. Shedding light on disulfide bond formation: Engineering a redox switch in green fluorescent protein. EMBO J 20: 5853–5862, 2001.

16. Ostergaard H, Tachibana C, and Winther JR. Monitoring disulfide bond formation in the eukaryotic cytosol. J Cell Biol 166: 337–345, 2004.

17. Fan Y, Chen Z, and Ai H-w. Monitoring redox dynamics in living cells with a redox-sensitive red fluorescent protein. Anal Chem 87: 2802-2810, 2015.

18. Shimomura O, Johnson FH, and Saiga Y. Extraction, purification and properties of aequorin, a bioluminescent protein from the luminous hydromedusan, Aequorea. J Cell Comp Physiol 59: 223–239, 1962.

19. Ormo¨ M, Cubitt AB, Kallio K, Gross LA, Tsien RY, and Remington SJ. Crystal structure of the Aequorea victoria green fluorescent protein. Science 273: 1392–1395, 1996.

20. Meech SR. Excited state reactions in fluorescent proteins. Chem Soc Rev 38: 2922–2934, 2009.

21. Tsien RY. The green fluorescent protein. Annu Rev Biochem 67: 509–544, 1998.

22. Wachter RM, Elsliger MA, Kallio K, Hanson GT, and Remington SJ. Structural basis of spectral shifts in the yellowemission variants of green fluorescent protein. Structure 6: 1267–1277, 1998.

23. Hanson GT, Aggeler R, Oglesbee D, Cannon M, Capaldi RA, Tsien RY, and Remington SJ. Investigating mitochondrial redox potential with redox-sensitive green fluorescent protein indicators. J Biol Chem 279: 13044–13053, 2004.

24. Meyer AJ, Brach T, Marty L, Kreye S, Rouhier N, Jacquot JP, and Hell R. Redox-sensitive GFP in Arabidopsis thaliana is a quantitative biosensor for the redox potential of the cellular glutathione redox buffer. Plant J 52: 973–986, 2007.

25. Zhao, Y.; Araki, S.; Wu, J.; Teramoto, T.; Chang, Y. F.; Nakano, M.; Abdelfattah, A. S.; Fujiwara, M.; Ishihara, T.; Nagai, T.; Campbell, R. E. Science 2011, 333, 1888−1891.

26. Hansen RE, Ostergaard H, and Winther JR. Increasing the reactivity of an artificial dithiol–disulfide pair through modification of the electrostatic milieu. Biochemistry 44: 5899–5906, 2005.

27. Schwarzla¨nder M, Fricker MD, Mu¨ ller C, Marty L, Brach T, Novak J, Sweetlove LJ, Hell R, and Meyer AJ. Confocal imaging of glutathione redox potential in living plant cells. J Microsc 231: 299–316, 2008.

28. Cannon MB and Remington SJ. Re-engineering redox sensitive green fluorescent protein for improved response rate. Protein Sci 15: 45–57, 2006.

29. Hansen JM, Go YM, and Jones DP. Nuclear and mitochondrial compartmentation of oxidative stress and redox signaling. Annu Rev Pharmacol Toxicol 46: 215–234, 2006.

30. Gutscher M, Pauleau AL, Marty L, Brach T, Wabnitz GH, Samstag Y, Meyer AJ, and Dick TP. Real-time imaging of the intracellular glutathione redox potential. Nat Methods 5: 553–559, 2008.

31. Delaunay A, Pflieger D, Barrault MB, Vinh J, and Toledano MB. A thiol peroxidase is an H2O2 receptor and redox transducer in gene activation. Cell 111: 471–481, 2002.

32. Belousov VV, Fradkov AF, Lukyanov KA, Staroverov DB, Shakhbazov KS, Terskikh AV, and Lukyanov S. Genetically encoded fluorescent indicator for intracellular hydrogen peroxide. Nat Methods 3: 281–286, 2006.

33. Kolossov VL, Spring BQ, Sokolowski A, Conour JE, Clegg RM, Kenis PJ, and Gaskins HR. Engineering redox-sensitive linkers for genetically encoded FRET-based biosensors. Exp Biol Med (Maywood) 233: 238–248, 2008.

34. Gutscher M, Sobotta MC, Wabnitz GH, Ballikaya S, Meyer AJ, Samstag Y, and Dick TP. Proximity-based protein thiol oxidation by H2O2-scavenging peroxidases. J Biol Chem 284: 31532–31540, 2009.

35. Dixon DP, Davis BG, and Edwards R. Functional divergence in the glutathione transferase superfamily in plants. Identification of two classes with putative functions in redox homeostasis in Arabidopsis thaliana. J Biol Chem 277: 30859–30869, 2002.

36. Fricker M, Runions J, and Moore I. Quantitative fluorescence microscopy: From art to science. Annu Rev Plant Biol 57: 79–107, 2006.

Chapter 2: Monitoring Redox Dynamics in Living Cells with a Redox-Sensitive Red Fluorescent Protein

2.1 Introduction

Reactive oxygen species (ROS) are generated in living organisms through a number of pathways, including aerobic metabolism and photosynthesis.[1] As a result, cells have been evolved to maintain a sophisticated antioxidant system to regulate redox homeostasis.[2,3] In response to stress signals, it is common to see ROS overproduction, resulting in a shift of the intracellular redox equilibrium to a more oxidized state. When ROS are generated beyond the detoxification ability of the antioxidant system, oxidative stress occurs to damage proteins, lipids and nucleic acids in cells.[4] This process has been linked to aging and a variety of human diseases, such as cancer, diabetes, atherosclerosis, asthma, Parkinson's disease and Alzheimer's disease.[5-7] On the other hand, cells may also alter the redox equilibrium to achieve necessary physiological functions. For example, ROS production has been found to be involved in cell signaling, immune response, stem cell proliferation and differentiation, and embryonic development. In this context, cellular redox potential changes have been recognized as very important information for understanding the relationships between ROS production, redox homeostasis and signaling, and diseases.[8,9]

In the past a few years, fluorescent protein-based redox sensors have gained increasing popularity for investigations of redox biology in living cells and organisms. Methods are now well established to deliver genetically encoded probes into specific subcellular domains or cell types to monitor real-time redox dynamics.[10,11] The first fluorescent protein-based redox sensor, rxYFP, was reported in 2001 by Winther and coworkers.[12,13] Two cysteine residues were introduced to the β-barrel surface of a yellow fluorescent protein (YFP). The two residues were spaced close enough, so that a reversible disulfide bond was formed when rxYFP was oxidized. The formation of the disulfide bond caused a subtle structural change in the protein scaffold, resulting in a ~ 50% fluorescence decrease compared to when it is reduced. Likewise, Remington *et al.* introduced cysteine disulfide bridges to the surface of green fluorescent proteins (GFPs) to create a series of redox-sensitive GFPs (roGFPs).[14-16] Different from rxYFP, roGFPs containing both protonated and deprotonated chromophores are fluorescent. Due to excited-state proton transfer (ESPT) of the protonated chromophore, only green fluorescence can be observed, and roGFPs are dual-excitation ratiometric probes. When expressed in living cells, both rxYFP and roGFPs were shown to faithfully report cellular glutathione redox potentials. Moreover, glutaredoxins have been fused to rxYFP or roGFP2 to create fluorescent probes that can more quickly equilibrate with intracellular thiols.[13,17,18,19] Similarly, a yeast peroxidase Orp1 has been linked to roGFP2 to create a redox relay between the two proteins, and the fusion construct has been shown to more selectively respond to hydrogen peroxide (H_2O_2).[20] Previous attempts to directly adapt the cysteine disulfide strategy to generate genetically encoded red fluorescent redox

probes have been unsuccessful. A recent conference abstract described the engineering of a reversible disulfide bridge in a red fluorescent protein (RFP), mKeima. Although responsive to dithiothreitol (DTT) reduction, the mutant protein was also sensitive to blue light illumination, making it less useful for redox sensing applications. In addition to these redox sensors based on disulfide bridges in fluorescent protein scaffolds, several other methods have been utilized to develop genetically encoded probes responsive to particular redox signaling molecules, such as H_2O_2,[23] organic hydroperoxide (ROOH),[24] oxidized and reduced nicotinamide adenine dinucleotide (NAD^+/NADH),[25,26] hydrogen sulfide (H_2S)[27,28] and peroxynitrite ($ONOO^-$).[29] This large family of fluorescent redox probes are useful research tools for studying redox biology.

Following their development, roGFPs and rxYFP have seen broad utilization in biological studies.[11] They both emit photons in the green to yellow-green spectral region; thus, monitoring redox changes in multiple cellular compartments, although is highly needed in many studies, is technically difficult. Moreover, redox probes with fluorescence in other spectral regions are expected to facilitate multiplex measurements, because most existing fluorescent protein fusion constructs or fluorescent protein-based biosensors emit light in the spectral region overlapping with that of rxYFP and roGFPs.[30] In addition, light used to excite rxYFP or roGFPs can also excite cell endogenous molecules, such as NADH/NADPH and flavins, leading to background fluorescence.[31] The auto fluorescence of doxycycline, a small molecule commonly used to achieve controlled protein expression, also overlaps with that of existing genetically encoded redox probes.[32] Furthermore, red-shifted fluorescent probes are expected to result in

reduced phototoxicity and increased tissue penetration.[33] A very recent work on a red-fluorescent H_2O_2 -specific HyPerRed sensor has partially alleviated these problems.[34] HyperRed was generated by fusing a bacterial H_2O_2–sensing OxyR domain with a circularly permuted red fluorescent protein (cpRFP). Upon oxidation, the red fluorescence of HyPerRed increases by ~ 80% from that in a fully reduced state. Because of the use of the OxyR domain, HyPerRed shows good selectivity toward H_2O_2.[34] Despite the progress, red fluorescent redox sensors that are analogous to rxYFP or roGFPs, are still highly needed for sensing general redox states and for creating proximity-based probes to detect other cellular redox-active components.

Previously, to derive rxYFP and roGFPs, reversible disulfide bridges were inserted to the β-barrel surfaces of fluorescent proteins in their native topology. However, the attempt to directly introduce disulfide bridges to a red fluorescent protein (RFP), mKeima, in its natural topology, has resulted in unsatisfactory results (e.g., a small dynamic range and photoconversion by blue illumination).[35] Concurrently, circularly permuted fluorescent proteins, containing more accessible chromophores than those of native fluorescent proteins, have been utilized to derive a large variety of single fluorescent protein-based sensors, including one of the first cpRFP-based Ca^{2+} biosensors, R-GECO1.[36] We therefore postulated that, adding reversible disulfide bridges between the N- and C termini of cpRFPs would be an effective way to generate redox sensitive fluorescent proteins. We tested this notion, and herein we present our results on the engineering, characterization and validation of a novel red fluorescent redox biosensor, rxRFP, based on a cpRFP scaffold derived from R-GECO1. The fluorescence

of rxRFP was highly responsive to reduction and oxidation, with a 4-fold fluorescence enhancement in the oxidized state compared to in the reduced state. We also demonstrated that rxRFP could be utilized to image general redox changes in living mammalian cells.

2.2 Materials and Methods

2.2.1 Materials

Synthetic DNA oligonucleotides were purchased from Integrated DNA Technologies (San Diego, CA). Restriction endonucleases were purchased from New England Biolabs (Ipswich, MA) or Thermo Scientific Fermentas (Vilnius, Lithuania). PCR products and products of restriction digestion were purified by gel electrophoresis and extracted using Syd Labs Gel Extraction columns (Malden, MA). Plasmid DNA was purified using Syd Labs Miniprep columns. Plasmid pCMV-R-GECO1 (Addgene plasmid 32444) was requested from Addgene (Cambridge, MA).[36] All chemicals were purchased from Sigma-Aldrich (St. Louis, MO) or Fisher Scientific (Hampton, NH) and used as received. DNA sequence was analyzed by the Genomics Core at the University of California, Riverside (UCR).

2.2.2 Construction of *E. coli* expression plasmids and libraries

Polymerase chain reactions (PCR) were utilized to amplify the cpRFP gene fragment from R-GECO1. Various synthetic oligonucleotide pairs (**see Table 2.1**) were purchased and used in these reactions to generate genes with different N- and C- termini. Oligonucleotides cpRFP_F1 and cpRFP_R1, and cpRFP_F2 and cpRFP_R2 were used for the identification of cpRFP scaffold self-sufficiently fluorescent. 1C_F, IC_R, 2C_F

and 2C_R were used for the initial test of cysteine residue sites. Oligonucleotides with degenerated codons at residue sites adjacent to the inserted cysteine residues were utilized to derive gene libraries for screening redox probes. pBAD_F was paired with either RCC_RCS or RCC_RSC to create mutants with only one C-terminal cysteine. Oligonucleotides pH_F and pH_R were used to create the library for screening pH-sensitive proteins. All amplified DNA fragments were treated with Xho I and Hind III, and ligated with a predigested compatible pBAD/His B plasmid (Life Technologies, Carlsbad, CA). The resulting ligation products were used to transform electrocompetent DH10B *E. coli* cells, which were next plated on LB agar plates supplemented with ampicillin (100 μg/ml) and L-arabinose (0.04%, w/v%).

Table 2.1. Oligonucleotides used in this study.

Primer name	Nucleotide Sequence
cpRFP_F1	5'- AACCACTCGAGTCCCGTGGTTTCCGAGCGGATG -3'
cpRFP_R1	5'- GACTGAAGCTTAGTGATGGTGATGGTGATGMNNMNNCGTAGCCTCCCAGCCCAT -3'
cpRFP_F2	5'- ATAACTCGAGCATAGGTCGGCTGAGCTCACCC -3'
cpRFP_R2	5'- TAGCAAGCTTAATGATGGTGGTGATGGTGTTGGTCACGCGTAGCCTCCCA -3'
1C_F	5'- GACTAGCTCGAGCTGCGCTATAGGTCGGCTGAGCTCA -3'
1C_R	5'- GTCGATAAGCTTAGCACAGTTGGTCACGCGTAGCCTCCCA -3'
2C_F	5'- GACTAGCTCGAGCTGCTGTGCTATAGGTCGGCTGAGCTCA -3'
2C_R	5'- GTCGATAAGCTTAACAGCACAGTTGGTCACGCGTAGCCTCCCA -3'
CXGR_F	5'- GACTAGCTCGAGCTGCNNKGGTCGGCTGAGCTCACCC -3'
CXIGR_F	5'- GACTAGCTCGAGCTGCNNKATAGGTCGGCTGAGCTCACCC -3'
XCIGR_F	5'- GACTAGCTCGAGCNNKTGCATAGGTCGGCTGAGCTCACCC -3'
CCXAI_F	5'- GACTAGCTCGAGCTGCTGTNNKGCTATAGGTCGGCTGAGCTCA -3'
DXCC_R	5'- GTCGATAAGCTTAACAGCAMNNGTCACGCGTAGCCTCCCA -3'
DQLXCC_R	5'- GTCGATAAGCTTAACAGCAMNNCAGTTGGTCACGCGTAGCCTCCCA -3'
DQXCC_R	5'- GTCGATAAGCTTAACAGCAMNNTTGGTCACGCGTAGCCTCCCA -3'
Ext_F	5'- GACTAGCTCGAGCNNKNNKNNKTGCGCTATAGGTCGGCTGAGCTCA -3'
Ext_R	5'- GTCGATAAGCTTAMNNMNNMNNGCAGCACCTTTGGTCACGCGTAGCCTCCCA -3'
pBAD_F	5'- ATGCCATAGCATTTTTATCC -3'
RCC_RCS	5'- GTCGATAAGCTTAAGAGCACCTTTGGTCACGCGTAGCCTCCCA -3'
RCC_RSC	5'- GTCGATAAGCTTAACAGGACCTTTGGTCACGCGTAGCCTCCCA -3'
pH_F	5'- GACTAGCTCGAGCNNKNNKGCTATAGGTCGGCTGAGCTCA -3'
pH_R	5'- GTCGATAAGCTTAMNNMNNCCTTTGGTCACGCGTAGCCTCCCA -3'
rxRFP-F	5'- ATACTAAAGCTTGCCGCCACCATGGGAGGTTCTCATCATCATCAT -3'
rxRFP-R	5'- CTGAAAATCTTCTCTCATCCGCCAAAGAATTCCAGCTTA -3'

2.2.3 Screening of *E. coli* colonies

DH10B *E. coli* cells on LB agar plates were incubated at 37 °C overnight to form colonies. A laboratory-built colony fluorescence imaging system was used to evaluate fluorescence intensities of individual bacterial colonies. Briefly, light from a Dolan-Jenner MH-100 Metal Halide Illuminator was passed through a 550/30 nm bandpass filter (Omega Optical, Brattleboro, VT) installed in a Thorlabs FW102C motorized filter wheel and a fiber optic ring light guide. Light exiting the ring light guide was used to illuminate agar plates containing bacterial colonies. Colony fluorescence was quantified with an 8-bit CCD Camera (The Image Source, Charlotte, NC), in front of which another Thorlabs FW102C motorized filter wheel was installed to harbor a 610/75 nm bandpass filter (Chroma, Bellows Falls, VT). The system was automated with the μManager software through a computer interface.[37] Digital images were acquired and processed with ImageJ to identify red fluorescence intensities of individual colonies.[38] A pair of forensic red goggles with a cutoff wavelength at ~ 590 nm was also used to directly observe fluorescence colonies by human eyes. Colonies with high to mediocre brightness were chosen and cultured in 5 mL liquid LB, containing 100 μg/ml ampicillin and 0.04% L-arabinose. They were incubated at 37 °C and 250 rpm overnight, and next, at room temperature and 200 rpm for another 6 h. Cells were pelleted by centrifugation. B-PER Bacterial Protein Extraction Reagents (Pierce, Rockford, IL) was added, followed by another centrifugation step to remove cell debris. Fluorescence emission of clear cell lysates, before and after a 15-min DTT (100 mM) treatment at room temperature, was quantified on a monochromator-based Synergy Mx Microplate Reader (BioTek,

Winooski, VT). Fluorescence excitation and emission wavelengths were set at 540 nm and 600 nm, respectively. Mutants showing large ratios of fluorescence intensities before and after DTT treatment were chosen for further studies. Corresponding plasmids were minipreped from cultured *E. coli* and sequenced with the oligonucleotide pBAD_F.

2.2.4 Protein purification

To prepare proteins for *in vitro* characterizations, pBAD plasmids harboring selected mutant genes were used to transform electrocompetent DH10B *E. coli* cells. A single colony was grown in a starter culture of 5 mL of LB broth with 100 μg/mL ampicillin at 37 °C and 220 rpm overnight. A saturated starter culture was diluted 100-fold into 2YT media supplemented with 100 μg/mL ampicillin, and grown under the same conditions. When the OD_{600} reached 0.6, the expression culture was induced with 0.2% L-arabinose. Cells continued to grow under the same conditions for 24 h, and then at room temperature and 200 rpm for an additional 24 h. Cells were next harvested and lysed. 6×His-tagged proteins were affinity-purified with Ni-NTA agarose beads (Pierce, Rockford, IL) under native conditions according to the manufacturer's instructions. Proteins were buffer-exchanged into Tris-HCl (5 mM, pH 7.4) using Thermo Scientific Snakeskin dialysis tubing (7K Molecular Weight Cutoff).

2.2.5 *In vitro* Characterizations

Absorption and fluorescence spectra were recorded on a BioTek Synergy Mx Microplate Reader. To record excitation spectra, the emission wavelength was set at 650 nm, and the excitation was scanned from 450 nm to 630 nm. To record emission spectra, the excitation was set at 540 nm, and the emission was scanned from 560 nm to 700 nm.

An alkali denaturation method was used to determine protein concentrations and molar absorption coefficients.[39] Quantum yields were determined by following a published protocol. mApple was used as the standard for quantum yield measurements (QY = 0.49).

To reduce oxidized proteins, DTT (50 mM) was incubated with concentrated proteins (30 μM) in sealed microcentrifuge tubes at room temperature overnight. DTT was next removed using Sartorius Vivaspin 500 ultrafiltration columns (Viva Products, Littleton, MA). To confirm the reduction state, proteins (3 μg) in 1× SDS sample loading buffer (with no reducing reagent), after denaturation at 95 °C for 10 minutes, were directly loaded to 16% SDS-PAGE gels. Different electrophoretic mobilities were observed for reduced and oxidized proteins.

To determine the pH-dependence of protein fluorescence, a series of buffer solutions containing 200 mM citric acid and 200 mM sodium phosphate with pH values ranging from 3 to 11 were used to dilute proteins to a final concentration of 1 μM. Relative fluorescence intensities at each pH were measured using a plate reader with excitation at 540 nm and emission at 600 nm. Absorbance was recorded at 576 nm, and subtracted by background values gained with buffers at the same wavelength.

To determine the fluorescence responses of proteins to different glutathione redox potentials, mixtures of oxidized glutathione (from 1 to 2000 μM) and reduced glutathione (from 1 to 70 mM) were incubated with proteins (1 μM) in N_2-purged Tris-HCl buffer (100 mM, pH 7.4) in sealed microcentrifuge tubes at room temperature for 8 h. Fluorescence intensities at 600 nm were recorded on a monochromator-based Synergy Mx Microplate reader with the excitation wavelength set at 540 nm.

To determine the oligomeric state of rxRFP, protein samples of reduced or oxidized rxRFP were passed through a HiPrep Sephacryl S-200 HR gel filtration column (GE Healthcare) in an elution buffer containing Tris-HCl (50 mM, pH 7.4) and NaCl (100 mM). Samples of the dimeric dTFP0.2 and the monomeric mCherry proteins were also expressed and purified as described above and used as size standards.[40,41] The UV detector of the Gilson PLC 2020 liquid chromatography system was set at 280 nm to monitor protein elution.

To assay the responses of reduced rxRFP to various redox active molecules, a reduced rxRFP protein stock solution was diluted with 1× Phosphate Buffered Saline (PBS) to a final concentration of 1 μM. Various redox-active molecules were added, and the mixtures were incubated at room temperature for 20 min. Fluorescence excitation and emission were set to 540 and 600 nm, respectively, to quantify fluorescence intensities. The results were represented as means ± SD from three independent measurements.

2.2.6 Construction of mammalian expression plasmids

Oligonucleotides rxRFP-F and rxRFP-R were used to amplify genes of fluorescent protein probes from their corresponding pBAD plasmids. The products were next digested with Hind III and EcoR I, and ligated into a pcDNA3 plasmid (Life Technologies, Carlsbad, CA) also pre-digested with Hind III and EcoR I.

2.2.7 Mammalian Cell Culture and Imaging.

Human Embryonic Kidney (HEK) 293T cells were cultured in Dulbecco's Modified Eagle's Medium (DMEM) supplemented with 10% fetal bovine serum (FBS). Cells were incubated at 37℃with 5% CO_2 in humidified air. Cells were split into 35-mm dishes and

transfected at 80% confluency with 3 μg plasmid DNA and 9 μg PEI (polyethyleneimine, linear, M.W. 25kD). Transfected cells were cultured in complete medium for 36 hours. Before imaging, cells were washed twice with 1× Dulbecco's Phosphate Buffered Saline (DPBS), and left in 1 mL DPBS containing 1 mM Ca^{2+}, 1 mM Mg^{2+} and 1% BSA (bovine serum albumin). For time-lapse series, images were acquired under a Motic AE31 epi-fluorescence microscope every minute. Stimulation chemicals were added to cells after a few acquisitions. To investigate the pH-dependence of rxRFP fluorescence in living cells, we followed a previously reported procedure to perfuse HEK 293T cells using a series of nigericin/high potassium buffers.[42] A 550/30 nm bandpass filter was used for selecting excitation light, and a 610/75 nm bandpass filter was used for emission collection. Images and time-lapse videos were processed with ImageJ.

2.3 Results and Discussion

2.3.1 Engineering disulfide bonds into a circularly permuted red fluorescent protein

Previously, rxYFP and roGFPs were developed by directly inserting reversible disulfide bridges to the β-barrel surfaces of fluorescent proteins in their native topology. Concurrently, circularly permuted fluorescent proteins containing more accessible chromophores than native fluorescent proteins have been utilized to derive a large variety of other single fluorescent protein-based sensors. We postulated that adding reversible disulfide bridges to the N- and C- termini of circularly permuted fluorescent protein could be an effective way to generate redox-sensitive fluorescent proteins. To test this notion, we first identified a cpRFP scaffold, which can maintain its autocatalytic fluorescence, from a red fluorescent calcium sensor, R-GECO1. In the previous study, a

vertebrate calmodulin (CaM) and the CaM-binding region of chicken myosin light chain kinase (M13) were fused to the N- and C- termini of circular permuted mApple to derive R-GECO1 (**Figure 2.1**).[36] We used two pairs of oligonucleotides (see the first 4 sequences in **Table 2.1**) to amplify circular permuted mApple fragments from R-GECO1. All these variants were only slightly different in their N- and C- terminal linker sequences, but showed drastically different fluorescence intensities when expressed in *E. coli*. A particular variant containing residues 53 to 306 of R-GECO1 (numbered following Protein Data Bank 4I2Y;[44] residues 6 to 259 in **Figure 2.1**) was found to be modestly fluorescent. We next introduced cysteine pairs to the N- and C- termini of this cpRFP

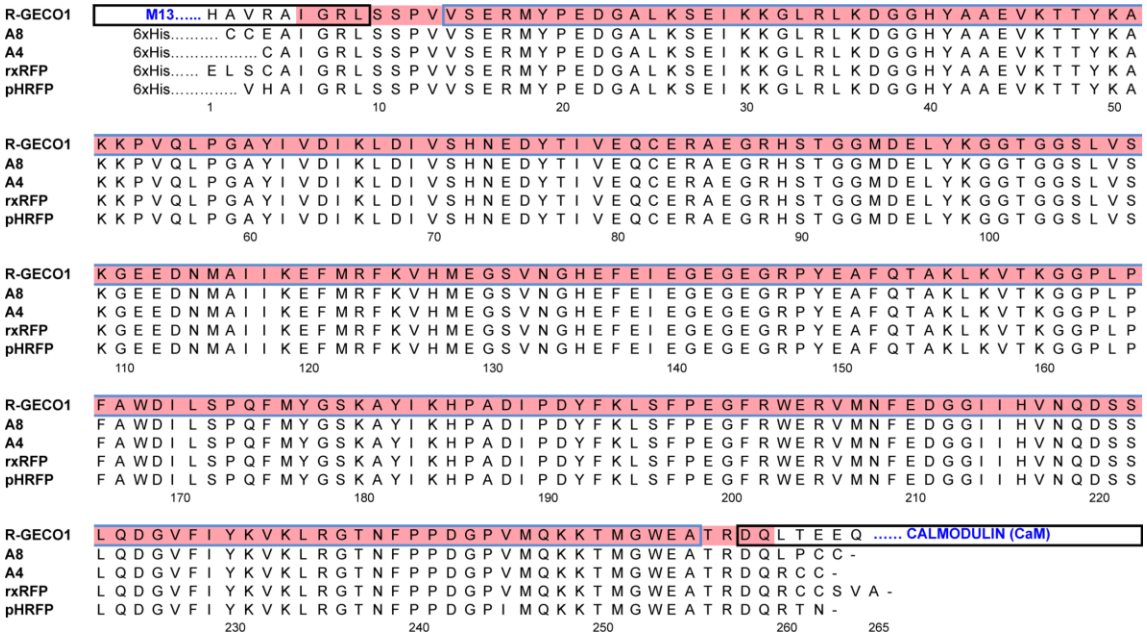

Figure 2.1. Sequence alignment of R-GECO1 and red fluorescent protein sensors described in this work. R-GECO1 is divided into three parts and individually boxed for sequences from M13, mApple and calmodulin. Residues 53 - 306 of R-GECO1 (6 - 259 in this figure) are highlighted in red, representing an autocatalytically fluorescent scaffold. The detailed sequences for the additional N- and C- termini of R-GECO1 and N-terminal 6×His tags are not shown. Residues in this figure are numbered according to the rxRFP sequence excluding residues encoded by the pBAD/His B plasmid.

variant. Four mutants (see the first 4 lines in **Table 2.2**) with different terminal sequences were made and crude proteins were prepared to test their responses to redox-active chemicals, such as DTT and H_2O_2. To our delight, when incubated with DTT, the fluorescence of all four mutants decreased, albeit marginally. Encouraged by the initial success, we next performed work to screen libraries to identify mutants showing improved redox-triggered fluorescence responses. To this end, additional oligonucleotides with varied lengths and randomized terminal residues were utilized to create 6 additional gene libraries, each encoding 20 or 400 protein variants (Libraries 1 - 6 in **Table 2.2**). From each library, a few of the most fluorescent bacterial colonies were chosen to inoculate liquid culture in 96-well plates, from which crude protein extracts were prepared. Adding the oxidizing reagent H_2O_2 to protein extracts typically led to little fluorescence change. We assumed that oxygen (O_2) in air was effective in oxidizing proteins to form disulfide bonds during preparation steps. The same phenomenon was also observed previously for rxYFP and roGFPs. In contrast, DTT was able to induce fluorescence responses of some clones in the libraries. Fluorescence intensities of cell extracts before and after DTT treatment were quantified. After examining ~ 24,000 individual colonies on LB agar plates and ~ 700 clones in liquid culture, we identified a few mutants showing large fluorescence responses to DTT treatment. Fluorescence intensities of the two best mutants, A4 and A8, in their oxidized states were ~ 3-fold higher than their intensities in the reduced states. A8 (**Figure 2.1**) contains two cysteines at its N-terminus and two additional cysteines at its C-terminus. Despite the fact that cysteines immediately adjacent to each other in peptides do not form disulfide bonds due

to geometric constraints, multiple cysteine combinations for disulfide bridges may be still possible in A8. Moreover, A8 was less fluorescent than A4, under both oxidizing and reducing conditions (**Figure 2.2a**). So we decided not to pursue this mutant further. A4 has one cysteine residue at its N-terminus and two cysteine residues at its C-terminus. To explore which C-terminal cysteine residue of A4 is more important for its redox sensitivity, we created two additional mutants by replacing each of the two C-terminal cysteines with serine. Serine substitution at the most C-terminal residue (A4-CS) resulted in a red fluorescent mutant, largely retaining the fluorescence brightness and dynamic range of A4 (**Figure 2.2a**). In contrast, the other mutant (A4-SC) was only dimly fluorescent and essentially unresponsive to DTT and H_2O_2 (data not shown). This result indicates that the second-most C-terminal cysteine residue of A4 is more important for its redox responsiveness.

To further improve A4, we optimized residues before its N-terminal cysteine and after its two C-terminal cysteines. Oligonucleotides with degenerated codons were used in a PCR reaction to construct a secondary library (**Library 7 in Table 2.2**) containing three fully randomized residues at each end of A4. After examining ~ 10,000 individual colonies on LB agar plates and ~ 500 colonies in liquid culture, we identified a further enhanced mutant, designated rxRFP (**Figure 2.1**), which showed up to 4-fold fluorescence increase in the oxidized state compared to in the reduced state (**Figure 2.2ab**). Both oxidized and reduced A4 and rxRFP proteins were subjected to SDS-PAGE analysis. The oxidized proteins migrated slightly faster than the reduced proteins (**Figure 2.2c**), suggesting a redox-dependent topological change in these proteins. It can be

reasoned that, in the oxidizing conditions, the N-terminal cysteine reacted with one of the C-terminal cysteines to form a cyclic structure with higher electrophoretic mobility. As the most promising redox-sensitive protein from our screening, rxRFP was subjected to further characterizations *in vitro* and in living mammalian cells.

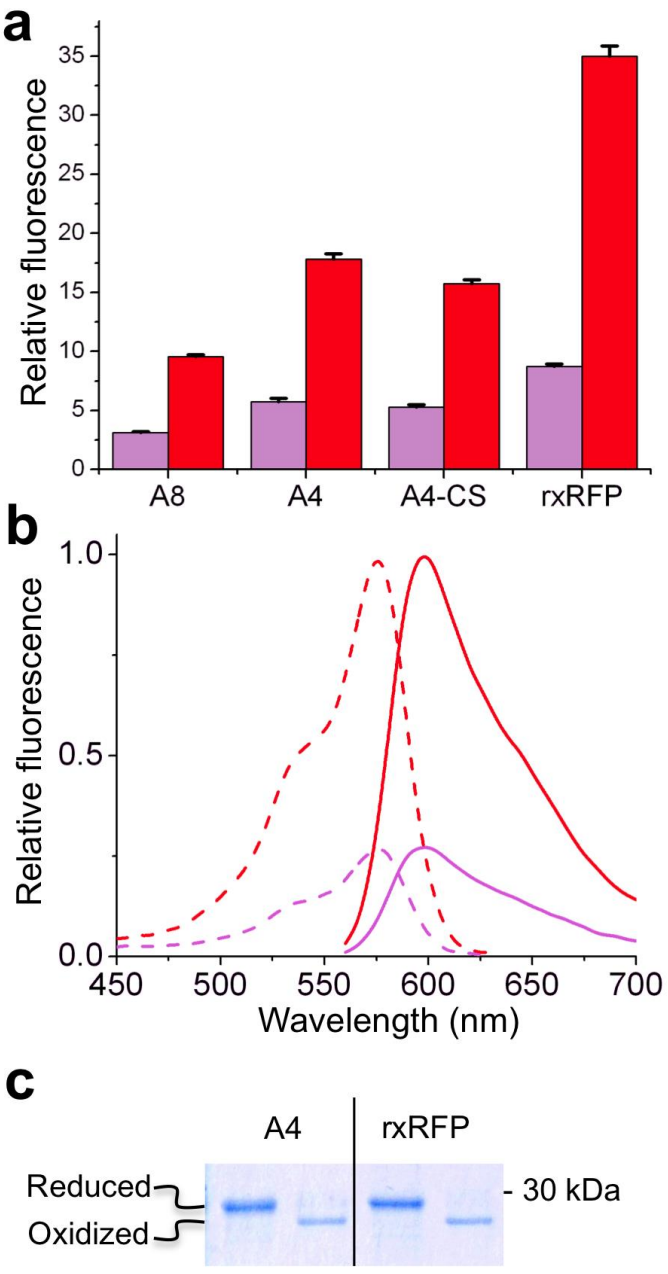

Figure 2.2. (**a**) Fluorescence intensity comparison of several rxRFP mutants at equal concentrations in their oxidized (red bar) or reduced (magenta bar) states. (**b**) Fluorescence excitation (dash line) and emission (solid line) spectra of oxidized (red) and reduced (magenta) rxRFP at pH 7.4. (**c**) Non-reducing SDS-PAGE analysis of A4 and rxRFP in the oxidized and reduced states.

Table 2.2. A list of mutants and libraries made for screening redox-sensitive proteins.

	PCR Primers	N-terminal sequence	C-terminal sequence	Note
	1C_F, 1C_R	CAIGR	RDQLC	Fluorescent but only weakly redox-responsive
	1C_F, 2C_R	CAIGR	RDQLCC	
	2C_F, 1C_R	CCAIGR	RDQLC	
	2C_F, 2C_R	CCAIGR	RDQLCC	
Library 1	CXGR_F, 2C_R	CXGR	RDQLCC	Mostly nonfluorescent
Library 2	CXIGR_F, 2C_R	CXIGR	RDQLCC	50% colonies were fluorescent
Library 3	XCIGR_F, 2C_R	XCIGR	RDQLCC	50% colonies were fluorescent
Library 4	1C_F, DXCC_R	CAIGR	RDXCC	10% colonies were fluorescent
Library 5	CCXAI_F, DQLXCC_R	CCXAIGR	RDQLXCC	80% colonies were fluorescent
Library 6	CXIGR_F, DQXCC_R	CXIGR	RDQXCC	50% colonies were fluorescent
Library 7	Ext_F, Ext_R	XXXCAIGR	RDQRCCXXX	70% colonies were fluorescent

C-terminal cysteines to form a cyclic structure with higher electrophoretic mobility. As the most promising redox-sensitive protein from our screening, rxRFP was subjected to further characterizations *in vitro* and in living mammalian cells.

2.3.2 Spectral and redox properties of rxRFP

At pH 7.4, both fully oxidized and reduced rxRFP have two major absorption bands with maxima at 448 nm and 576 nm, which correspond to the protonated and deprotonated states of the chromophore, respectively (**Figure 2.3ab**). Excitation of the high-energy absorption band at 448 nm led to very low fluorescence, while excitation of the low-energy absorption band at 576 nm resulted in strong red fluorescence with a peak at 600 nm (**Figure 2.2b**). Different from our original perception that the disulfide bond may block small molecules (e.g. H_2O) from accessing the chromophore of oxidized rxRFP to enhance its fluorescence quantum yield, the measured quantum yields of rxRFP under both oxidation conditions were essentially the same (**Table 2.2**). Instead, the ratio of the two absorption bands was redox-sensitive. When rxRFP was incubated under more oxidizing conditions, its absorption peak at 576 nm increased at the expense of the absorbance at 448 nm, compared to its absorption peaks under more reducing conditions (**Figure 2.3b**).

We also investigated the fluorescence response of oxidized and reduced rxRFP to pH changes. Fluorescence measurements from pH 5.5 to 11 yielded apparent pK_a value of 8.7 for both oxidized and reduced proteins (**Figure 2.3c**). The same pK_a values were also derived from absorbance measurements at 576 nm. Interestingly, in the high pH range where the chromophore was dominantly deprotonated, the absorptivity of oxidized rxRFP was ~ 4-fold higher than the absorptivity of reduced rxRFP. If this can be extrapolated to the condition at pH 7.4, the formation of the disulfide bond bridge in rxRFP modulates its absorptivity, which should be the main cause for the observed 4-fold

dynamic range at pH 7.4 (**Table 2.2**). The actual equilibrium shift caused by oxidation at pH 7.4, from a protonated chromophore to a deprotonated chromophore, would only be a minor factor.

The fluorescence response of rxRFP to a series of buffers with different redox potentials was also investigated (**Figure 2.3d**). Purified rxRFP was incubated and equilibrated with different mixtures of reduced and oxidized glutathiones (GSH/GSSH) at pH 7.4, room temperature. Fluorescence intensities were used to derive the apparent equilibrium constant for the oxidation reaction (K_{ox} = 3.3 M), assuming that the amount of protein-glutathione mixed disulfide was negligible at equilibrium. Based on the standard redox potential of - 240 mV for the GSH/GSSG redox pair at pH 7,[45] the midpoint redox potential of rxRFP was determined to be - 290 mV at pH 7.4. This number is close to the midpoint redox potentials of rxYFP and roGFPs, and also the previously reported redox potentials of cytosols and several other organelles in mammalian cells. The fluorescence excitation and emission of rxRFP are red-shifted, rendering it well-suited and complementary to other current research tools for studying redox dynamics in live cells.

To investigate the oligomeric state of rxRFP in the oxidized or reduced state, we carried out gel filtration chromatography (Figure 2.4a). By comparing the elution time of rxRFP to the elution time of two dimeric and monomeric fluorescent protein standards, we determined that reduced rxRFP is a pure monomer. Interestingly, rxRFP is a mixture of dimer and monomer in its oxidized state. About 10% of the oxidized protein formed a dimeric structure, likely because of interpeptide disulfide bonds. We also examined the

direct reactivity of reduced rxRFP with various common redox-active chemicals at physiologically relevant concentrations (Figure 2.4b). As expected, the fluorescence of reduced rxRFP was highly responsive to GSSG. In addition, $ONOO^-$ and superoxide ion ($O2^{\bullet-}$) also oxidized reduced rxRFP. In contrast, reduced rxRFP was unreactive to H_2O_2, hypochlorite (OCl^-) and hydroxyl radical (•OH) at the tested concentrations. This result further confirms our original notion that rxRFP is a suitable fluorescent probe for general redox changes, but not a specific redox probe toward a single ROS/RNS. It is also worthwhile to note that, when rxRFP is expressed in living cells, the overproduction of ROS, such as H_2O_2, may eventually affect the GSSG/GSH equilibrium to impact the fluorescence of rxRFP.

Table 2.3. Fluorescent properties of rxRFPs and mApple.

Protein		λ_{ab} (nm) with ε (mM^{-1} cm^{-1}) in parenthesis[1]	λ_{em} (nm) with Φ in parenthesis[1]	Brightness[2] (mM^{-1} cm^{-1})	pK_a[3]	Dynamic range[4]	Standard midpoint potential (mV)[5]
rxRFP	Oxidized	448 (34.3), 576 (26.0)	600 (0.14)	3.64	8.7	4.0×	− 290
	Reduced	448 (36.7), 576 (6.5)	600 (0.14)	0.91	8.7		
pHRFP		448 (17.1), 576 (9.8)	600 (0.20)	1.96	8.6	NA[6]	NA[6]

[1] Measured at pH 7.4. [2] Defined as the product of ε and Φ. [3] Defined as the pH value at which 50% of the maximal fluorescence is maintained. [4] Defined as the ratio of emission intensities in the oxidized and reduced states at pH 7.4. [5] Derived from fluorescence measurements of proteins equilibrated with GSH and GSSG. [6] Not applicable.

2.3.3 Developing a red fluorescent control pH probe

pH sensitivity is a common problem associated with many fluorescent protein-based sensors. To accurately interpret data derived from these fluorescent protein-based sensors, control pH probes are highly needed to assure that observed changes are not caused by pH variations. Previous studies have generated several genetically encoded red fluorescent pH sensors, such as mNectarine, pHTomato, and pHRed. These existing probes, however, have pK_a values quite different from rxRFP. Thus, they are not best suited for use as a pH control probe in rxRFP-involved experiments.

To derive a pH-sensitive fluorescent protein showing similar pH responses to rxRFP, we used a pair of oligonucleotides with degenerated codons (NNK) to amplify cpRFP from R-GECO1 (**Table 2.1**). Cysteines were intentionally excluded, except for those encoded by NNK codons. We screened the resultant library for high fluorescence brightness and the unresponsiveness to DTT and H_2O_2. We derived a particular mutant, named pHRFP, insensitive to redox changes and having a pK_a of 8.6 (**Figure 2.3e**). pHRFP and rxRFP, based on the same cpRFP scaffold, responded to pH changes almost identically. Sequencing of pHRFP confirmed that it is only different from rxRFP in a few amino acid residues.

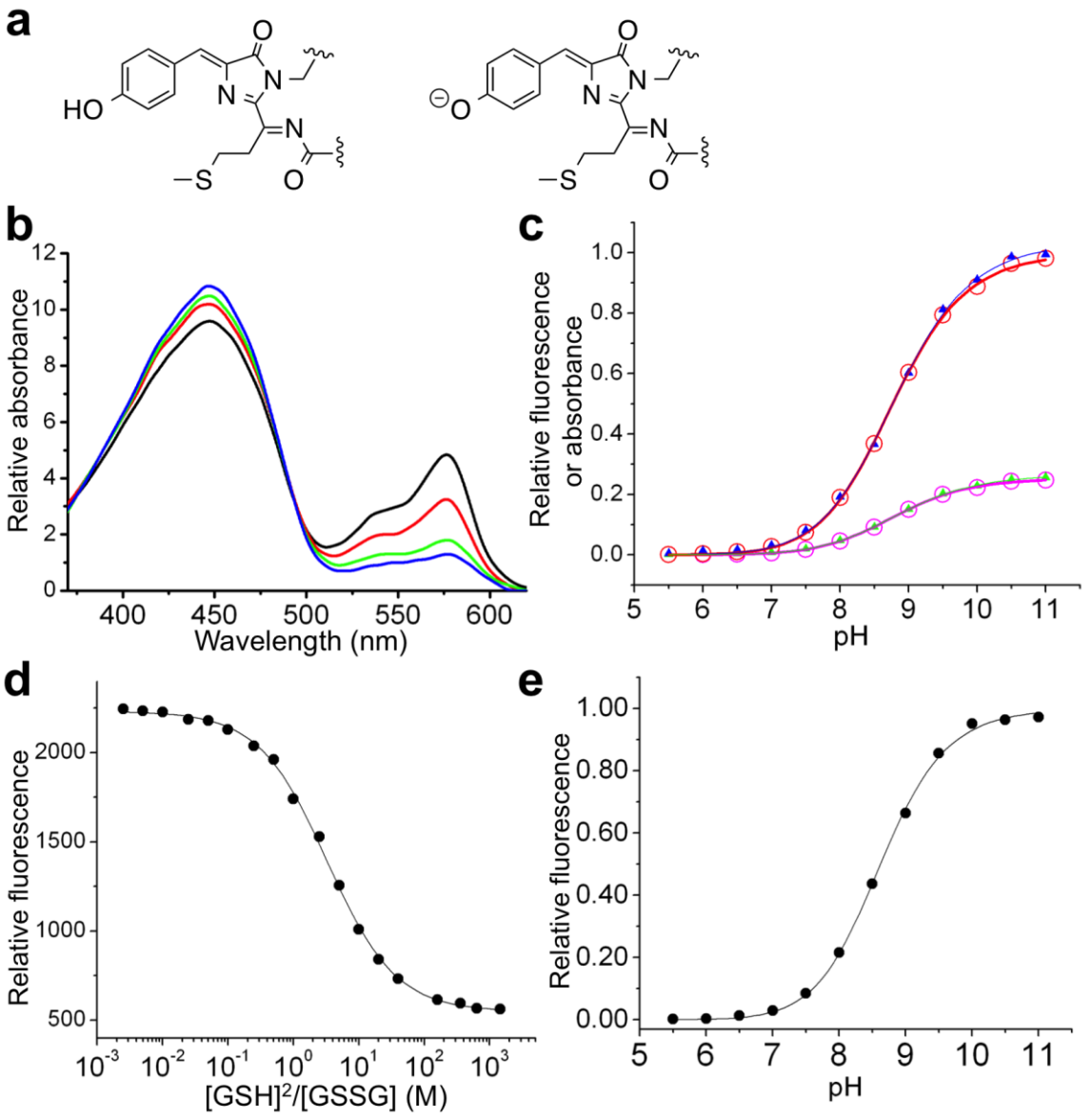

Figure 2.3. (**a**) Chemical structures of the protonated (left) and deprotonated (right) rxRFP chromophores. (**b**) Absorption spectra of rxRFP in redox buffers with $[GSH]^2/[GSSG]$ ratios of 10^{-4} M (black), 0.025 M (red), 40 M (green) and 1960 M (blue), respectively. (**c**) pH-dependent fluorescence and absorbance of rxRFP (*red circle*: fluorescence of oxidized rxRFP; *magenta circle*: fluorescence of reduced rxRFP; *blue triangle*: absorbance of oxidized rxRFP; *green triangle*: absorbance of reduced rxRFP). The data were normalized to the maximal obtained fluorescence or absorbance value, respectively. (**d**) Redox titration of rxRFP with reduced and oxidized glutathiones. (**e**). pH-dependent fluorescence of pHRFP.

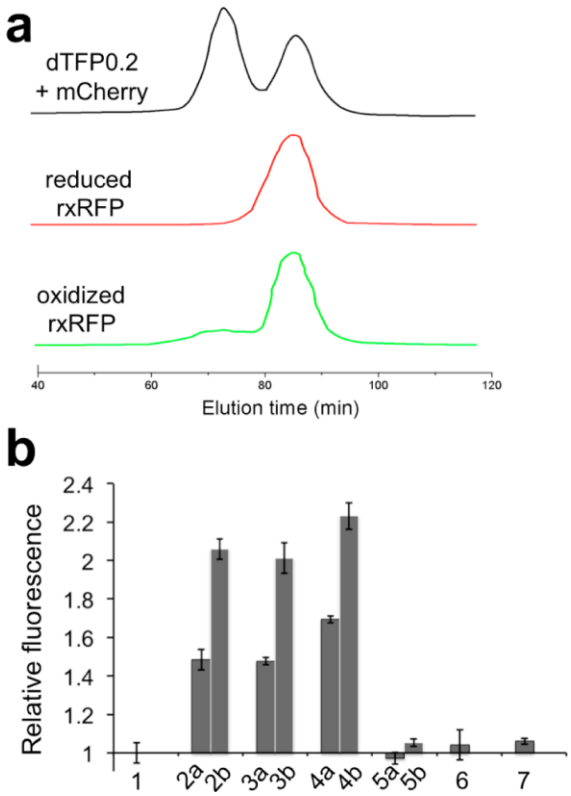

Figure 2.4. (**a**) Gel filtration chromatography elution profile of reduced (red) and oxidized (green) rxRFP. Detection is at 280 nm. For comparison, the upper profile is a co-injection of dimeric dTFP0.2 and monomeric mCherry. (**b**) Fluorescence responses of reduced rxRFP to various oxidants at physiologically relevant concentrations (1, PBS; 2, GSSG at 100 μM (a) and 1 mM (b); 3, $O_2^{\bullet-}$ at 1 μM (a) and 10 μM (b); 4, $ONOO^-$ at 10 μM (a) and 100 μM (b); 5, H_2O_2 at 100 μM (a) and 1 mM (b); 6, 100 μM OCl^-; 7, •OH (100 μM H2O2 + 1 mM Fe^{2+}).

2.3.4 Imaging redox dynamics in living mammalian cells

To validate the use of rxRFP for imaging redox dynamics in living mammalian cells, we transiently expressed it in HEK 293T cells. Bright red fluorescence was observed under fluorescence microscopy, suggesting that the chromophore of rxRFP was successfully formed in cells. rxRFP-expressing cells responded quickly to stimulation with a cell-permeable oxidant, aldrithiol-2 (200 μM). The fluorescence intensities of most cells increased by ~ 60% within 2 min (**Figure 2.4ab**). Following the initial escalation, the fluorescence of rxRFP-expressing cells decreased gradually, suggesting that living mammalian cells can activate intracellular antioxidant pathways to mitigate excessive oxidants. HEK 293T cells were also subjected to DTT perturbation (10 mM), and a sharp decrease in rxRFP fluorescence was observed (**Figure 2.4ab**). Moreover, we expressed pHRFP in HEK 293T cells, and insignificant fluorescence response was observed from identically treated cells (**Figure 2.4bc**). The sensitivity of pHRFP to pH changes was also cross-verified with HEK 293T cells in DPBS at pH 7.4 and 7.6 (**Figure 2.5**). These experiments suggest that the observed rxRFP fluorescence changes in HEK 293T cells were caused by redox changes, but not pH fluctuations.

We next explored the use of rxRFP to monitor the intracellular redox potential changes induced by a glutathione reductase inhibitor, 2-acetylamino-3-[4-(2-acetylamino-2-carboxyethylsulfanylthiocarbonylamino)phenylthiocarbamoylsulfanyl]propionic acid (2-AAPA). The inhibition of glutathione reductase by 2-AAPA is expected to increase GSSG and decrease GSH in cells. Indeed, when stimulated with 2-AAPA (100 μM), the fluorescence of rxRFP-expressing HEK 293T cells increased gradually, suggesting that

2-AAPA slowly shifted the redox potential to more positive states (**Figure 2.6ab**). A control experiment with pHRFP was also carried out, and the fluorescence of pHRFP did not change in the same magnitude compared to rxRFP under the same experimental condition (**Figure 2.6bc**). All these data support that rxRFP is a sensitive and robust fluorescent probe, and its fluorescence can be used as an indicator for redox changes in living mammalian cells.

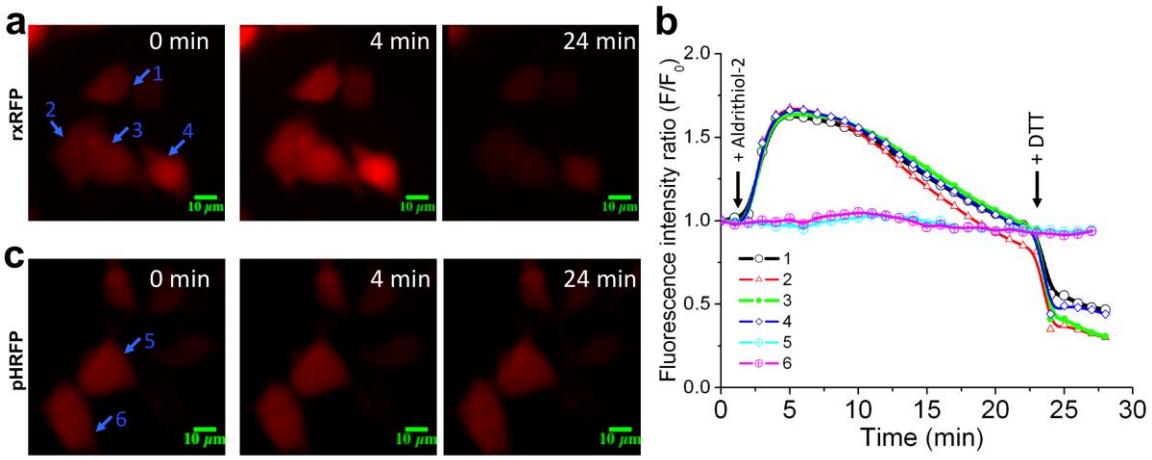

Figure 2.5. (**a**) Live fluorescence imaging of representative rxRFP-expressing HEK 293T cells at the indicated time points. Aldrithiol-2 (200 μM) and DTT (10 mM) were added at 2 and 23 min, respectively. (**b**) Quantified fluorescence intensities of individual cells indicated by arrows in panels **a** and **c**. The intensities were normalized to the initial intensities at 0 min. (**c**) Live fluorescence imaging of representative pHRFP-expressing HEK 293T cells, identically treated as the cells in panel **a**.

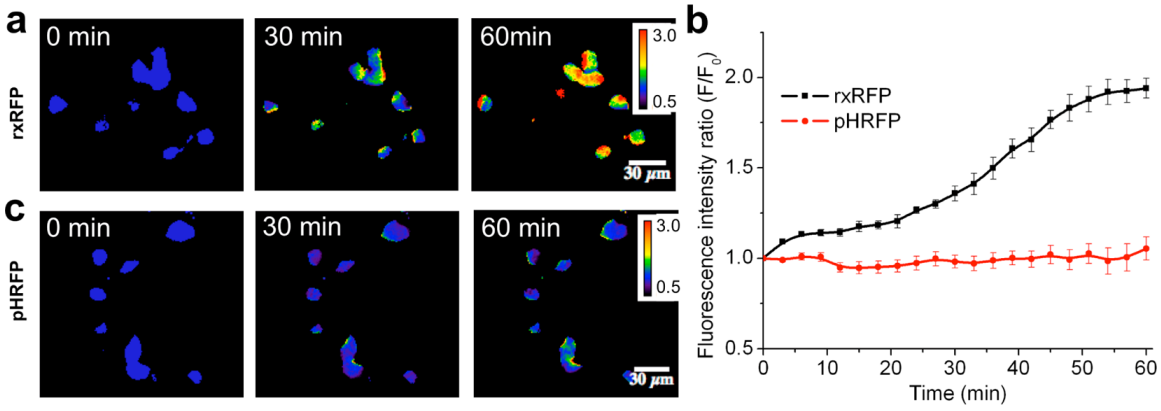

Figure 2.6. (**a**) Pseudocolored ratio images of representative rxRFP-expressing HEK 293T cells at the indicated time points. Cells were treated with 2-AAPA (200 μM) at 0 min. Color bar represents the ratios of fluorescence at the indicated time point to that at 0 min. (**b**) Fluorescence intensities of 2-AAPA-treated HEK 293T cells, normalized to the initial intensities at 0 min. The data were shown as means ± SD derived from the intensities of individual cells. (**c**) Pseudocolored ratio images of representative pHRFP-expressing HEK 293T cells, identically treated as the cells in panel **a**.

2.4 CONCLUSIONS

Our work reported here has expanded the family of genetically encoded redox probes into a longer wavelength region. We engineered a novel red fluorescent redox sensor, rxRFP, by introducing disulfide bridges to the N- and C- termini of circularly permuted fluorescent protein. Directed protein evolution was performed to optimize terminal sequences for increased redox-sensitivity and fluorescence brightness. The derived probe showed ~ 4-fold fluorescence increase upon oxidation, and has been utilized to image redox changes in mammalian cells.

Reference

1. Bartosz, G. Biochem. Reactive oxygen species: destroyers or messengers? Pharmacol. 2009, 77, 1303−1315.

2. Crow, J. P. Dichlorodihydrofluorescein and dihydrorhodamine 123 are sensitive indicators of peroxynitrite in vitro: implications for intracellular measurement of reactive nitrogen and oxygen species. Nitric Oxide 1997, 1, 145−157.

3. Finkel, T. Nitric oxide, mitochondria, and cell death. IUBMB Life 2001, 52, 3−6.

4. Klomsiri, C.; Karplus, P. A.; Poole, L. B. Cysteine-based redox switches in enzymes. Antioxid. Redox Signal. 2011, 14, 1065−1077.

5. Gius, D.; Spitz, D. R. Redox signaling in cancer biology. Antioxid. Redox Signal. 2006, 8, 1249−1252.

6. Spitaler, M. M.; Graier, W. F. Role of Nitrosative Stress and peroxynitrite in the pathogenesis of diabetic complications, Curr Med Chem 2002, 45, 476−494.

7. Zhang, S.; Liu, X.; Bawa-Khalfe, T.; Lu, L. S.; Lyu, Y. L.; Liu, L. F.; Yeh, E. T. Identification of the molecular basis of doxorubicin-induced cardiotoxicity. Nat. Med. 2012, 18, 1639−1642.

8. Halliwell, B. Reactive species and antioxidants. Plant Physiol. 2006, 141, 312−322.

9. Nikolaidis, M. G.; Kyparos, A.; Spanou, C.; Paschalis, V.; Theodorou, A. A.; Vrabas, I. S. Redox biology of exercise: an integrative and comparative consideration of some overlooked issues. J. Exp. Biol. 2012, 215, 1615−1625.

10. Ren, W.; Ai, H. W. Genetically encoded fluorescent redox probes. Sensors 2013, 13, 15422−15433.

11. Meyer, A. J.; Dick, T. P. Fluorescent protein-based redox probes. Antioxid. Redox Signal. 2010, 13, 621− 650.

12. Ostergaard, H.; Henriksen, A.; Hansen, F. G.; Winther, J. R. Shedding light on disulfide bond formation: engineering a redox switch in green fluorescent protein. EMBO J. 2001, 20, 5853−5862.

13. Ostergaard, H.; Tachibana, C.; Winther, J. R. Monitoring disulfide bond formation in the eukaryotic cytosol. J. Cell Biol. 2004, 166, 337−345.

14. Hanson, G. T.; Aggeler, R.; Oglesbee, D.; Cannon, M.; Capaldi, R. A.; Tsien, R. Y.; Remington, S. J. Investigating mitochondrial redox potential with redox-sensitive green fluorescent protein. J. Biol. Chem. 2004, 279, 13044− 13053.

15. Cannon, M. B.; Remington, S. J. Re-engineering redox-sensitive green fluorescent protein for improved response rate. Protein Sci. 2006, 15, 45−57.

16. Ai, H. W. Fluorescent protein-based probes: General principles and practices. Anal. Bioanal. Chem. 2015, 407, 9−15.

17. Meyer, A. J.; Brach, T.; Marty, L.; Kreye, S.; Rouhier, N.; Jacquot, J. P.; Hell, R. Redox-sensitive GFP in *Arabidopsis thaliana* is a quantitative biosensor for the the redox potential of the cellular glutathione redox buffer. Plant J. 2007, 52, 973−986.

18. Bjornberg, O.; Ostergaard, H.; Winther, J. R. Mechanistic insights provided by glutaredoxin within a fusion to redox-sensitive yellow fluorescent protein. Biochemistry 2006, 45, 2362−2371.

19. Gutscher, M.; Pauleau, A. L.; Marty, L.; Brach, T.; Wabnitz, G. H.; Samstag, Y.; Meyer, A. J.; Dick, T. P. Real-time imaging of the intracellular glutathione redox potential. Nat. Methods 2008, 5, 553− 559.

20. Gutscher, M.; Sobotta, M. C.; Wabnitz, G. H.; Ballikaya, S.; Meyer, A. J.; Samstag, Y.; Dick, T. P. Proximity-based protein thiol oxidation by H_2O_2-scavenging peroxidases. J. Biol. Chem. 2009, 284, 31532− 31540.

21. Bhaskar, A.; Chawla, M.; Mehta, M.; Parikh, P.; Chandra, P.; Bhave, D.; Kumar, D.; Carroll, K. S.; Singh, A. Reengineering redox sensitive GFP to measure mycothiol redox potential of *Mycobacterium tuberculosis* during infection. PLoS Pathog. 2014, 10, No. e1003902.

22. Pal, R.; Basu Thakur, P.; Li, S.; Minard, C.; Rodney, G. G. Real-time imaging of NADPH oxidase activity in living cells using a novel fluorescent protein reporter. PLoS One 2013, 8, No. e63989.

23. Belousov, V. V.; Fradkov, A. F.; Lukyanov, K. A.; Staroverov, D. B.; Shakhbazov, K. S.; Terskikh, A. V.; Lukyanov, S. Genetically encoded fluorescent indicator for intracellular hydrogen peroxide. Nat. Methods 2006, 3, 281−286.

24. Zhao, B. S.; Liang, Y.; Song, Y.; Zheng, C.; Hao, Z.; Chen, P. R. A highly selective fluorescent probe for visualization of organic hydroperoxides in living cells. J. Am. Chem. Soc. 2010, 132, 17065−17067.

25. Zhao, Y.; Jin, J.; Hu, Q.; Zhou, H. M.; Yi, J.; Yu, Z.; Xu, L.; Wang, X.; Yang, Y.; Loscalzo, Genetically encoded fluorescent sensors for intracellular NADH detection. J. Cell Metab. 2011, 14, 555−566.

26. Hung, Y. P.; Albeck, J. G.; Tantama, M.; Yellen, G. Imaging cytosolic NADH-NAD(+) redox state with a genetically encoded fluorescent biosensor. Cell Metab. 2011, 14, 545−554.

27. Chen, S.; Chen, Z. J.; Ren, W.; Ai, H. W. Reaction-based genetically encoded fluorescent hydrogen sulfide sensors. J. Am. Chem. Soc. 2012, 134, 9589−9592.

28. Chen, Z. J.; Ai, H. W. A highly responsive and selective fluorescent probe for imaging physiological hydrogen sulfide. Biochemistry 2014, 53, 5966−5974.

29. Chen, Z. J.; Ren, W.; Wright, Q. E.; Ai, H. W. Genetically encoded fluorescent probe for the selective detection of peroxynitrite. J. Am. Chem. Soc. 2013, 135, 14940−14943.

30. Frommer, W. B.; Davidson, M. W.; Campbell, R. E. Genetically encoded biosensors based on engineered fluorescent proteins. Chem. Soc. Rev. 2009, 38, 2833−2841.

31. Monici, M. Biotechnol. Cell and tissue autofluorescence research and diagnostic applications. Annu. Rev. 2005, 11, 227−256.

32. Khader, H.; Solodushko, V.; Al-Mehdi, A. B.; Audia, J.; Fouty, B. Overlap of doxycycline fluorescence with that of the redox-sensitive intracellular reporter of roGFP. J. Fluoresc. 2013, 24, 305−311.

33. Chu, J.; Haynes, R. D.; Corbel, S. Y.; Li, P.; Gonzalez-Gonzalez, E.; Burg, J. S.; Ataie, N. J.; Lam, A. J.; Cranfill, P. J.; Baird, M. A.; Davidson, M. W.; Ng, H. L.; Garcia, K. C.; Contag, C. H.; Shen, K.; Blau, H. M.; Lin, M. Z. Non-invasive intravital imaging of cellular differentiation with a bright red-excitable fluorescent protein. Nat. Methods 2014, 11, 572−578.

34. Ermakova, Y. G.; Bilan, D. S.; Matlashov, M. E.; Mishina, N. M.; Markvicheva, K. N.; Subach, O. M.; Subach, F. V.; Bogeski, I.; Hoth, M.; Enikolopov, G.; Belousov, V. V. Red fluorescent genetically encoded indicator for intracellular hydrogen peroxide. Nat. Commun. 2014, 5, 5222.

35. Magpiong, I.; Koon, N.; Yei, S. M.; Risenmay, A. J.; Kallio, K.; Remington, S. J. J. Biomol. Technol. 2011, 22 (Suppl), S52 Poster in ABRF 2011.

36. Zhao, Y.; Araki, S.; Wu, J.; Teramoto, T.; Chang, Y. F.; Nakano, M.; Abdelfattah, A. S.; Fujiwara, M.; Ishihara, T.; Nagai, T.; Campbell, R. E. An expanded palette of genetically encoded Ca^{2+} indicators. Science 2011, 333, 1888−1891.

37. Edelstein, A.; Amodaj, N.; Hoover, K.; Vale, R.; Stuurman, N. Current Protocols in Molecular Biology; Ausubel, F. M., Ed.; 2010; Chapter 14, Unit 14.20.

38. Schneider, C. A.; Rasband, W. S.; Eliceiri, K. W. NIH image to imageJ: 25 years of image analysis. Nat. Methods 2012, 9, 671−675.

39. Ai, H. W.; Baird, M. A.; Shen, Y.; Davidson, M. W.; Campbell, R. E. Engineering and characterization monomeric fluorescent proteins for live-cell imaging applications. Nat. Protoc. 2014, 9, 910−928.

40. Ai, H. W.; Olenych, S. G.; Wong, P.; Davidson, M. W.; Campbell, R. E. Hue-shifted monomeric variants of *Clavulariacyan* fluorescent protein: identification of the molecular determinants of color and applications in fluorescence imaging. BMC Biol. 2008, 6, 13.

41. Shaner, N. C.; Campbell, R. E.; Steinbach, P. A.; Giepmans, B. N.; Palmer, A. E.; Tsien, R. Y. Improved monomeric red, orange and yellow fluorescent proteins derived from *Discosoma* sp. Red fluorescent protein. Nat. Biotechnol. 2004, 22, 1567−1572.

42. Johnson, D. E.; Ai, H. W.; Wong, P.; Young, J. D.; Campbell, R. E.; Casey, J. R. Red fluorescent protein pH biosensor to detect concentrative nucleoside transport. J. Biol. Chem. 2009, 284, 20499−20511.

43. Kardash, E.; Bandemer, J.; Raz, E. Imaging protein activity in live embryos using fluorescence resonance energy transfer biosensors. Nat. Protoc. 2011, 6, 1835−1846.

44. Akerboom, J.; Carreras Calderon, N.; Tian, L.; Wabnig, S.; Prigge, M.; Tolo, J.; Gordus, A.; Orger, M. B.; Severi, K. E.; Macklin, J. J.; Patel, R.; Pulver, S. R.; Wardill, T. J.; Fischer, E.; Schuler, C.; Chen, T. W.; Sarkisyan, K. S.; Marvin, J. S.; Bargmann, C. I.; Kim, D. S.; Kugler, S.; Lagnado, L.; Hegemann, P.; Gottschalk, A.; Schreiter, E. R.; Looger, L. L. Genetically encoded calcium indicators for multi-color neural activity imaging and combination with optogenetics. Front. Mol. Neurosci. 2013, 6, 2.

45. Appenzeller-Herzog, C. Glutathione- and non-glutathione-based oxidant control in the endoplasmic reticulum. J. Cell Sci. 2011, 124, 847−855.

46. Li, Y.; Tsien, R. W. Localized microstimulation of primate pregenual cingulate cortex induces negative decision-making. Nat. Neurosci. 2012, 15, 1047−1053.

47. Tantama, M.; Hung, Y. P.; Yellen, G. Imaging intracellular pH in live cells with a genetically encoded red fluorescent protein probe. J. Am. Chem. Soc. 2011, 133, 10034−10037.

48. Seefeldt, T.; Zhao, Y.; Chen, W.; Raza, A. S.; Carlson, L.; Herman, J.; Stoebner, A.; Hanson, S.; Foll, R.; Guan, X. Characterization of a novel dithiocarbamate glutathione reductase inhibitor and its use as a tool to modulate intracellular glutathione. J Biol Chem2009, 284, 2729−2737.

Chapter 3: Development of redox-sensitive red fluorescent proteins for imaging redox dynamics in cellular compartments

3.1 Introduction

The biochemistry and functions of eukaryotic cells are organized within distinct cellular compartments separated by physical barriers such as lipid-containing membranes.[1] Cellular compartmentation is important for eukaryotic biology, since it provides the basis for spatiotemporal regulation of biomolecules, biomolecular reactions, and signaling. Redox signaling and oxidative stress play critical biological roles,[2,3] and it is long accepted that redox regulation systems exist in the major compartments of mammalian cells, such as mitochondria, the cell nucleus, and the secretory pathway.[4] Each of these compartments shows unique redox characteristics, with mitochondria as the most reducing compartments and the endoplasmic reticulum (ER) as the most oxidizing intracellular environments.[4] Variations in the redox states of individual cellular compartments affect, or even sometimes determine, biological consequences,[5] thereby impacting diverse cellular processes, including proliferation, differentiation, and apoptosis.

Genetically encoded fluorescent redox probes, such as redox-sensitive green fluorescent proteins (roGFPs)[6,7] and redox-sensitive yellow fluorescent protein (rxYFP),[8]

have been instrumental in understanding redox controls and pathways within compartments, because fusing them with subcellular localization sequences allows precise targeting of these sensors into various subcellular domains.[9-11] The fluorescence of these sensors can be monitored with fluorometers, fluorescence plate readers, or fluorescence microscopy to derive precious information on redox dynamics of these cellular organelles. Our laboratory recently reported a redox-sensitive red fluorescent protein (rxRFP), which comprises of a circularly permuted red fluorescent protein with cysteine residues appended to the N- and C- termini for redox-dependent, reversible formation of a disulfide bridge.[12] We also demonstrated that, rxRFP could be expressed in living mammalian cells to monitor redox changes induced by various oxidants and reductants, in addition to a glutathione reductase inhibitor, 2-AAPA.[12] In the basal state, rxRFP maintained both an oxidized portion and a reduced portion in the cytosol of HEK 293T cells, indicating that the midpoint redox potential of rxRFP is close to the redox potential of the cytosol and rxRFP is a suitable sensor for cytosolic redox dynamics. This expansion of the palette of redox-sensitive fluorescent proteins has enabled new capabilities for multicolor and multiplex images. Moreover, different from roGFPs and rxYFP, which respond to oxidation, either excitation-ratiometrically or inversely, the fluorescence of rxRFP is simply positively correlated with the extent of oxidation, making it a highly attractive redox sensor.[12] The use of long wavelength light for excitation of rxRFP1 also reduces the concerns on intracellular oxidation induced by short wavelength light for excitation of roGFPs.[11,13]

Since individual cellular compartments have quite different basal redox states, monitoring redox dynamics in these compartments therefore requires fluorescent probes showing different midpoint redox potentials to match the redox states of these compartments. Herein, we report the development of several rxRFP mutants (**Figure 3.1**) showing *in vitro* midpoint redox potentials spanning from -314 mV to -268 mV. We also show that the fluorescence of these sensors is indicative for redox changes in cellular compartments, such as mitochondria, the cell nucleus, and ER. In particular, a mitochondrially localized rxRFP mutant, Mito-rxRFP1.1, was utilized to monitor doxorubicin-induced oxidative stress,[14] a process related to the cardiotoxic adverse effect of cancer chemotherapy.

3.2 Materials and Methods

3.2.1 Materials, Reagents, and General Methodology

Synthetic DNA oligonucleotides were purchased from Integrated DNA Technologies (San Diego, CA). Restriction endonucleases were purchased from New England Biolabs (Ipswich, MA) or Thermo Scientific Fermentas (Vilnius, Lithuania). Products of PCR and restriction digestion were purified by gel electrophoresis and extracted using Syd Laboratories Gel Extraction columns (Malden, MA). Plasmid DNA was purified using Syd Laboratories Miniprep columns. All chemicals were purchased from Sigma-Aldrich (St. Louis, MO) or Fisher Scientific (Hampton, NH) and used as received. DNA sequences were analyzed by Retrogen (San Diego, CA).

3.2.2 Construction of *Escherichia coli* Expression Plasmids and Libraries

pBAD-rxRFP were used as our cloning template. In several polymerase chain reactions (PCR), oligonucleotide pBAD_F (see **Table 3.2**) was paired with either RCK_R, or RCE_R, or RCS_R to directly generate rxRFP mutants with point mutations at residue 262. In addition, oligonucleotides 3X_F and 3X_R, which contain several degenerate NNK codons (in which N = A, T, G, or C, and K = G or T), were used to generate a C262S point mutation and full randomization at residues 1-3 and 263-265. All amplified DNA fragments were treated with Xho I and Hind III, and ligated into a predigested compatible pBAD/His B plasmid (Life Technologies, Carlsbad, CA). The resultant ligation products were used to transform DH10B *Escherichia coli* cells, which were next plated on LB agar plates supplemented with ampicillin (100μg/mL) and L-arabinose (0.04%, w/v%).

3.2.3 Library Screening

To screen the library generated from rxRFP and oligonucleotides 3X_F and 3X_R, we used a laboratory-built colony fluorescence imaging system, which has been described previously, to evaluate fluorescence intensities of individual colonies on LB agar plates after overnight incubation at 37 °C. We used a digital camera and ImageJ[15] to quantify red fluorescence intensities of individual colonies. A pair of forensic red goggles with a cutoff wavelength at ~ 590 nm was also utilized to assist in identification of bacterial colonies on LB agar plates by human eyes. Colonies with high to mediocre brightness were selected and cultured in 5 mL liquid LB supplemented with 100 μg/mL ampicillin and 0.04% L-arabinose. Cells were first incubated at 37 °C and 250 rpm

overnight, and next, at room temperature and 200 rpm for another 6 h. After centrifugation to pellet the cells, B-PER Bacterial Protein Extraction Reagents (Pierce, Rockford, IL) were added, followed by another centrifugation step to remove cell debris. Before and after a 15-min DTT (100 mM) treatment at room temperature, we quantified the fluorescence of the resultant clear cell lysates on a monochromator-based Synergy Mx Microplate Reader (BioTek, Winooski, VT) with excitation and emission wavelengths at 540 and 600 nm, respectively. We selected mutants showing large ratios of fluorescence intensities before and after DTT treatment for further characterization.

3.2.4 Protein Purification and *in vitro* Characterization

6×His-tagged proteins were purified using Ni-NTA agarose beads by following a previously described procedure. Next, they were buffer-exchanged into Tris-HCl (5mM, pH7.4) using Thermo Scientific Snakeskin dialysis tubing (7k molecular weight cutoff). Absorption and fluorescence spectra, quantum yields, molar absorption, and pH sensitivity (pKa) were determined as previously described. To prepared reduced proteins, protein stocks were incubated in DTT (50 mM) overnight in a nitrogen (N_2) glove box. DTT was removed using Sartorius Vivaspin 500 ultrafiltration columns (Viva Products, Littleton, MA) right before other characterization experiments. To determine the fluorescence responses of proteins to oxidized and reduced glutathione (GSSG/GSH) mixtures showing different redox potentials, proteins (1 μM) were incubated with GSSG (from 1 to 2000 μM) and GSH (from 1 to 100 mM) overnight in N_2-purged Tris-HCl buffer (100mM, pH 7.4), and allowed to equilibrate in a N_2 glove box at room temperature. Fluorescence intensities were next measured using a monochromator-based

Synergy Mx Microplate Reader. The equilibrium constant for oxidation reactions, K_{ox}, was determined by fitting the data to $F = F_{red} + (F_{ox}-F_{red})/(1+([GSH]^2/[GSSG])/K_{ox})$, where F_{red} and F_{ox} represent the fluorescence of reduced and oxidized proteins, respectively. The half reaction of rxRFP reduction is $rxRFP_{ox}+2H+ + 2e- \leftrightarrow rxRFP_{red}$, and the half-reaction of GSSG reduction is $GSSG+2H+ + 2e- \leftrightarrow GSH$. Based on the standard redox potential of the GSH/GSSG redox pair at pH 7,[6,16] the redox potentials of rxRFPs could then be calculated from the Nernst equation, $E = E^{\phi} + RT/nF (Ln K_{ox})$, where EØ is the standard redox potential of the GSH/GSSG pair, R is the gas constant (8.315 $J•K^{-1}$ mol^{-1}), T is the absolute temperature, n is the number of transferred electrons, and F is the Faraday constant (9.649×10^4 $C•mol^{-1}$). To further correct for the pH difference, the redox potential ($E_{7.4}$) at pH 7.4 can be derived from the redox potential (E_7) at pH 7 using the following equation: $E_{7.4} = E_7 – 2.303RT/F \times (7.4-7)$

3.2.5 Construction of Mammalian Expression Plasmids

To create a plasmid for mitochondrial expression of the rxRFP mutant, rxRFP1.1, we used oligonucleotides Mito_F and Mito_RCK_R, and Mito_RCK_F and rxRCK_R to amplify a mitochondrial targeting sequence (MLSLRQSIRFFKPATRTLCSSRYLL) from pMito-hsGFP[17] and the rxRFP1.1 gene fragment from pBAD-rxRFP1.1, respectively. Next, an overlap PCR with oligonucleotides Mito_F and rxRCK_R was utilized to assemble the two fragments. The resultant DNA was digested with Hind III and Xba I, and then ligated into a predigested pcDNA3 plasmid to generate pMito-rxRFP1.1. To construct a plasmid for ER localization of the rxRFP mutant, rxRFP1.4, we used oligonucleotides ER_RCS_F1, ER_RCS_F2, ER_RCS_F3, and ER_RCS_R to

amplify the rxRFP1.4 gene fragment from pBAD-rxRFP1.4 and further extend it to include an N-terminal ER localization sequence (MLLSVPLLLGLLGLAAAD) and a C-terminal ER retention sequence (KDEL). The resultant DNA was again digested with Hind III and Xba I, and then ligated into a predigested pcDNA3 plasmid to generate pER-rxRFP1.4. To construct a plasmid for nuclear expression of rxRFP, we used oligonucleotides Nuc_F, RCC_Nuc1, Nuc2, and Nuc3 to amplify the rxRFP gene fragment from pBAD-rxRFP and further extend it to include C-terminal three repeats of nuclear localization sequence (DPKKKRKV). The PCR product was digested with Hind III and Xba I and ligated into a predigested pcDNA3 plasmid to derive pNuc-rxRFP. A pNuc-rxRFP1.1 plasmid was also generated based on the same strategy, except for that the oligonucleotide RCK_Nuc1 was used to replace RCC_Nuc1 to amplify rxRFP1.1 from pBAD-rxRFP1.1 in the initial PCR reaction.

3.2.6 Cell Culture and Transfection

HEK 293T cells were cultured in Dulecco's Modified Eagle's Medium (DMEM) supplemented with 10% fetal bovine serum (FBS), and incubated at 37°C under 5% CO_2 in humidified air. The day before transfection, approximately 2.5×10^5 cells were seeded into individual 35-mm culture dishes. In the next day, 3 μg plasmid DNA and 9 μg PEI (polyethylenimine, linear, M.W. 25 kD) were mixed in fresh DMEM (500 μL) with no FBS. After incubation at room temperature for 15 min, the mixture was added into a 35-mm cell culture dish containing HEK 293T cells. Three hours later, the culture medium was replaced with fresh DMEM containing 10% FBS. Cells were cultured for another 48 h before imaging or only 36 h before treatment of doxorubicin.

3.2.7 Fluorescence Imaging

Cells were washed twice with 2 mL Dulbecco's Phosphate Buffered Saline (DPBS) containing 1 mM Ca^{2+} and 1 mM Mg^{2+} (DPBS++), and left in 1 mL DPBS++ for immediate imaging on either a Motic AE31 inverted epi-fluorescence microscope equipped with a 20× objective Lens or a Leica SP5 confocal fluorescence microscope with a 40× objective Lens. For time-lapse series, images were acquired every 1 min and stimulating chemicals were added between acquisitions.

For understanding the redox status of rxRFPs within different compartment, cells were treated with 0.02% (w/v) digitonin for complete permeabilization and high concentrated aldrithiol-2 (1 mM) were added for maximal oxidation in cells. Images were taken after no more fluorescence increase was observed. Aldrithiol-2 was removed from cells followed by DTT (10 mM) addition for maximal reduction in cells. Again images were taken after reduction reaches equilibrium.

Time-dependence of doxorubicin in mitochondria was determined by taking images every one hour for a total duration of 12 h after doxorubicin treatment. Cells were cultured in medium supplemented with 2 μM doxorubicin and washed three times with DPBS right before imaging. Treated cells were maintained at 37°C whenever not being imaged. Doxorubicin toxicity within cytoplasm was also studied by treating cells with 2 μM doxorubicin for 12 h. Images were taken and analyzed for comparison between cytoplasm and mitochondria. Concentration-dependency was determined by treating cells with doxorubicin from 100 nM to 2 μM. Images were taken 12 hours after treatment. Cells not treated with doxorubicin were also imaged as control experiment to indicate

intrinsic fluorescence changes by time. Representative fluorescence intensity of at least 30 cells from different fields is shown as mean ± sd. A 550/30 nm bandpass filter was used for selecting excitation light, and a 610/75 nm bandpass filter was used for emission collection. All images were taken under the same microscopy setting with exposure of 150 ms and gain of 200. ImageJ was used to process the images.

3.3 Results and Discussion

3.3.1 Engineering of rxRFP Mutants

Our previously reported red fluorescent redox sensor, rxRFP, has a redox potential matching the basal redox state of the cell cytosol. To generate rxRFP mutants showing different redox potentials, we hypothesized that residues in close proximity to the two cysteine residues （C241 and C261） responsible for the formation of a reversible disulfide bridge between the N- and C- termini of rxRFP, should effectively modulate the redox potential of rxRFP. To test this notion, we introduced point mutations (C262K, C262S, or C262E) into rxRFP, because C262 is close to C261 but not involved in the formation of the reversible disulfide bridge. We intentionally chose lysine, serine, and glutamate for the replacement, because they represent a positively charged, a neutral and structurally similar, and a negatively charged residue, respectively. We named these three mutants as rxRFP1.1, rxRFP1.2 and rxRFP1.3, respectively (**Figure 3.1**).

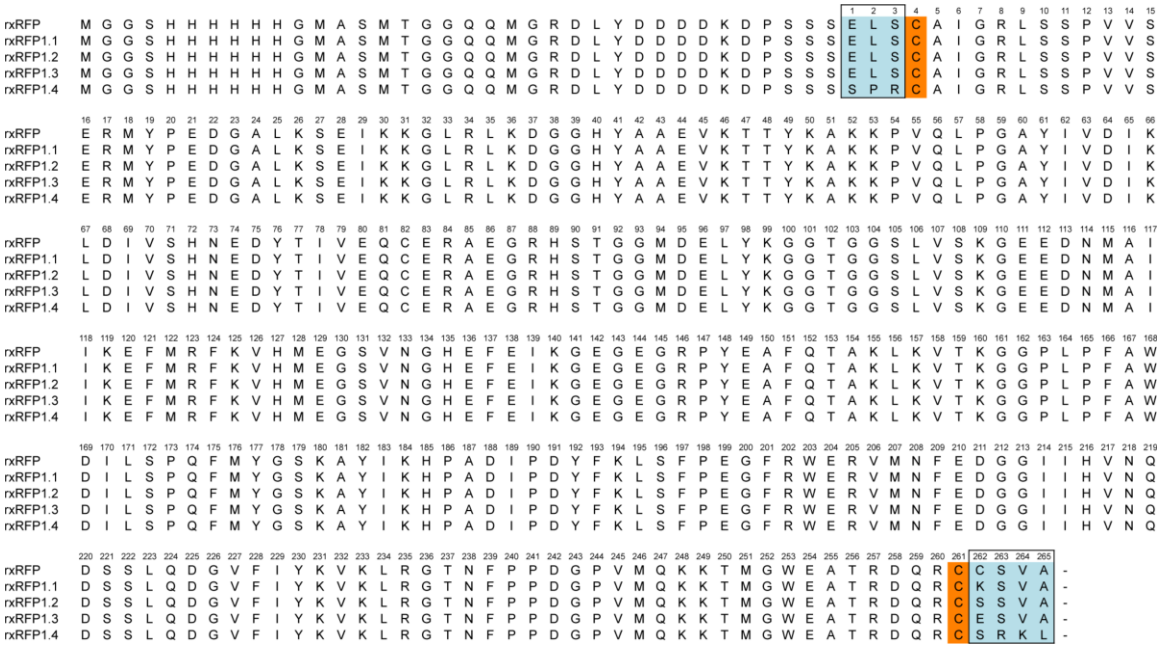

Figure 3.1. Sequence alignment of redox-sensitive red fluorescent protein mutants described in this work. Unnumbered N-terminal residues (including the His_6 Tag) are encoded in the plasmid backbone of pBAD/His B. Two cysteine residues for reversible disulfide bond formation (residues 4 and 261) and amino acid residues different among these mutants (residues 1-3 and 262-265) are highlighted in orange and cyan, respectively.

During the evolution of rxRFP, we previously derived an A4-CS mutant, the sequence of which starts with an N-terminal cysteine and ends with a C-terminal cysteine followed by a serine residue. We utilized oligonucleotides with degenerate codons to extend it from both ends with an original intention to enhance its brightness. The oligonucleotides were designed to match the length of rxRFP and randomize residues 1-3 and 263-265 (numbered according to rxRFP). We screened ~ 10000 individual colonies on LB agar plates and ~ 400 clones in liquid culture. We eventually identified a promising clone, which showed bright red fluorescence on a LB agar plate and high

responsiveness to reduction in an assay based on crude cell lysates. This mutant is different from rxRFP in seven mutations (E1S/L2P/S3R/C262S/S263R/V264K/A265L), and was named rxRFP1.4.

3.3.2 Characterization of rxRFP Mutants Showing Varied Midpoint Redox Potentials

All abovementioned four variants of rxRFP showed red fluorescence, which increased as the proteins were converted from more reduced states to more oxidized states. The maxima of their absorbance and fluorescence excitation and emission were identical to those of rxRFP. Excitation of the high-energy absorption bands at 448 nm, which corresponded to neutral chromophores, essentially led to no fluorescence, whereas excitation of deprotonated chromophores at 576 nm generated strong red fluorescence with maxima at 600 nm. The dynamic ranges, defined as the ratios of emission intensities of proteins in oxidized states to their intensities in reduced states, were roughly 4-fold (**Table 3.1**). Compared to rxRFP, the brightness of rxRFP1.2 and rxRFP1.3 was reduced, while rxRFP1.1 and rxRFP1.4 were ~ 45% – 65% brighter than rxRFP under oxidized or reduced conditions. We also determined the pH sensitivity of these proteins, and their pK_a values in the oxidized and reduced states were between 8.2 and 10.2 (**Table 3.1**).

We next determined the thermodynamic stabilities of the disulfide bonds of these rxRFP mutants (**Figure 3.2**). We incubated purified proteins with mixtures of reduced and oxidized glutathione (GSH/GSSH) at pH 7.4. After equilibration at room temperature, their fluorescence intensities were measured to derive the apparent equilibrium constants for their oxidation reactions (K_{ox} = 83.6 M, 1.71 M, 0.36 M, and

0.22 M for rxRFP1.1, rxRFP1.2, rxRFP1.3, and rxRFP1.4, respectively), based on the assumption that mixed disulfides between proteins and glutathione were negligible at equilibration. Since the standard redox potential of the GSH/GSSG redox pair is – 240 mV at pH 7, we consequently derived the midpoint redox potentials of rxRFP1.1, rxRFP1.2, rxRFP1.3, and rxRFP1.4 at pH 7.4 to be – 321 mV, – 271 mV, – 250 mV, and – 244 mV, respectively. In comparison, the midpoint redox potential of the initial rxRFP was determined to be – 279 mV using the same procedure.

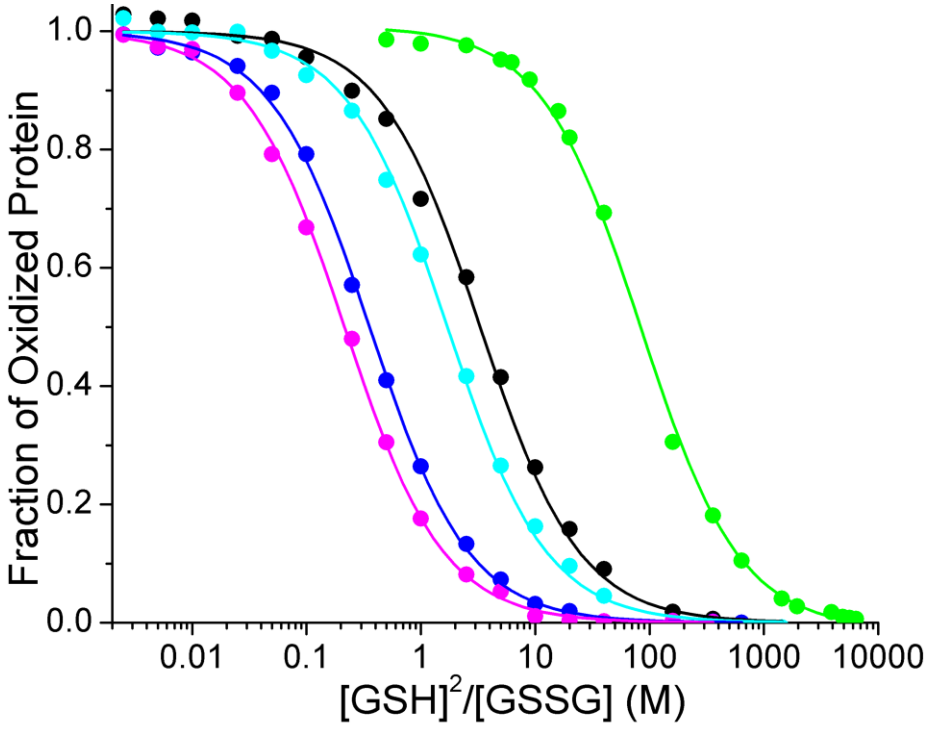

Figure 3.2. Redox titration with reduced and oxidized glutathiones, showing different midpoint redox potentials for rxRFP (black), rxRFP1.1 (green), rxRFP1.2 (cyan), rxRFP1.3 (blue), and rxRFP1.4 (magenta). The fractions of oxidized proteins were determined based on fluorescence intensities of rxRFP mutants in equilibration with mixtures of reduced and oxidized glutathiones.

Our mutagenesis and protein evolution have derived rxRFP mutants showing quite different midpoint redox potentials. Placing a positively charged lysine and a negatively charged glutamate at residue 262 increased and reduced the thermodynamic stability of the disulfide bond, respectively. A single residue difference between rxRFP1.1 and rxRFP1.3 was able to vary the midpoint redox potentials by 71 mV. This contradicts our initial assumption and some previous examples on roGFP and rxRFP mutants, in which positively charged residues stabilize thiolate species to weaken disulfide bonds. On the other hand, rxRFP1.4, which was engineered from a library with several fully randomized residues, was enriched with positively charged residues at residues 3, 263, and 264. These mutations decreased the thermodynamic stability of the disulfide bond, leading to the most positive midpoint redox potential among this group. Based on these results, the interplay between the thermodynamic stability of the disulfide bond and its surrounding residues seems to be rather complex and not simply determined by side-chain charges of these residues. Presumably, other factors, such as geometric strain, may also play important roles. Further research is needed to understand the mechanisms regarding the order of the midpoint redox potentials of rxRFP and its mutants.

3.3.3 Imaging of Real-Time Redox Changes in Cellular Compartments

After development of rxRFP mutants showing very different redox potentials, we next used them to detect redox dynamics in subcellular domains. To monitor subcellular redox dynamics, the redox potentials of fluorescent probes should be close to the basal redox states of particular compartments, so that the probes are maintained in equilibrium between reduced and oxidized portions. Mitochondria have usually been considered as

the most reduced cellular organelles, due to a high rate of electron transfer during mitochondrial respiration to molecular oxygen (O_2). We therefore, genetically fused rxRFP1.1, the mutant with the lowest midpoint redox potential among the group, with a mitochondrial targeting sequence (MTS) derived from the leader sequence of cytochrome c oxidase subunit IV. With this fusion construct (pMito-rxRFP1.1), rxRFP1.1 should be expressed and automatically sorted into the mitochondrial matrix. Similarly, we fused rxRFP1.4, the rxRFP mutant with the highest midpoint redox potential, with peptide sequences responsible for localization and retention of proteins in ER, the most oxidizing intracellular compartment. To create constructs for sensing redox dynamics in the nucleus, which is a relatively reducing cellular compartments but also considered less reduced than the mitochondria, we appended a nuclear localization sequence (NLS) to the C-terminus of either rxRFP or rxRFP1.1. Imaging of HEK293T cells expressing the abovementioned constructs show proper subcellular localization in all experiments (**Figure 3.3a, 3.4a, 3.5a**).

To analyze the response of Mito-rxRFP1.1 upon exogenous redox stimulation, time-lapse images were taken using fluorescence microscopy. Mito-rxRFP1.1-expressing cells responded quickly to the stimulation of cell-permeable oxidants, both aldrithiol-2 and H_2O_2. Addition of the oxidants evoked fluorescence intensities increase by 81% and 42%, aldrithiol-2 and H_2O_2 respectively, within 10 minutes (**Figure 3.3b**). An immediate decrease in fluorescence intensities was also observed after the cells were subjected to DTT perturbation. These proved that Mito-rxRFP1.1 is only partially reduced in HEK 293T cell mitochondria, which makes it effective to measure changes with more

oxidizing or reducing states. rxRFP1.1 was fully oxidized or reduced in these cells after addition of AT-2 or DTT because supplementing additional AT-2 or DTT did not trigger any further fluorescence change in either condition. Based on these intensity values, we estimated that in the basal state, ~36 % of rxRFP1.1 was oxidized in the mitochondrial matrix of HEK 293 T cells. Providing that rxRFP1.1 equilibrates with GSSG and GSH in vivo the same as it does in vitro, we further estimated the redox potential for the mitochondrial matrix of HEK 293 T cells to be −329 mVat pH 7.4 and 37 °C. Because the pH of mitochondria has been estimated to be 7.98,[18] the redox potential was further corrected to be −365 mV at pH 7.98 and 37 °C (Table 3.3), based on the assumption that the equilibrium between rxRFP1.1 and glutathiones was not affected by pH changes from 7.4 to 7.98. Our estimated value (−365 mV) is close to the value (−360 mV) reported by Hanson and coworkers, who used roGFP1 to estimate the mitochondrial redox potential of HeLa cells. Our experiments support that rxRFP1.1 is an effective probe for monitoring both oxidative and reductive changes in mammalian mitochondria.

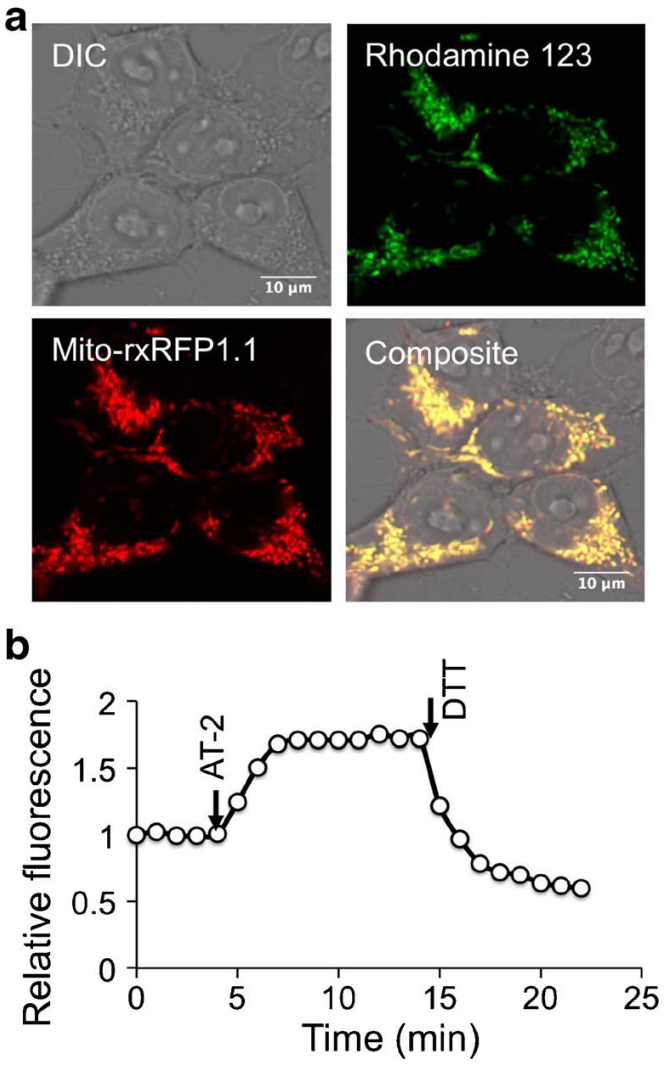

Figure 3.3. (**a**) Fluorescence imaging of HEK 293 T cells, showing mitochondrial localization of rxRFP1.1. Rhodamine 123, a known mitochondrial probe, was used for comparison. (**b**) A representative trace of fluorescence intensities (normalized to the intensity value at 0 min) of a HEK 293 T cell expressing mitochondrial rxRFP1.1, treated with AT-2 (1 mM) and DTT (10 mM) at 4 and 14 min, respectively.

Another target of interest is endoplasmic reticulum, which has very oxidizing conditions to introduce structural disulfides in protein folding for membrane and exported proteins. Targeting genetically encoded redox-sensitive fluorescent probes to ER has always been insufficient, considering midpoint potential in ER to be beyond the useful dynamic range of the probes. Of all the rxRFP derived variants, rxRFP1.4 has the most oxidizing potential, which makes it possibly suitable for targeting the subcellular ER. Indeed, a gradual increase of fluorescence (up to 50% within 15 minutes) in ER-rxRFP1.4-expressing cells was observed after the cells were treated with aldrithiol-2 and as expected a sharp decrease in fluorescence was achieved by treating the cells with DTT (**Figure 3.4a, b**). This confirmed that ER-rxRFP1.4 is not fully oxidized in endoplasmic reticulum of HEK 293T cells and we believe it is one of the few reported ER-targeting fluorescent probes to sense redox changes. We observed that the direct addition of DTT (10 mM) in the imaging medium was unable to fully reduce rxRFP1.4 in the ER, so we further developed a procedure to permeabilize cell membranes with digitonin. We co-treated HEK 293 T cells with digitonin (0.02 %, w/v) and AT-2 (1 mM)

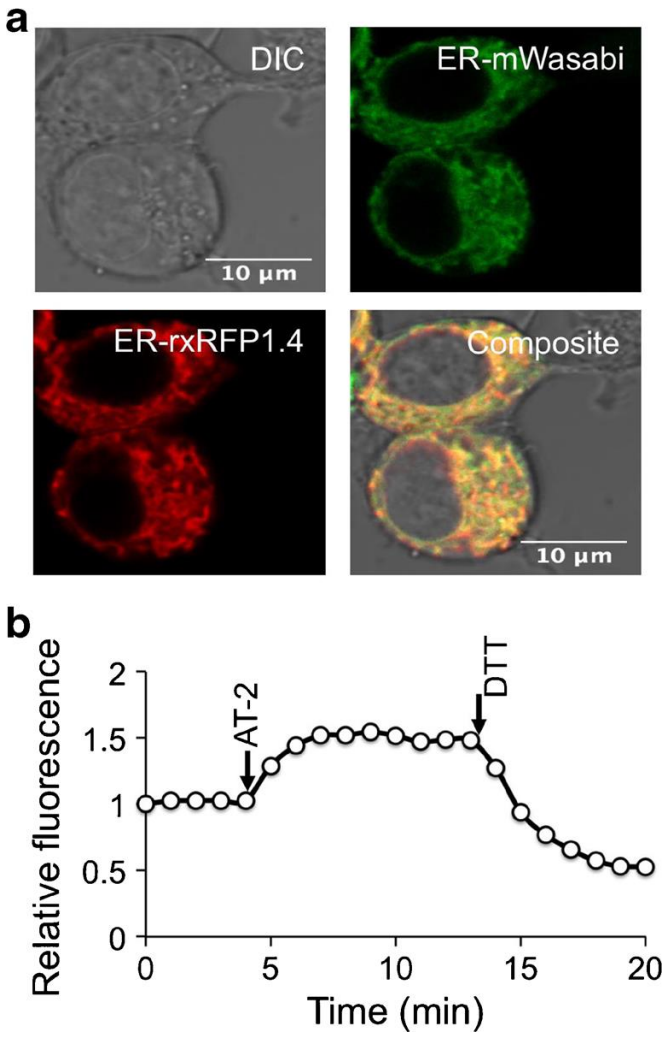

Figure 3.4. (**a**) Fluorescence imaging of HEK 293 T cells, showing ER localization of rxRFP1.4. A previously validated green fluorescent ERmWasabi probe was used for comparison. (**b**) A representative trace of fluorescence intensities (normalized to the intensity value at 0 min) of a HEK 293 T cell expressing rxRFP1.4 in the ER, by addition of AT-2 (1 mM) and DTT (10 mM) in the culture medium at 4 and 13 min, respectively.

or DTT (10 mM), and estimated that ~73 % rxRFP1.4 was in the oxidized state before any treatment. We further estimated that the basal redox potential for the ER of HEK 293 T cells was −209 mVat pH 7.0 and 37 °C (Table 3.3). This was based on the same assumptions mentioned previously for estimating the redox potential of mitochondria, except that pH 7.0 was used as the typical pH of the ER.[20] We want to note that the reported values for the redox potential of ER have been quite inconsistent, at least ranging from −118 mV to −242 mV.[21-24] The inconsistency in the literature may be caused by several reasons: first, those studies used different organisms or cell lines, and their biological differences may be truly significant; second, cell culture methods and sample preparation may have an impact on the redox states of ER; third, redox sensors and ER-endogenous redox components may not reach a complete thermodynamic equilibrium, and their redox states are kinetically separated, thereby leading to different numbers reflecting the reducing power of different ER redox components.[25] Our derived value is close to the number (−208 mV at pH 7.0) reported in a recent study,[26] which used a glutaredoxin-coupled roGFP to estimate the ER glutathione redox potential in HeLa cells.

Table 3.3. Basal redox potentials of cellular compartments, estimated by using rxRFP mutants

Cellular location	Probe used	Estimated basal redox potential (pH and temperature)
Mitochondria	Mitochondrial rxRFP1.1	−365 mV (pH 7.98 and 37 °C)
Cell nucleus	Nuclear rxRFP1.1	−326 mV (pH 7.4 and 37 °C)
ER	ER-localized rxRFP1.4	−209 mV (pH 7.0 and 37 °C)
Cytosol	Cytosolic rxRFP1	−277 mV (pH 7.4 and 37 °C)

We next want to utilize the probes to measure redox status in mammalian nucleus. Original rxRFP was first fused with nuclear localization sequence and the resulting recombinant Nuc-rxRFP was expressed in HEK 293T cells (**Figure 3.5a**). An increase in fluorescence intensity up to 140% was observed 10 minutes after aldrithiol-2 perturbation (**Figure 3.5b**). However, no noticeable fluorescence decrease was observed after DTT perturbation. We believe Nuc-rxRFP is fully reduced in mammalian cell nucleus. Since rxRFP1.1 has a relatively more reducing midpoint potential compared with rxRFP, we again fuse nuclear localization sequence with rxRFP1.1. Recombinant Nuc-rxRFP1.1 shows a quicker response after aldrithiol-2 perturbation and up to 60% fluorescence increase was observed within 5 minutes (**Figure 3.5c**). Moreover, immediate decrease in fluorescence was also observed for Nuc-rxRFP1.1-expressing cells upon DTT treatment, which proves that unlike Nuc-rxRFP, Nuc-rxRFP1.1 is not fully reduced in cell nucleus. We believe generally rxRFP1.1 is suitable in relatively more reducing cellular compartments, including mitochondria and nucleus. It is also worth mentioning that the

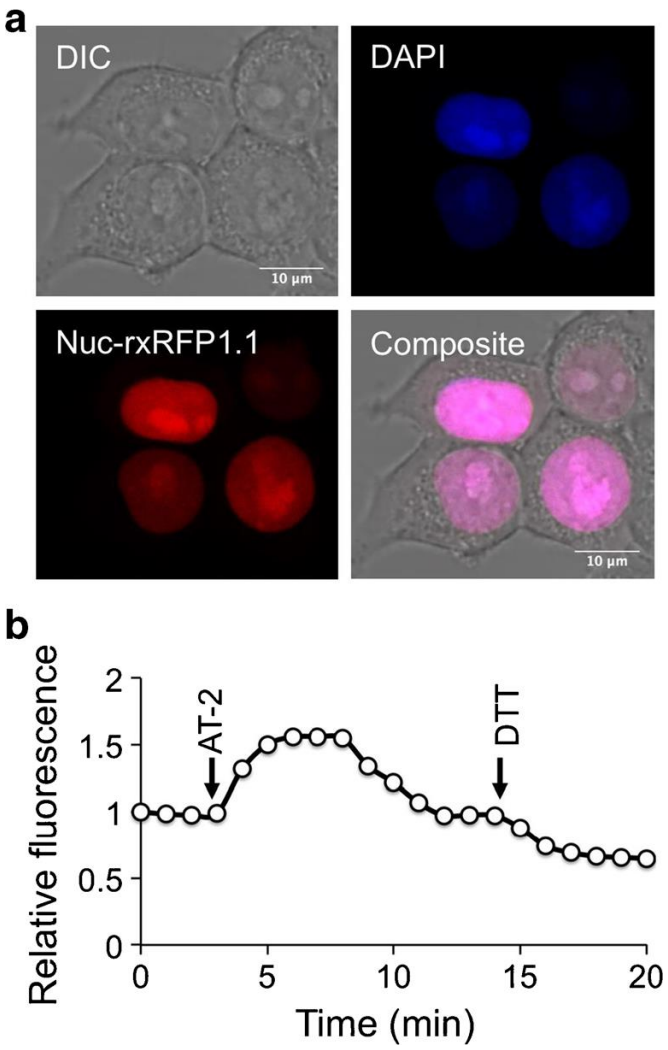

Figure 3.5. (**a**) Fluorescence imaging of HEK 293 T cells, showing nuclear localization of rxRFP1.1. DAPI was also utilized to stain cell nuclei. (**b**) A representative trace of fluorescence intensities (normalized to the intensity value at 0 min) of a HEK 293 T cell expressing nuclear rxRFP1.1, treated with AT-2 (1 mM) and DTT (10 mM) at 3 and 14 min, respectively.

fluorescence of both Nuc-rxRFP and Nuc-rxRFP1.1-expressing cells decreased gradually following the initial escalation.[27] This suggests that the subcellular nuclear antioxidant pathways were activated to mitigate the excessive exogenous oxidants thus avoiding DNA damage.

We further sought to estimate the cytoplasmic redox potential of HEK 293 T using rxRFP1. Considering its comparable size to other single fluorescent proteins, the untagged rxRFP1 can likely passively diffuse through the nuclear pore.[27] The observed whole-cell fluorescence was therefore affected by the redox potentials of the cytosol and the nucleus, the redox reaction kinetics of rxRFP1, and the intercompartmental protein-transport kinetics. Indeed, when an rxRFP1-expressing cell was imaged at a high resolution and magnification, the fluorescence of the nucleus seemed to be dimmer than the fluorescence of the cytosol (**Figure 3.6a**), supporting that the cell nucleus is more reduced than the cytosol and the cytosol-nucleus rxRFP1-transport is not much faster than the redox reaction of rxRFP1. We next expressed rxRFP1 fused with three copies of a nuclear export signal peptide. The fusion protein was exclusively in the cytosol (Fig. 6b). We performed the oxidation and reduction experiments with AT-2 (1 mM) and DTT (10 mM), respectively (**Figure 3.6c**). We estimated that ~56 % of rxRFP1 was oxidized before treatment, corresponding to a redox potential of −277 mV for the cytosol of HEK 293 T (Table 3.3). We want to note that the dynamic ranges of these rxRFP probes in cell compartments may not exactly match the dynamic ranges determined in vitro with purified proteins because the absolute fluorescence intensities are often sensitive to other environmental factors (e.g., pH, temperature, and ionic strength). However, the redox

equilibrium itself is less affected by small environmental changes,[8] and it is reasonable to estimate the fractions of oxidized proteins based on the fluorescence intensity values before treatment and in the corresponding fully oxidized and reduced conditions. In fact, in order to estimate the redox potentials for mitochondria (pH 7.98) and the ER (pH 7.0), we assumed that the equilibria between rxRFPs and glutathiones were not changed even though the in vitro glutathione titration experiment was done at pH 7.4.We further validated this assumption by incubating rxRFP1.1 or rxRFP1.4 with mixtures of GSH and GSSG at pH 8 and pH 7, respectively. The equilibrium between rxRFP1.1 or rxRFP1.4 and glutathiones at pH 8 or pH 7 was identical to the corresponding equilibrium at pH 7.4 (**Figure 3.7**), further suggesting that our estimation was appropriate.

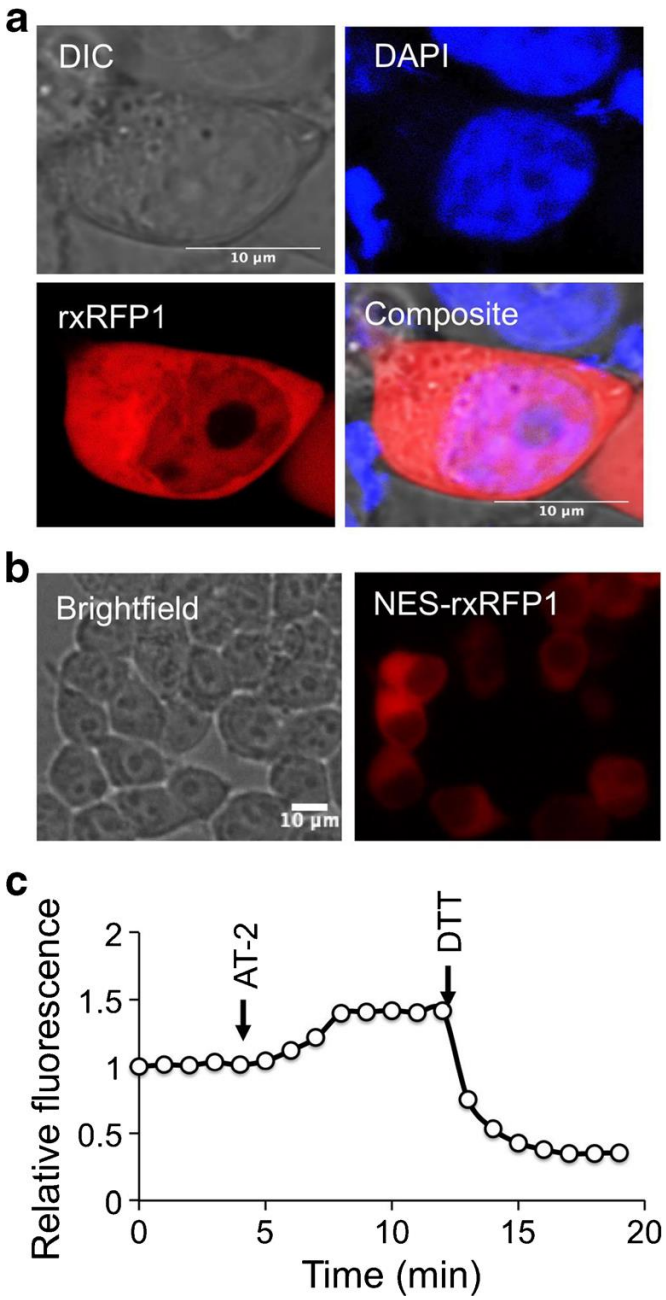

Figure 3.6. (**a**) Fluorescence imaging of HEK 293 T cells expressing unlocalized rxRFP1. The cell nucleus was less fluorescent than the cytosol, and rxRFP1 seemed to be excluded from a condensed nuclear subdomain. (**b**) Fluorescence imaging of HEK 293 T cells expressing rxRFP1 fused with nuclear export signal (NES). (**c**) A representative trace of fluorescence intensities (normalized to the intensity value at 0 min) of a HEK 293 T cell expressing cytosolic rxRFP1, treated with AT-2 (1 mM) and DTT (10 mM) at 4 and 12 min, respectively.

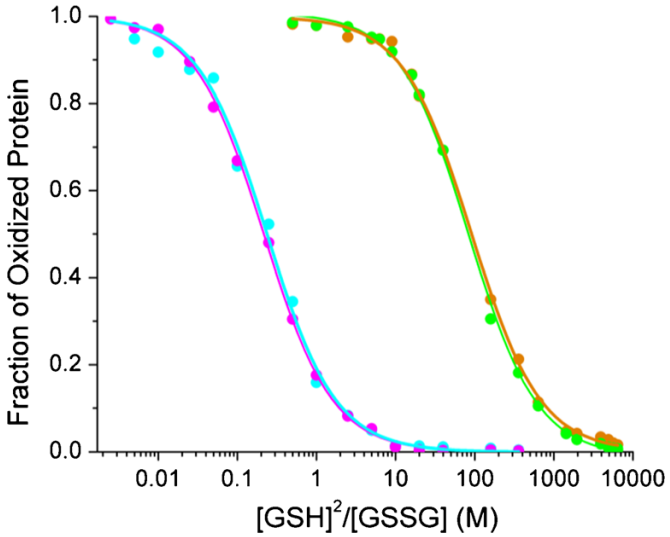

Figure 3.7. Redox titration of rxRFP1.1 with reduced and oxidized glutathiones at pH 7.4 (green) and pH 8 (dark orange), and rxRFP1.4 at pH 7.4 (magenta) and pH 7 (cyan), suggesting that the corresponding equilibrium was not shifted in these pH ranges.

3.3.4 Monitoring of Mitochondrial Oxidative Stress Induced by Doxorubicin

Doxorubicin is a chemotherapy drug routinely used to treat many kinds of cancer.[14,28] Doxorubicin is known to mediate ROS production, which has been utilized to explain its anticancer activity and its adverse cardiotoxic effect. In particular, recent evidences indicate that ROS production may enhance, but is not essential for, the anticancer activity of doxorubicin is a major limitation for doxorubicin therapy, whereas the acute and chronic cardiotoxicity of doxorubicin is typically attributed to ROS/RNS[29] resulting from the redox cycling of doxorubicin at the mtETC and/or hydroxyl radical (·OH) generated in mitochondria of cardiac cells.

We further utilized Mito-rxRFP1.1 to monitor the intracellular redox potential changes induced by an anticancer drug, doxorubicin (DOX), which is widely used in treatment of a broad spectrum of cancers. DOX-induced cardiotoxicity is known being caused mainly by ROS generation, especially in mitochondria. Cells were first treated

with various concentrations of DOX, from 100 nM to 2 μM. Images were taken 12 hours after the treatment. Fluorescence intensity was modestly increased in a dose-dependent manner, and maximum increase (240 ± 19%) was observed at 2 μM DOX (**Figure 3.8a**). A more oxidizing state in mitochondria was induced by DOX treatment, causing increase in fluorescence intensity as we expected. We next want to explore the effects of DOX in a time-dependent manner. After stimulated with 2 μM DOX, the fluorescence started to gradually increase from 1 hour, and reached plateau at approximately 6 hours, then sustained the same after that (**Figure 3.8b**). Fluorescence increased up to 254 ± 27%, which is qualitatively similar to the responses in dose-dependency experiment. The results support that Mito-rxRFP1.1 is a sensitive and robust probe and it can be used as a fluorescence indicator for exogenous as well as endogenous redox changes in the mitochondria of living mammalian cells.

Doxorubicin is often administered at 20–50 mg/m2 every 3 or 4 wk to treat cancer.[30] In a pharmacokinetics study on patients with AIDS-related Kaposi's sarcoma, a single dose of 20 mg/m^2 doxorubicin infused over 30 min generated a peak plasma doxorubicin concentration of 8.34 μg/mL (~15 μM).[31] This further suggests that our observed mitochondrial oxidative stress is likely of clinical relevance.

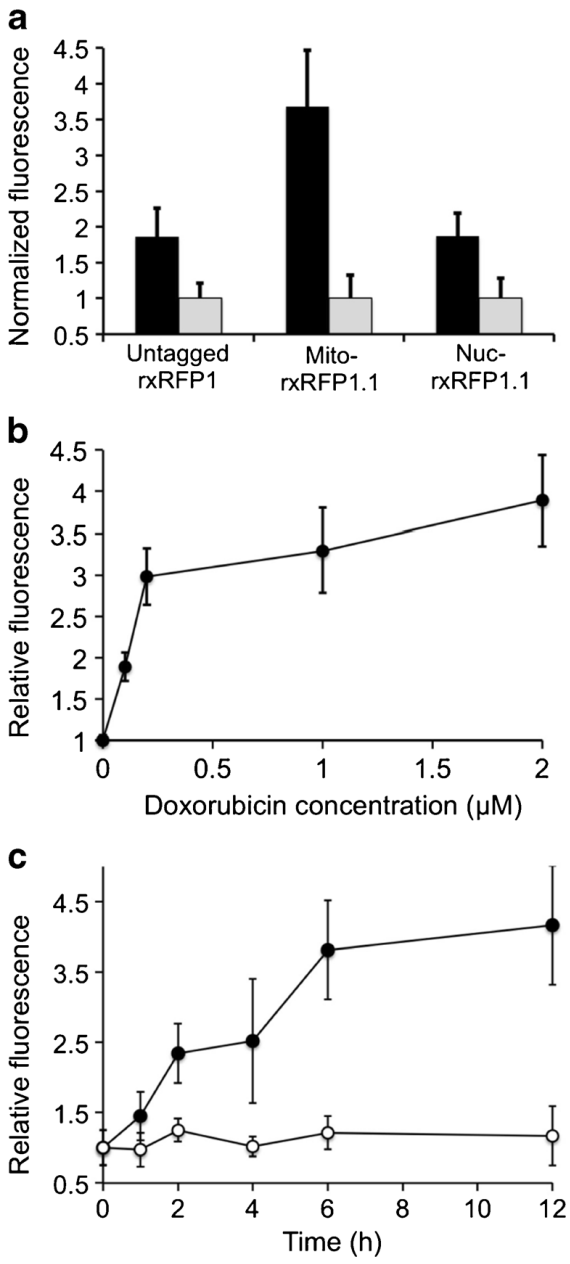

Figure 3.8. (**a**) Comparison of fluorescence intensities of cells expressed untagged rxRFP1, or mitochondrial rxRFP1.1, or nuclear rxRFP1.1, and treated or untreated with doxorubicin (2 μM). Fluorescence intensities were normalized to the values of untreated cells in their corresponding groups. (**b**) Dose-dependent fluorescence increase of HEK 293 T cells expressing mitochondrial rxRFP1.1. Fluorescence intensities were normalized to the values of untreated cells. (**c**) Time dependent fluorescence increase of HEK 293 T cells expressing mitochondrial rxRFP1.1, treated (filled circle), or untreated (open circle) with doxorubicin (2 μM). Fluorescence intensities were normalized to the values of untreated cells at 0 h.

3.4 Conclusion

Redox-sensitive RFPs with various midpoint potentials were developed by different substitutions near the key cysteine residues of rxRFP. These variants were targeted specifically to different cellular compartments, including mitochondria, nucleus and endoplasmic reticulum. Upon treatment of these recombinant probes with exogenous redox changes, we were able to confirm that those rxRFP proteins are robust and versatile fluorescent probes to provide a convenient approach of redox dynamics with subcellular resolution. In addition, Mito-rxRFP1.1 is effectively responsive to the biologically mitochondria-generated reactive oxygen species, induced by anticancer drug, doxorubicin. These rxRFP-derived variants extend our abilities to observe and measure clearly defined redox processes happening in subcellular locations. They are expected to be extremely useful for providing new insights into cellular redox biology.

Reference

1. Diekmann Y, Pereira-Leal JB. Evolution of intracellular compartmentalization. Biochem J. 2013;449(2):319–31.

2. Gius D, Spitz DR. Redox signaling in cancer biology. Antioxid Redox Signal. 2006;8(7/8):1249–52.

3. Stone JR, Yang S. Hydrogen peroxide: a signaling messenger. Antioxid Redox Signal. 2006;8(3/4):243–70.

4. Go YM, Jones DP. Redox compartmentalization in eukaryotic cells. Biochim Biophys Acta. 2008;1780(11):1273–90.

5. Jones DP, Go YM. Redox compartmentalization and cellular stress. Diabetes Obes Metab. 2010;12 Suppl 2:116–25.

6. Hanson GT, Aggeler R, Oglesbee D, Cannon M, Capaldi RA, Tsien RY, et al. Investigating mitochondrial redox potential with redox sensitive green fluorescent protein indicators. J Biol Chem. 2004;279(13):13044–53.

7. Cannon MB, Remington SJ. Re-engineering redox-sensitive green fluorescent protein for improved response rate. Protein Sci. 2006;15(1):45–57.

8. Ostergaard H, Tachibana C, Winther JR. Monitoring disulfide bond formation in the eukaryotic cytosol. J Cell Biol. 2004;166(3):337–45.

9. Meyer AJ, Dick TP. Fluorescent protein-based redox probes. Antioxid Redox Signal. 2010;13(5):621–50.

10. Ren W, Ai HW. Genetically encoded fluorescent redox probes. Sensors. 2013;13(11):15422–33.

11. van Lith M, Tiwari S, Pediani J, Milligan G, Bulleid NJ. Real-time monitoring of redox changes in the mammalian endoplasmic reticulum. J Cell Sci. 2011;124(Pt 14):2349–56.

12. Fan Y, Chen Z, Ai HW. Monitoring redox dynamics in living cells with a redox-sensitive red fluorescent protein. Anal Chem. 2015;87:2802–10.

13. Kolossov VL, Beaudoin JN, Hanafin WP, DiLiberto SJ, Kenis PJ, Gaskins HR. Transient light-induced intracellular oxidation revealed by redox biosensor. Biochem Biophys Res Commun. 2013;439(4):517–21.

14. Thorn CF, Oshiro C, Marsh S, Hernandez-Boussard T, McLeod H, Klein TE, et al. Doxorubicin pathways: pharmacodynamics and adverse effects. Pharmacogenet Genomics. 2011;21(7):440–6.

15. Schneider CA, Rasband WS, Eliceiri KW. NIH Image to ImageJ: 25 years of image analysis. Nat Methods. 2012;9(7):671–5.

16. Appenzeller-Herzog C.Glutathione- and non-glutathione-based oxidant control in the endoplasmic reticulum. J Cell Sci. 2011;124(Pt6):847–55.

17. Chen ZJ, Ai HW. A highly responsive and selective fluorescent probe for imaging physiological hydrogen sulfide. Biochemistry. 2014;53(37):5966–74.

18. Llopis J, McCaffery JM, Miyawaki A, Farquhar MG, Tsien RY. Measurement of cytosolic, mitochondrial, and Golgi pH in single living cells with green fluorescent proteins. Proc Natl Acad Sci U S A. 1998;95(12):6803–8.

19. Ai HW, Olenych SG,Wong P, DavidsonMW, Campbell RE. Hue-shifted monomeric variants of Clavularia cyan fluorescent protein: identification of the molecular determinants of color and applications in fluorescence imaging. BMC Biol. 2008;6:13.

20. Kim JH, Johannes L, Goud B, Antony C, Lingwood CA, Daneman R, et al. Noninvasive measurement of the pH of the endoplasmic reticulum at rest and during calciumrelease. Proc Natl Acad Sci U S A. 1998;95(6):2997–3002.

21. Sarkar DD, Edwards SK, Mauser JA, Suarez AM, Serowoky MA, Hudok NL, et al. Increased redox-sensitive green fluorescent protein reduction potential in the endoplasmic reticulum following glutathione-mediated dimerization. Biochemistry. 2013;52(19): 3332–45.

22. Delic M, Rebnegger C, Wanka F, Puxbaum V, Haberhauer-Troyer C, Hann S, et al. Oxidative protein folding and unfolded protein response elicit differing redox regulation in endoplasmic reticulum and cytosol of yeast. Free Radic Biol Med. 2012;52(9):2000–12.

23. Kolossov VL, Leslie MT, Chatterjee A, Sheehan BM, Kenis PJ, Gaskins HR. Forster resonance energy transfer-based sensor targeting endoplasmic reticulum reveals highly oxidative environment. Exp Biol Med. 2012;237(6):652–62.

24. Lohman JR, Remington SJ. Development of a family of redoxsensitive green fluorescent protein indicators for use in relatively oxidizing subcellular environments. Biochemistry. 2008;47(33): 8678–88.

25. Appenzeller-Herzog C. Updates on "endoplasmic reticulum redox.". Antioxid Redox Signal. 2012;16(8):760–2.

26. Birk J, Meyer M, Aller I, Hansen HG, Odermatt A, Dick TP, et al. Endoplasmic reticulum: reduced and oxidized glutathione revisited. J Cell Sci. 2013;126(Pt 7):1604–17.

27. Miyawaki A. Proteins on the move: insights gained from fluorescent protein technologies. Nat Rev Mol Cell Biol. 2011;12(10):656–68.

28. Chatterjee K, Zhang J, Honbo N, Karliner JS. Doxorubicin cardiomyopathy. Cardiology. 2010;115(2):155–62.

29. Stowe DF, Camara AK. Mitochondrial reactive oxygen species production in excitable cells: modulators of mitochondrial and cell function. Antioxid Redox Signal. 2009;11(6):1373–414.

30. Zhang S, Liu X, Bawa-Khalfe T, Lu LS, Lyu YL, Liu LF, et al. Identification of the molecular basis of doxorubicin-induced cardiotoxicity. Nat Med. 2012;18(11):1639–42.

31. Duggan ST, KeatingGM. Pegylated liposomal doxorubicin: a review of its use in metastatic breast cancer, ovarian cancer, multiple myeloma, and AIDS-related Kaposi's sarcoma. Drugs. 2011;71(18): 2531–58.

Chapter 4: Monitoring thioredoxin redox in live cells with a genetically encoded red fluorescent protein biosensor

4.1 Introduction

Disruption of redox signaling and homeostasis is tightly associated with the toxicity of many toxicants and medications, aging, and a variety of human diseases, such as cancer, diabetes, arteriosclerosis, Alzheimer's disease, and Parkinson's disease.[1-4] Along with glutathione, thioredoxin (Trx) is one of the two major thiol-dependent antioxidants in mammals[5]. The NADPH-dependent reduction of Trx is catalyzed by the flavoenzyme Trx reductase (TrxR), whereas the oxidation of Trx is catalyzed by Trx-dependent peroxiredoxins (Prx) also known as Trx peroxidases (TPx) (**Fig. 4.7**).[5,6] Consequently, the Trx system shuttles electrons from NADPH to TPx, leading to rapid removal of reactive oxygen species (ROS). Trx also plays important roles in modulating protein activities through the modulation of the redox states of cysteine and methionine residues.[5] Trx can reduce oxidized cysteine residues in some important proteins, such as ribonucleotide reductase involved in DNA synthesis and repair,[7] a number of redox-sensitive transcription factors including NF-κB and Ref-1/AP-1,[8,9] apoptosis signal regulating kinase 1 (ASK1),[10] and methionine sulfoxide reductases responsible for reduction of oxidized methionine residues in proteins.[11,12] In addition, the Trx system has

been linked to immune responses,[13] bacterial and viral infection,[14,15] cell proliferation,[16] apoptosis,[17] and pancreatic β-cell functions.[18] Moreover, the abnormality of the Trx system has been observed in cancer.[19] Numerous reports suggest that high Trx levels could contribute to the resistance to chemotherapies,[20,21] while others support that TrxR is crucial for carcinogenesis and invasion.[22,23] The Trx system, especially TrxR, has been considered as a promising target for cancer therapy.[24]

Our current understanding of redox biology remains largely elusive. Redox signaling, which involves diverse reactive oxygen, nitrogen and sulfur species (ROS, RNS and RSS), small-molecule thiols, cysteine- and methionine- containing proteins, and other types of molecules, is incredibly sophisticated.[25] Although thermodynamics drives redox reactions in live cells and organisms, the specificity of the reactions is largely determined by the spatial organization of redox signaling components and the kinetics of competitive reactions.[26] Such complexity is further compounded by the scarcity of research tools that can monitor the redox of specific redox-signaling components in live cells with appropriate spatiotemporal resolution. Previous studies have reported a family of genetically encoded fluorescent protein (FP)-based biosensors that can sense live-cell redox dynamics.[27,28] Reversible disulfide bridges have been introduced to the surfaces of a yellow FP (YFP) and green FPs (GFPs), and recently, to the N- and C- termini of a circularly permuted red FP (cpRFP) to derive redox sensitive rxYFP, roGFPs, and rxRFPs.[29-32] Genetically encoded biosensors (**Fig. 4.7**) are also available for the monitoring of various ROS, RNS and RSS such as hydrogen peroxide (H_2O_2),[33-35] organic hydroperoxides (ROOH),[36] peroxynitrite ($ONOO^-$)[37] and hydrogen sulfide

(H_2S).[38,39] in addition to biosensors for reduced nicotinamide adenine dinucleotide (NADH)[40,41] that is a cofactor involved in redox reactions and methionine sulfoxide[42] that is a post-translational modification derived from the oxidation of methionine residues. Moreover, rxYFP and roGFPs have been genetically linked to glutaredoxin (Grx), resulting in selective biosensors for the redox dynamics of the oxidized and reduced glutathione (GSSG/GSH) pair.[43,44] Despite the progress, there is currently no genetically encoded biosensor for probing the redox changes of the Trx system. Effort has previously been made to fuse rxYFP or roGFPs to Trx, but failed to yield any effective biosensor likely due to the steric hindrance that prevents a proper alignment of thiols in Trx and rxYFP or roGFPs for disulfide exchange reactions.[26,44,45] The current strategy for probing the redox status of Trx is based on the alkylation of Trx thiols in the cell lysis buffer followed by electrophoresis.[46] This low-throughput method only allows end-point measurements and cannot avoid additional Trx oxidation during preparation and lysis of cells. The technical difficulty in direct monitoring of the redox status of Trx in live cells has greatly hindered investigations on the physiological and pathological roles of the Trx redox system and the interplays between Trx and other cell signaling components.

Herein we report the first fluorescent probe that can directly monitor the redox status of the active-site cysteines of Trx in live mammalian cells. Our new probe, namely TrxRFP1, was developed by creating and optimizing a redox relay between human Trx1 and rxRFP1—a redox-sensitive red fluorescent protein previously developed in our laboratory.[31] rxRFP1, which has a circularly permuted topology different from those of rxYFP and roGFPs, permits an effective intramolecular disulfide exchange with the

active-site cysteines of Trx1. The resultant optimized biosensor, TrxRFP1, is fully genetically encoded and can be expressed in live cells without the need of external factors. We have utilized TrxRFP1 to monitor the dynamics of Trx redox induced by various chemicals, such as H_2O_2, auranofin, and arsenic trioxide. We further localized TrxRFP1 to the cell nucleus and mitochondria, validated TrxRFP1 in a variety of mammalian cell lines, and combined TrxRFP1 with a green fluorescent Grx1-roGFP2 biosensor for simultaneous imaging of Trx and glutathione redox dynamics. We were able to observe redox changes under physiologically relevant conditions, including epidermal growth factor (EGF) and serum stimulation. We demonstrated that, under certain conditions, the redox of glutathione and the active-site cysteines of Trx could be individually altered without affecting the other. The results support the notion that the two antioxidant systems residing in the same cellular space are not thermodynamically equilibrated.

4.2 Materials and Methods

4.2.1 Reagents and general methods

The human Trx1 gene fragment and all other synthetic DNA oligonucleotides were purchased from Integrated DNA Technologies (San Diego, CA). The genes for human TrxR1 and TPx1 were purchased from DNASU Plasmid Repository (Tempe, AZ). Restriction endonucleases were purchased from Thermo Scientific Fermentas (Vilnius, Lithuania). Accura high-fidelity DNA polymerase and EconoTaq DNA polymerase were purchased from Lucigen (Middleton, WI). Products of PCR and restriction digestion were purified using gel electrophoresis and Syd Laboratories Gel Extraction columns (Malden,

MA). Plasmid DNA was purified using Syd Laboratories Miniprep columns (Malden, MA). DNA sequences were analyzed by Retrogen (San Diego, CA). All other chemicals were purchased from Sigma-Aldrich (St. Louis, MO), Fisher Scientific (Hampton, NH), and VWR (Radnor, PA), unless otherwise noted. Anti-human Trx1 antibody (Cat # 11538) and rat recombinant TrxR1 (Cat # 14638) were purchased from Cayman Chemical (Ann Arbor, MI). Anti-human/mouse/rat TrxR1 antibody (Cat # MAB7428-SP) was purchased from R&D Systems (Minneapolis, MN). Secondary antibodies and the anti-β-actin antibody (Cat # sc-130656) were purchased from Santa Cruz Biotechnology (Santa Cruz, CA). Human recombinant EGF (Cat # 354052) was purchased from Corning (Painted Post, NY). Glutathione reductase (Cat # G3664) was purchased from Sigma-Aldrich (St. Louis, MO).

4.2.2 Plasmid construction

To build TrxRFP0.1, oligonucleotide Trx-F was paired with 0.1-R1, 0.1-R2, 0.1-R3, or 0.1-R4 (**Table 4.1**) stepwise in four individual polymerase chain reactions (PCR) using a purchased human Trx1 gene as the template in the first reaction and the product of a previous reaction as the template in the subsequent reaction. Oligonucleotides 0.1-F and pBAD-R were used to amplify an rxRFP1 gene fragment from a previously reported pBAD-rxRFP1 plasmid. Next, an overlap PCR reaction was performed to assemble the two fragments using Trx-F and pBAD-R to afford a full-length TrxRFP0.1 gene. TrxRFP0.2, TrxRFP0.3, TrxRFP0.4 were constructed similarly using Trx-F/2-R and 2-F/pBAD-R, Trx-F/3-R and 3-F/TrxRFP3-R, and Trx-F/4-R and 4-F/pBAD-R oligonucleotide pairs, respectively. To introduce the C32S mutation to TrxRFP0.1,

pBAD-F/C32S-R and C32S-F/pBAD-R were used to amplify two fragments from TrxRFP 0.1, and subsequently, an overlap PCR reaction was performed using pBAD-F and pBAD-R. Similarly, the C35S mutant and the C32S/ C35S double mutant of TrxRFP0.1 were made using C35S-F, C35S-R, C32C35S-F and C32C35S-R. To construct TrxRFP0.2, we utilized Trx-F/C62S-R, C69/73S-F/pBAD-R for to amplify two fragments from TrxRFP 0.1, which were next linked together by using an overlap PCR reaction with Trx-F and pBAD-R. To introduce the C217Y mutation to TrxRFP0.9, we utilized a similar overlap PCR strategy based on Trx-F, C217S-R, C217S-F and pBAD-R. Because C397 is close to the N-terminus, C397-R was used to replace pBAD-R to introduce a C397S mutation. To create the $TrxRFP1_{sscc}$ (C32S/C35S/S62C/S69C) mutant, oligonucleotide pairs pBAD-F and 32/35S-R, 32/35S-F and 62/69C-R, and 62/69C-F and pBAD-R were utilized to amplify three individual fragments from TrxRFP1, which were next assembled in an overlap PCR with pBAD-F and pBAD-R. To construct the plasmid for bacterial expression of human TrxR1, a purchased gene was amplified with oligonucleotides TRND-F and TRND-R. Similarly, PRX-F and PRX-R were used to amplify the gene of human TPx1. To construct the plasmids for human Trx1, $Trx1_{CCSS}$, and $Trx1_{SSCC}$, Trx-F and Trx-R were used to amply the gene from TrxRFP0.1, TrxRFP1 and $TrxRFP_{SSCC}$, respectively. To construct the plasmid for bacterial expression of human Grx1, Grx-F and Grx-R were used to amplify the gene from a HEK 293 cDNA library (Biosettia, San Diego, CA). All aforementioned assembled or amplified gene fragments were digested with Xho I and Hind III, and ligated into a pre-treated compatible pBAD/His B plasmid (Life Technologies, Carlsbad, CA, USA). The wild-type human

TrxR1 has a selenocysteine (Sec) residue encoded by a TGA codon upstream to a Sec insertion sequence (SECIS). In our plasmid for expression of TrxR1, the Sec residue has been replaced with Cys to afford a mutant retaining ~ 30% of the activity. We used either this TrxR1 mutant or rat TrxR from Cayman in *in vitro* assays. Oligonucleotides CMV-F1 and CMV-TrxRFP1-R were used to amplify the gene of TrxRFP1 from its corresponding pBAD plasmid. To construct a plasmid for nuclear expression of TrxRFP1, we used CMV-F1, Nuc-R1, Nuc-R2, and Nuc-R3 to amplify the gene of TrxRFP1 and further append three repeats of a nuclear localization sequence (DPKKKRKV). To construct the plasmid for mitochondrial expression of TrxRFP1, oligonucleotides Mito-F and Mito-TrxRFP-R were used amplify a mitochondrial targeting sequence (MLSLRQSIRFFKPATRTLCSSRYLL) from pMito-rxRFP1.1, and Mito-TrxRFP-F and CMV-TrxRFP1-R were used amplify the TrxRFP1 fragment. The products were assembled in an overlap PCR with Mito-F and CMV-TrxRFP1-R. These assembled or amplified gene fragments were next digested with Hind III and Xba I, and ligated into a pre-digested pcDNA3 plasmid (Life Technologies, Carlsbad, CA). To add nuclear exclusion sequence to TrxRFP1 for cytosolic expression, NES-F1 and NES-F2 was paired sequentially with NES-R in a two-step PCR and the resultant gene was digested with BamHI and XbaI, and ligated into a pre-digested pNES-rxRFP[3]. To construct untagged, cytosol-localized and nucleus-localized HyPer-3, a purchased HyPer-3 gene was used as template, HyPer-F and HyPer-R, HyPer-NES-F ad HyPer-NES-R, and HyPer-F, HyPer-Nuc-R1, Nuc-R2, Nuc-R3 were used, respectively. Resultant gene fragments were digested with appropriate restriction enzymes and ligated into pre-

digested pcDNA3. All ligation products were used to transform DH10B *Escherichia coli* cells, which were next plated on LB agar plates supplemented with ampicillin (100 μg/mL). Individual colonies were used to seed liquid culture for preparation of DNA. All constructs were confirmed by DNA sequencing.

4.2.3 Random mutagenesis and library screening

Randomization was limited to the gene fragment encoding the GS-rich linker and rxRFP1. First, rxRFP0.2 was amplified with oligonucleotides Trx-F/0.2-R and 0.2_F/pBAD_R. The fragments were digested with Xho I and BamH I, and BamH I/Hind III, respectively, and ligated into a pre-treated compatible pBAD/His B plasmid. This procedure inserted a new BamH I restriction site downstream to Trx1 without change the protein sequence. Error-prone PCR reactions were next carried out with oligonucleotides 0.2_F and pBAD_R according to a reported procedure[3]. The DNA was digested with BamH I and Hind III and ligated into the pre-digested, aforementioned plasmid. The resultant gene library was introduced into DH10B cells and plated onto LB agar plate supplemented with 100 μg/mL ampicillin and 0.1% (w/v) L-arabinose. Colonies were imaged using a previously described setup. Fluorescence before and after spraying of DTT (50 mM) was quantified and the fluorescence ratios of individual colonies were evaluated using the Fiji image analysis software. Colonies showing large fluorescence changes were selected and cultured in 96-well plates containing 2YT medium supplemented with 100 μg/mL ampicillin and 0.2% (w/v) L-arabinose. Bacterial cells were first shaken at 37°C and 250 rpm for 24 h, and next, at room temperature for another 12 h. Cells were pelleted and lysed using B-PER Bacterial Protein Extraction

Reagents (Pierce, Rockford, IL). Cell debris was removed by centrifugation. Fluorescence emission of clear cell lysates was quantified on a BioTek Synergy Mx Microplate Reader before and after treatments of TrxR1 (10 μM)/NADPH (200 μM). Three clones with largest dynamic ranges were selected and corresponding plasmids were minipreped. Their mixture was used as the template for the next round of random mutagenesis.

4.2.4. Protein expression and purification

All proteins were expressed and purified as previously described. The purities of the prepared proteins were analyzed by SDS-PAGE (sodium dodecyl sulfate polyacrylamide gel electrophoresis, see **Fig. 4.15**). To prepare reduced sensor proteins or the reduced forms of Grx1 and TRP-14, we incubated the proteins with 100 molar equivalent of DTT at room temperature overnight, which were next dialyzed into 1x phosphate buffered saline (PBS) using Thermo Scientific Snakeskin dialysis tubing (7k molecular weight cutoff) in an N_2-filled anaerobic chamber. Purified recombinant TrxR1 and TPx1 proteins were also buffer-exchanged into 1x PBS, aliquoted to 10 μL each at 50 μM, and stored at -80°C for long-term use.

4.2.5 *In vitro* characterization

Protein concentrations were determined using the Bradford assay. The fluorescence of proteins was measured using a BioTek Synergy Mx Microplate Reader with the excitation wavelength at 540 nm and the emission wavelength at 600 nm. Sensor proteins were diluted to desired concentrations with 1x PBS (pH 7.4). Reduction and oxidation kinetics was monitored at room temperature. Unless otherwise stated, oxidized sensor

proteins (1 μM) were reduced with either our prepared recombinant TrxR1 or rat recombinant TrxR and NADPH (200 μM) or GSH; reduced sensor proteins (0.5 μM) were mixed with our purified recombinant TPx1 (0.5 μM) and H_2O_2 at desired concentrations. For reduction and re-oxidation in the same reaction vessel, oxidized TrxRFP1 (1 μM) was first reduced with rat recombinant TrxR1 (50 nM) and NADPH (200 μM), and next, TPx1 and H_2O_2 at the indicated concentrations were added. For absorbance based kinetic assays, different Trx-1 mutants (60 μM), TrxRFP1 (60 μM) or $TrxRFP1_{sscc}$ (60 μM) were treated with either NADPH (200 μM) and rat recombinant TrxR (10nM), or a mixture containing NADPH (200 μM), glutathione reductase (45 nM), Grx1 (5 μM), and GSH (10 mM). The consumption of NADPH was determined by monitoring the absorbance at 340 nm. For determination of K_m and V_{max} values of human Trx-1 and TrxRFP1, Trx-1 or TrxRFP1 concentrations were varied from 1-50 μM. Assays were conducted at room temperature using a reaction mixture volume of 1mL consisting of buffer (100mM phosphate, 2mM EDTA, pH 7.4) and 200 μM NADPH. The assay was started with 10nM rat TrxR and NADPH oxidation was measured spectrophotometrically at 340 nm. K_m and V_{max} values were obtained applying the Michaelis-Menten equation.

4.2.6 Cell culture and live-cell imaging

HEK 293T, SW620, MCF-7, and HeLa cells were cultured in Dulbecco's Modified Eagle's Medium (DMEM) supplemented with 10% (v/v) FBS, and SH-SY5Y cells were cultured in DMEM/F12 (1:1) supplemented with 10% (v/v) FBS. All cells were kept at 37°C in humidified air containing 5% CO_2. Cells were seeded and transfected as

previously described[1], and analyzed 72 h post transfection. Cells were rinsed twice with Dulbecco' s Phosphate Buffered Saline (DPBS), and left in the imaging medium containing DPBS supplemented with 1 mM Ca^{2+}, 1 mM Mg^{2+} and 1% (w/v) BSA. For the serum stimulation experiment, cells were first rinsed three times with DMEM containing no FBS, maintained in DMEM containing no FBS for 6 h at 37°C, and next stimulated by adding 10% (v/v) FBS. All single-color images were taken with a Motic AE31 inverted epi-fluorescence microscope as previously described. A Leica SP5 confocal microscope was used to simultaneously image TrxRFP1 and Grx1-roGFP2. TrxRFP1 was excited with a 543 nm HeNe laser, and the red fluorescence emission was collected between 580-630 nm with a hybrid detector (HyD). Grx1-roGFP2 was excited with a 405 nm UV laser and a 488 nm argon-ion laser sequentially, and the green fluorescence emission was collected between 500-530 nm with a PMT (photomultiplier tube) detector. Time-lapse series was acquired at the indicated interval and fluorescence emissions from all channels were scanned sequentially with the "between frames" mode. All images were analyzed using the Fiji image analysis software[4] and the ratios of the images were processed according to a published procedure.

4.2.7 Cell responses to chemical treatments, cell viability, and proliferation assays

To study the responses of cells expressing fluorescent biosensors to H_2O_2, transfected cells were rinsed twice with DPBS and left in the abovementioned imaging medium. Fluorescence was quantified after 10 min incubation at 37°C. For auranofin, arsenic trioxide, and 2-AAPA, chemicals were added into the fresh culture medium and cells were incubated in the medium for 3 h at 37°C. Cells were collected and cell

suspensions were used for quantification. All samples were prepared and measured in triplicates to derive averages and standard deviations. To determine cell viabilities, cells were treated with chemicals for 24 h at 37°C, and we followed the manufacturer's protocol and used RealTime-Glo™ MT cell viability assays (Promega) to determine cell viability. All fluorescence response and viability data were fitted with a modified Hill equation:

$$y = A + \frac{B * x^n}{x^n + k^n}$$

in which *k* is the EC_{50} or LC_{50} reported in the manuscript, n is the Hill coefficient, A is the initial value, and B is the magnitude of change (positive for growth and negative for decay). To compare the growth of non-transfected cells and TrxRFP1 expressing cells, we seeded HEK 293T cells into 35mm and transfected cells at 70% confluency. Cells were then collected at different time points to determine cell numbers. Briefly, cells were washed, trypsinized and re-suspended by 1 mL PBS and cell suspension were diluted by appropriate factors and mixed with 0.4% trypan blue. Viable cell numbers were counted by using hemacytometer following manufacturer's protocol.

4.2.8 Western blotting

To examine the expression levels of Trx1 and TrxR1, we prepared cell lysates from the same number ($6x10^6$) of HEK 293T, SW620, MCF-7, Hela and SH-SY5Y cells using a CelLytic M cell lysis buffer (Sigma-Aldrich) supplemented with cOmplete™ Protease Inhibitor Cocktail (Roche). The Bradford assay was used to determine total protein concentrations in the cell lysates. 5 μg of total proteins were loaded to each lane and resolved on a 12% SDS-PAGE. Proteins were next transferred to a nitrocellulose

membrane. The membrane was first blocked with 5% skim milk in TBST, and next, incubated with one of the anti-Trx1 (1:5000), anti-TrxR (1:10000) and anti-β-actin (1:10000) antibodies. After washing with TBST, the corresponding horseradish peroxidase (HRP) conjugated secondary antibodies were added. The membrane was visualized with SuperSignal West Pico Chemiluminescent substrate (Thermo Fisher) on a Bio-Rad Gel Doc XR System.

4.2.9 Redox immunoblotting

We modified a reported procedure[7] to performed redox immunoblotting on TrxRFP1 in HEK 293T cells. Untreated, H_2O_2-treated, or auranofin-treated cells ($6x10^6$) were quickly washed twice with ice-cold 1x PBS, pelleted by a brief centrifugation, and lysed with 200 μL urea lysis buffer (1 mM EDTA, 8 M urea, and 50 mM Tris-HCl, pH 8.3) freshly supplemented with 10 mM iodoacetamide. Free thiols in cells were alkylated with iodoacetamide at 37°C for 30 min. Cell debris was next removed by centrifugation and proteins in clear cell lysates were precipitated with ice-cold acetone containing 20 mM HCl. The resultant precipitates were washed twice with ice-cold acetone containing 20 mM HCl and re-suspended in 50 μL urea lysis buffer containing 3.5 mM DTT. After incubation at 37°C for 30 min, 2.5 μL of freshly prepared 600 mM iodoacetic acid was added, followed by another 30-min incubation at 37°C to alkylate additional free thiols resulting from DTT reduction. Total protein concentrations in cell lysate were determined by bicinchoninic acid (BCA) assay and 10 μg of total proteins were loaded to each lane followed by separation with 12% urea-PAGE. Before we loaded our protein samples, we first prerun the urea-PAGE for at least 30 min to heat the gel up and remove remaining

urea. After samples were applied we run the gel at constant 100 v with temperature constant at 50°C during the run. Next proteins were transferred to a nitrocellulose membrane at 80 v for 90 min. The membranes were first blocked with 5% skim milk in TBST, followed by incubation with anti-Trx (1:5000) antibodies for overnight. After 5 times washing with TBST, HRP-conjugated anti-goat secondary antibody was added. SuperSignal West Pico Chemiluminescent substrate was used to visualize the membrane on a Bio-Rad Gel Doc XR System.

4.3 Results and Discussion

4.3.1 Engineering of fluorescent biosensors for the redox status of the active-site cysteines of Trx

We recently introduced cysteine residues to the N- and C- termini of a cpRFP and subsequently optimized surrounding residues to derive a red fluorescent biosensor, rxRFP1, showing ~ 4-fold fluorescence increase from a fully reduced state to a fully oxidized state[31]. Compared to rxYFP and roGFPs, rxRFP1 has more red-shifted emission that is attractive for biological imaging. Thus, we sought to develop additional biosensors by fusing rxRFP1 with other redox-sensory proteins. We genetically linked rxRFP1 to Trx1, the human Trx found in cytoplasmic and nuclear compartments. We reasoned that, with an appropriate topological rearrangement, the redox of the active-site cysteine residues (C32 and C35) of Trx1 might be coupled with the redox of the cysteine pair at the termini of rxRFP1 (**Figure 1a,b**). Because Trx1 and rxRFP1 are forced into proximity in the fusion construct, such redox coupling may be kinetically favored.

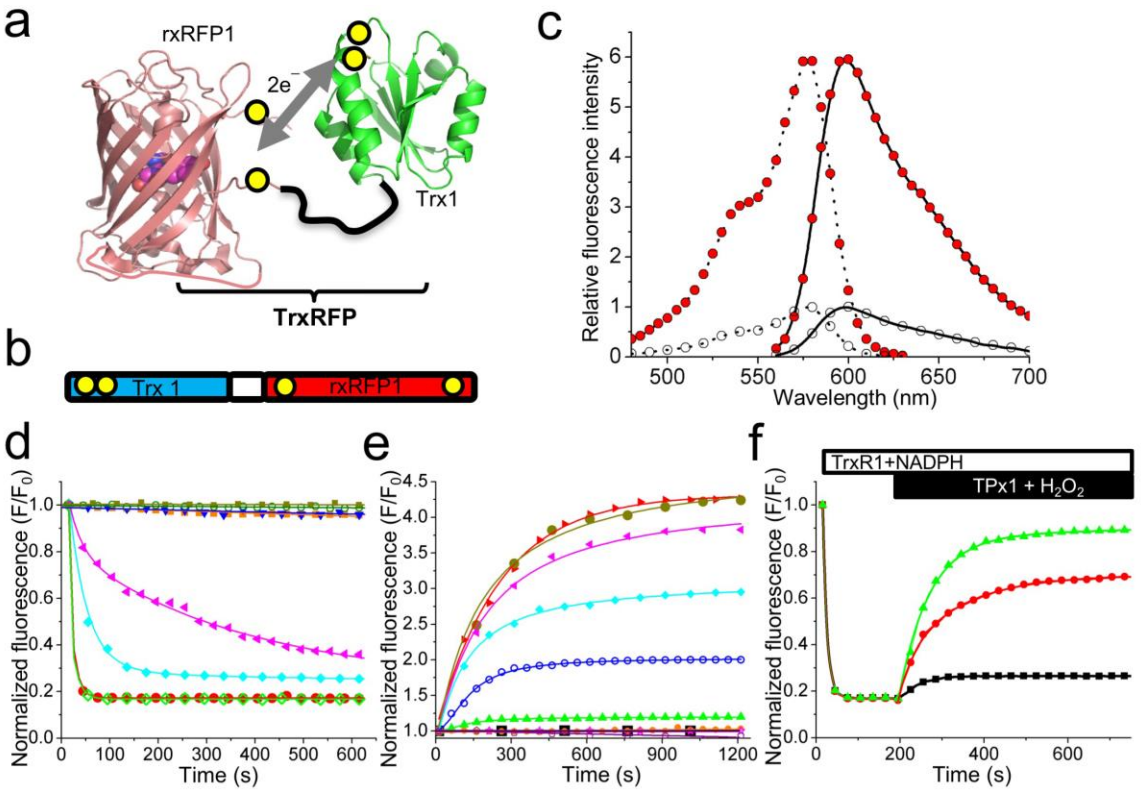

Figure 4.1. Design and fluorescence characterization of TrxRFP biosensors. (**a**) Schematic representation of the mechanism for TrxRFP sensors. By positioning rxRFP1 and Trx1 in proximity, the redox of rxRFP1 and Trx1 may be kinetically coupled so that the fluorescence of rxRFP1 becomes an indicator for the redox status of Trx1. The yellow circles indicate cysteine residues involved in the redox coupling. (**b**) Primary structural arrangement of TrxRFP1. (**c**) Excitation (dotted line) and emission (solid line) spectra of reduced (black open circle) and oxidized (red filled circle) TrxRFP1. Spectra were normalized to the maximal fluorescence of the reduced form. (**d**) Kinetic traces for the reduction of oxidized proteins (from top to bottom: ■ TrxRFP1 + 10 mM L-ascorbic acid, ○ TrxRFP1 + 10 mM L-cysteine, ▼ rxRFP1 + 10 µM TrxR1 + NADPH, ■ TrxRFP1 + 1 mM GSH, ◀ TrxRFP1 + 2 µM TrxR1 + NADPH, ◆ TrxRFP1 + 5 µM TrxR1 + NADPH, ● TrxRFP1 + 10 µM TrxR1 + NADPH, and ◇ TrxRFP1 + 10 µM TrxR1 + NADPH + 100 µM GSSG). (**e**) Kinetic traces for oxidation of reduced proteins (from top to bottom: ▶ TrxRFP1 + TPx1 + 100 µM H_2O_2, ● TrxRFP1 + TPx1 + 100 µM H_2O_2 + 10 mM GSH, ◀ TrxRFP1 + TPx1 + 10 µM H_2O_2, ◆ TrxRFP1 + TPx1 + 1 µM H_2O_2, ○ TrxRFP1 + TPx1 + 100 nM H_2O_2, ▲ TrxRFP1 + TPx1 + 10 nM H_2O_2, ● TrxRFP1 + 100 µM H_2O_2 only, ■ TrxRFP1 + TPx only, ★ TrxRFP1 + 100 µM GSSG, and ⬟ rxRFP1 + TPx1 + 100 µM H_2O_2). (**f**) Kinetic traces for TrxRFP1 reduced with 10 µM TrxR1 / 200 µM NADPH and reversibly oxidized by addition of TPx1/H_2O_2 (■ 0.5 µM TPx1 + 10 µM H_2O_2, ● 0.5 µM TPx1 + 200 µM H_2O_2, and ▲ 2 µM TPx1 + 200 µM H_2O_2).

Therefore, the fluorescence of rxRFP1 would become an indicator for the redox status of Trx1. We next constructed four chimeric proteins varying in the lengths of their linkers and the relative order of Trx1 and rxRFP1 (Constructs 1-4 in **Fig. 4.8**). One of the four variants, which has a 30-amino-acid Gly-Ser-rich linker between the C-terminus of Trx1 and the N-terminus of rxRFP1, showed a 4-fold fluorescence change in response to the reduction from a fully oxidized state in the presence of recombinant human TrxR1 and NADPH (**Fig. 4.9**). We named this mutant TrxRFP0.1 (**Fig. 4.10**) and characterized it further. Oxidized TrxRFP0.1 was unresponsive to various tested reducing reagents such as L-ascorbic acid and L-cysteine at millimolar concentrations, and reduced glutathione only caused a small, less than 10% fluorescence decrease (**Fig. 4.11a**). In addition, reduced TrxRFP0.1 could be effectively oxidized by H_2O_2 in the presence of recombinant human TPx1, leading to a prompt fluorescence increase (**Fig. 4.11b**). Such response required the TPx1 enzyme and was dependent on the concentrations of H_2O_2 (**Fig. 4.11b**). In comparison, rxRFP1 alone in either an oxidized or a reduced state was unresponsive to TrxR1/NADPH and TPx1/H_2O_2 (**Fig. 4.11a,b**), further confirming that the observed fluorescence changes of TrxRFP0.1 were particularly caused by the redox dynamics of Trx1. Furthermore, we mutated each of the two or both active-site cysteine residues of Trx1 to serine and replaced Trx1 in TrxRFP0.1 with one of the three mutants. None of them responded to TrxR1/NADPH or TPx1/H_2O_2 (**Fig. 4.11c,d**), supporting that both active-site cysteine residues of Trx1 are directly involved in the redox coupling between Trx1 and rxRFP1.

Trx1 has a total of five cysteine residues. Its three non-active-site cysteine residues (C62, C69, and C73) have been previously reported for regulatory roles,[47] and an additional disulfide bond may be formed between C62 and C69 to crosstalk with the glutaredoxin/glutathione system.[48] To eliminate possible interferences caused by these non-active-site cysteines, we mutated all three to serine to derive TrxRFP0.2 (**Fig. 4.8**). Next, we randomized the gene fragment encoding rxRFP1 and screened for TrxRFP mutants showing increased dynamic ranges. After three rounds of directed evolution, we arrived at TrxRFP0.9 with three additional mutations (G142S/D228G/V399Q) and a 5.7-fold fluorescence increase from the fully reduced state to the fully oxidized state (**Fig. 4.9,4.10**). Compared to TrxRFP0.1, oxidized and reduced TrxRFP0.9 were more reactive toward TrxR1/NADPH and TPx1/H_2O_2, respectively (**Fig. 4.11e,f**). In particular, reduced TrxRFP0.9 showed a notable response to as low as 10 nM H_2O_2 in our TPx1 oxidation assay, and remained unreactive to 100 μM H_2O_2 alone.

Besides the two cysteine residues forming the reversible disulfide bond in rxRFP1, rxRFP1 has two additional cysteine residues. We next created a mutant of TrxRFP0.9 with all nonessential cysteines removed (C217Y/C397S). The C217Y mutation was chosen because mApple,[49] the parental protein of rxRFP1, has a tyrosine residue at this site, whereas the C397S mutation has previously been shown to have little impact on the spectral and redox properties of rxRFP1.[32] This final mutant was named TrxRFP1 (**Fig. 4.10**) and subjected to thorough characterization.

4.3.2 Characterization of TrxRFP1 *in vitro* and in HEK 293 cells

Our freshly purified TrxRFP1, which was fully oxidized by molecular oxygen (O_2) in air during the preparation, showed an excitation peak at 576 nm and an emission peak at 600 nm (**Fig. 4.1c**), identical to the peaks of rxRFP1.[31] In the presence of dithiothreitol (DTT) or TrxR1/NADPH, TrxRFP1 was reduced quickly to show a nearly 6-fold fluorescence decrease (**Fig. 4.1d** and **Fig. 4.9**). In comparison, rxRFP1 could be reduced by DTT, but not by TrxR1/NADPH. The speed and extent of the reduction were dependent of the concentrations of TrxR1 (**Fig. 4.1d**). TrxRFP1 inherited excellent specificity from TrxRFP0.1, as millimolar L-cysteine and L-ascorbic acid did not decrease the fluorescence of oxidized TrxRFP1. Interestingly, through this evolution process, the sensitivity of TrxRFP1 to glutathione was further reduced. Millimolar reduced glutathione alone triggered almost no fluorescence response, and in the presence of 100 μM oxidized glutathione, which is considered an upper concentration limit for typical mammalian cells,[50] the reduction of TrxRFP1 by TrxR1/NADPH was not impacted (**Fig. 4.1d**). The fully reduced TrxRFP1, freshly prepared by DTT reduction and dialysis in a nitrogen (N_2)-filled anaerobic chamber, responded to TPx1-catalyzed oxidation by H_2O_2 (**Fig. 4.1e**). The response was dependent of the concentrations of H_2O_2. In parallel, reduced TrxRFP1 was unreactive to 100 μM H_2O_2 or oxidized glutathione. In the presence of 10 mM reduced glutathione, oxidation of reduced TrxRFP1 by TPx1/H_2O_2 was also not affected (**Fig. 4.1e**). We further investigated the response of TrxRFP1 to reducing and oxidizing enzymes in the same reaction vessel. As expected, TrxRFP1 reduced by TrxR1/NADPH could be re-oxidized by addition of

TPx1/H_2O_2 (**Fig. 4.1f**). The final fluorescence of TrxRFP1 was determined by the interplay between the reduction and oxidation reactions. With the same amount of TrxR1/NADPH, the degree of re-oxidation was dependent of the concentrations of H_2O_2 and TPx1 (**Fig. 4.1f**).

We also tested the responses of TrxRFP1 to Trx-like, redox-sensitive proteins such as glutaredoxin 1 (Grx1) and thioredoxin (Trx)-related protein TRP14. Neither oxidation nor reduction took place (**Fig. 4.12)**, suggesting that the redox states of these proteins are kinetically separated and TrxRFP1 is a specific biosensor. In 2012, Holmgren and co-workers reported the reduction of oxidized Trx1 by glutathione enzymatically coupled with Grx1, glutathione reductase, and NADPH,[51] so we further examined our oxidized TrxRFP1 under this condition. In both of our *in vitro* fluorescence and NADPH absorbance assays, no reaction was detectable for TrxRFP1 (**Fig. 4.13**). We also created a TrxRFP1 mutant (C32S/C35S/S62C/S69C) in which only a non-active-site disulfide bond can form. This new mutant was reduced under this condition as observed from the NADPH absorbance change at 340 nm (**Fig. 4.13**), suggesting that the glutaredoxin/glutathione system is involved in the reduction of the non-active-site disulfide bond, but not the active-site disulfide bond, of Trx1. This finding corroborates another report by Holmgren *et al*. in 2013.[48]

To examine the performance of TrxRFP1 in live cells, we transiently expressed it in human embryonic kidney (HEK) 293T cells. Live mammalian cells express TPx to transform ROS and, at the same time, oxidize Trx (**Fig. 4.7**). Not surprisingly, addition of a single bolus of 16.7 μM H_2O_2 to the imaging medium caused an immediate and

dramatic fluorescence increase for TrxRFP1-expressing cells (**Fig. 4.2a**, **Fig. 4.14**), suggesting the change of Trx to a more oxidized state. The TrxRFP1 sensor remained oxidized during our imaging period until the addition of 10 mM DTT 9 min later. We also imaged H_2O_2-treated TrxRFP1-expressing cells for a longer period or with less H_2O_2 and found that the oxidation of TrxRFP1 could be spontaneously reverted (**Fig. 4.13**), suggesting the presence of an efficient intracellular system to maintain the redox homeostasis of Trx. Furthermore, we treated TrxRFP1-expressing cells with 10 μM auranofin, a previously reported gold(I)-containing TrxR reductase inhibitor.[52] Like H_2O_2, auranofin also shifted Trx to a more oxidized state indicated by gradual fluorescence increase over the monitored period (**Fig. 4.2b**, **Fig. 4.14**). In comparison, we did not observe substantial fluorescence increase for H_2O_2- or auranofin- treated control cells expressing either rxRFP1 or a genetically encoded pH indicator pHRFP[31] (**Fig. 4.2c,d** and **Fig. 4.16**). All data collectively support that perturbation of either TPx or TrxR may change the redox status of Trx in live cells and TrxRFP1 is effective in detecting the redox dynamics of Trx.

To further explore the sensitivity of TrxRFP1 in live cells, we characterized the responses of TrxRFP1 to various concentrations of H_2O_2 and auranofin (**Fig. 4.2e,f)**. The EC_{50}'s (the concentration to give a half-maximal response) for 10-min H_2O_2 treatment and 3-h auranofin treatment were 13.5±0.7 μM (fit-value ± s.e. of fit) and 3.2±1.1 μM, respectively. In the tested concentration ranges, H_2O_2 and auranofin did not cause appreciable fluorescence increase for rxRFP1-expressing HEK 293T cells. We further performed redox urea-polyacrylamide gel electrophoresis (PAGE) immunoblotting

analysis of TrxRFP1 in HEK 293T cells treated with different concentrations of H_2O_2 or auranofin. We adopted a previously established method[48] to first treat cells with neutral alkylating agent iodoacetamide and subsequently treat reduced cell lysates with acidic alkylating agent iodoacetic acid. We were able to separate the TrxRFP1 protein based on its redox states. As the concentration of H_2O_2 or auranofin increases, the oxidation of TrxRFP1 increases (**Fig. 4.2g,h)**, corroborating our measurements based on the fluorescence of TrxRFP1. These results further confirm that TrxRFP1 is a selective indicator for Trx redox and the engineered redox relay in TrxRFP1 is necessary for sensing Trx redox changes.

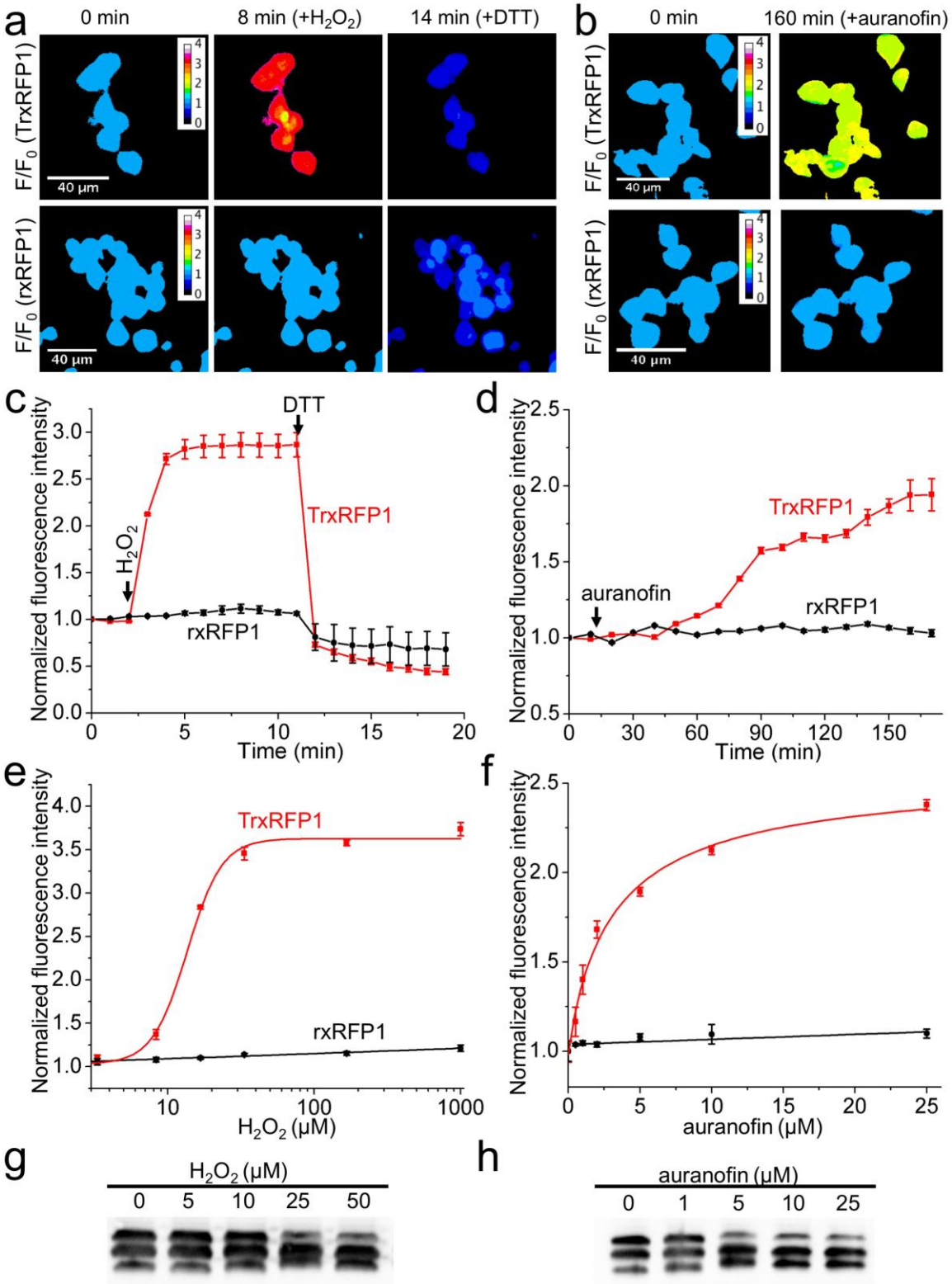
a
0 min
8 min (+H2O2)
14 min (+DTT)
F/F0 (TrxRFP1)
F/F0 (rxRFP1)
40 μm
b
0 min
160 min (+auranofin)
c
DTT
H2O2
TrxRFP1
rxRFP1
Normalized fluorescence intensity
Time (min)
d
TrxRFP1
auranofin
rxRFP1
Time (min)
e
TrxRFP1
rxRFP1
H2O2 (μM)
f
auranofin (μM)
g
H2O2 (μM)
0 5 10 25 50
h
auranofin (μM)
0 1 5 10 25

Figure 4.2. Characterization of TrxRFP1 in HEK 293T cells. (**a,b**) Time-lapse pseudocolored fluorescence images (F/F_0) of HEK 293T cells expressing either TrxRFP1 or rxRFP1 sequentially treated with 16.7 μM H_2O_2 and 10 mM DTT (**a**) or treated with 10 μM auranofin (**b**), showing H_2O_2- and auranofin- induced fluorescence changes of TrxRFP1 but not rxRFP1. H_2O_2 and auranofin were added at t = 2 min and t = 12 min, respectively. (**c,d**) Fluorescence intensity traces for TrxRFP1 or rxRFP1 in HEK 293T. The intensities were normalized to the value at t = 0 min and shown as the mean and s.d. of randomly selected eight cells. The red and black lines are for TrxRFP1 and rxRFP1, respectively. The arrows indicate the time points for addition of 16.7 μM H_2O_2, 10 mM DTT, or 10 μM auranofin. (**e,f**) Fluorescence responses of TrxRFP1 (red) or rxRFP1 (black) in HEK 293T to various concentrations of H_2O_2 (**e**) or auranofin (**f**), suggesting that TrxRFP1 can selectively sense the redox changes of Trx in live cells. Data are shown as mean and s.d. of three independent experiments. (**g,h**) Redox urea-PAGE/immunoblotting analysis of TrxRFP1 in HEK 293T cells treated with H_2O_2 (**g**) or auranofin (**h**) at the indicated concentrations, showing the increase of protein oxidation in response to the increase of the H_2O_2 or auranofin concentration. The three bands from top to bottom are interpreted as the TrxRFP1 protein containing no, one, and two disulfide bonds, respectively.

It is a general concern that the use of redox sensors in live cells may inevitably perturb their intrinsic physiology. In our case, expression of TrxRFP1 may result in the additional Trx1 domain and rxRFP1 which also contains cysteines. Fortunately, Trx1 is a highly abundant protein in mammalian cells,[53] whereas cysteines in rxRFP1 are not very reactive because rxRFP1 alone does not respond to micromolar and even low millimolar H_2O_2 *in vitro* and in live cells (**Fig. 4.1e, 4.2e**). We assessed the effect of TrxRFP1 expression on the responses of HEK 293T to H_2O_2 and auranofin, which both are known modulators of the thioredoxin redox system, in terms of cell viabilities. We utilized a commercialized bioluminescence assay to evaluate the viabilities of HEK 293T cells after 24 h incubation with difference concentrations of H_2O_2 or auranofin. To our delight, we did not observe any substantial difference for the viabilities of H_2O_2- or auranofin-treated HEK 293T cells with or without TrxRFP1 overexpression (**Fig. 4. 11a,b**), suggesting that expression of TrxRFP1 does not affect cellular redox homeostasis. We repeated the experiment in several other mammalian cell lines (*e.g.* HeLa, MCF-7, and SW620), and still, no substantial difference in cell viabilities was observed (**Fig. 4.17c-h**).

4.3.3 Localization of TrxRFP1 to subcellular compartments

Besides the cytosol, the Trx redox system exists in the cell nucleus and mitochondria of human cells, we therefore next subcellularly localized TrxRFP1 to monitor compartmentalized Trx redox dynamics. We appended a nuclear localization sequence (NLS) or a mitochondrial targeting sequence (MTS) to TrxRFP1. This led to the proper nuclear localization of TrxRFP1 in either the cell nucleus or mitochondria in mammalian cells, as confirmed by the co-localization of TrxRFP1 with a nuclear and chromosome

stain DAPI (**Fig. 4.3a**) or a mitochondrial stain MitoTracker Green (**Fig. 4.3b**). Treating the cells expressing nuclear or mitochondrial TrxRFP1 with either H_2O_2 or auranofin resulted in robust fluorescence increases (**Fig. 4.18**). However, both nuclear and mitochondrial TrxRFP1 are less sensitive to exogenously added H_2O_2 and auranofin than unlocalized TrxRFP1, as higher concentrations are needed to trigger the fluorescence responses (**Fig. 4.3c,d**). In particular, the EC_{50}'s for 10-min H_2O_2 treatment were 62.6±3.6 μM (fit-value ± s.e. of fit) and 69.6±9.7 μM for nuclear and mitochondrial TrxRFP1, respectively. The EC_{50}'s for 3-h auranofin treatment were 7.9±0.8 and 17.1±1.2 μM for nuclear and mitochondrial TrxRFP1, respectively. These observations are reasonable, since exogenous H_2O_2 and auranofin have to cross additional cellular space and membranes to reach nuclear or mitochondrial Trx redox system and the effective concentrations of H_2O_2 and auranofin in the nucleus or mitochondria could be significantly reduced. Moreover, the Trx redox system in mammalian mitochondria is based on Trx2 and TrxR2,[54] which is homologous to, but distinct from the cytosolic and nuclear Trx redox system based on Trx1 and TrxR1. Therefore, although our Trx1-based TrxRFP1 biosensor displayed cross-reactivity,[55] it may not have the optimal kinetics to sense the redox dynamics of the mitochondrial Trx system.

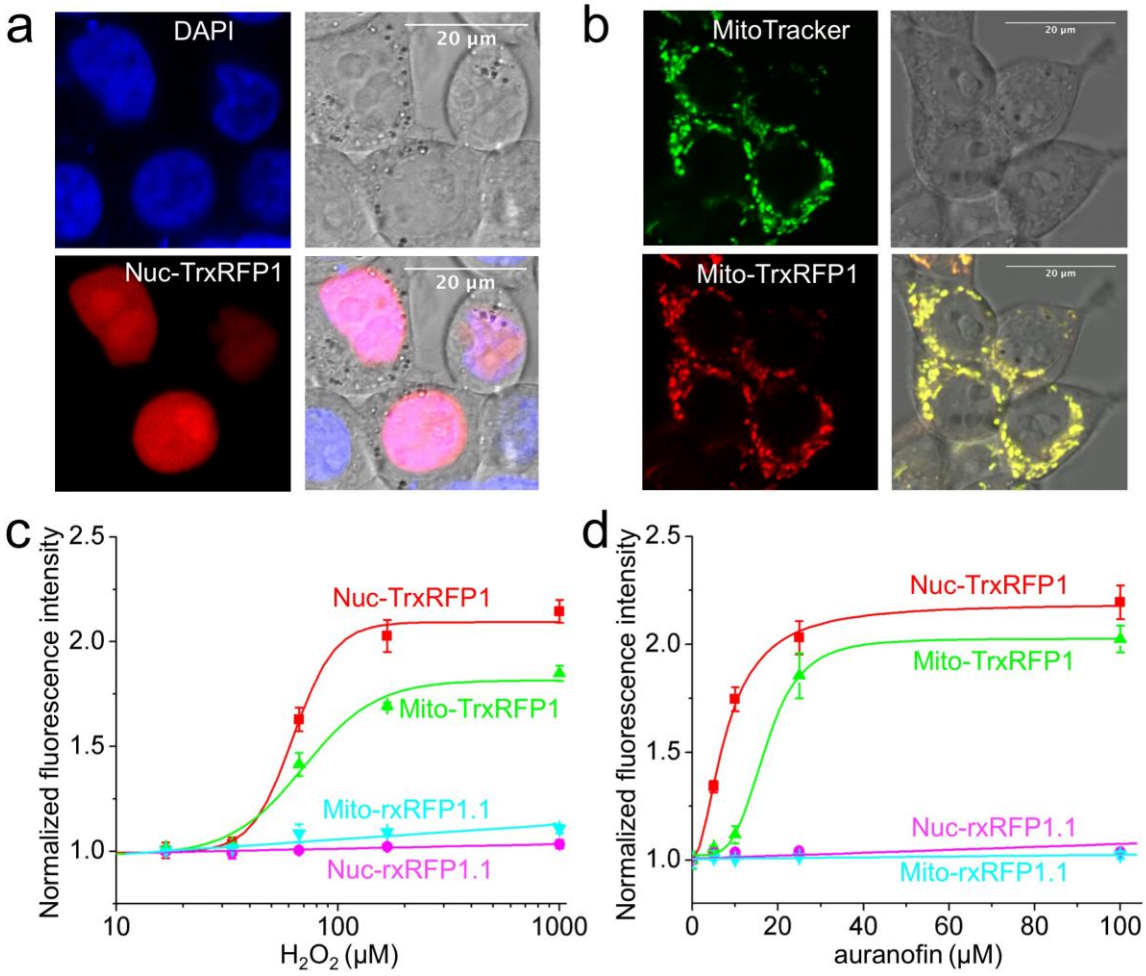

Figure 4.3. Subcellularly localized TrxRFP1. (**a,b**) Co-localization of nuclear (**a**) and mitochondrial (**b**) TrxRFP1 with a nuclear stain DAPI and a mitochondrial stain MitoTracker Green, respectively. (**c,d)** Fluorescence responses of nuclear (red) and mitochondrial (green) TrxRFP1 in HEK 293T to various concentrations of H_2O_2 (**c**) or auranofin (**d),** suggesting that TrxRFP1 can selectively sense the subcellular redox changes of Trx in live cells. Fluorescence responses of nuclear (cyan) and mitochondrial (magenta) rxRFP1.1 are also shown as control groups. Data are represented as mean and s.d. of three independent experiments.

4.3.4 Monitoring of induced Trx redox dynamics in various mammalian cells

To demonstrate the general applicability of TrxRFP1 for monitoring mammalian Trx redox changes, we expressed TrxRFP1 in several additional mammalian cell lines, including cervical cancer HeLa cells, breast cancer MCF-7 cells, colon carcinoma SW620 cells, and neuroblastoma SH-SY5Y cells. Fluorescence responses to H_2O_2- and auranofin- induced Trx oxidation were observed in all cell lines (**Fig. 4.4**, **Fig. 4.19**). We further compared the responses of TrxRFP1 in different cell lines to various concentrations of auranofin after a 3-h incubation period. Each showed different sensitivity to auranofin with an EC_{50} of 1.7±0.5 μM (fit-value ± s.e. of fit) for HeLa, 7.9±5.7 μM for MCF-7, 28.1±9.8 μM for SW620, and 2.5±0.5 μM for SH-SY5Y (**Fig. 4.4a-d**). Moreover, the magnitudes of their fluorescence responses were also different with approximately 2.95-fold, 3.83-fold, 2.73-fold, 1.94-fold maximal changes for HeLa, MCF-7, SW620, and SH-SY5Y, respectively. To understand the biological meanings of the differences across various cell lines, we further determined the viability responses of various cell lines to auranofin after 24-h incubation. The LC_{50}'s (the concentration to kill half cells) were determined to be ~ 6.5, 4.5, 11.7, 88.4, 5.3 μM for HEK 293T, HeLa, MCF-7, SW620, and SH-SY5Y, respectively (**Fig. 4.4e**). These LC_{50} values roughly correlate with the EC_{50} values derived from the fluorescence measurements of TrxRFP1 (**Fig. 4.4f**), suggesting that TrxR is indeed a cellular target of auranofin to cause cell growth inhibition and death. The differences in EC_{50} and LC_{50} values across various cell lines were likely due to differences in bioavailability and drug permeability.[56] On the other hand, it is difficult to rationalize the differences in the magnitudes of auranofin-

induced fluorescence changes across various cell lines. We probed the expression levels of Trx1 and TrxR1 in various cell types (**Fig. 4.4g**), and did not observe much difference for the expression of Trx1 but observed dramatic differences for TrxR1 across various cell lines. SH-SY5Y, which has a very low level of TrxR1, indeed showed a relatively small fluorescence change in response to high concentrations of auranofin, suggesting that Trx1 in untreated SH-SY5Y is likely more oxidized compared to Trx1 in other tested cell lines. However, when all tested cell lines are considered together, the correlation between the maximal fluorescence changes and the TrxR1 levels is weak (**Fig. 4.4f**). We reason that the redox of Trx1 is determined by the interplay between oxidation and reduction reactions of Trx1, and the TrxR1 expression level is not the only factor. Moreover, we found that intracellular TrxRFP1 was not fully oxidized by high concentrations of auranofin, because addition of H_2O_2 could drive TrxRFP1 to even higher fluorescence levels (**Fig 4.2e,f**). This suggests that cells have complicated systems regulating Trx redox in response to auranofin treatment, and such systems may be different in various types of cells. This may also contribute to the observed differences in TrxRFP1 fluorescence responses across various cell lines.

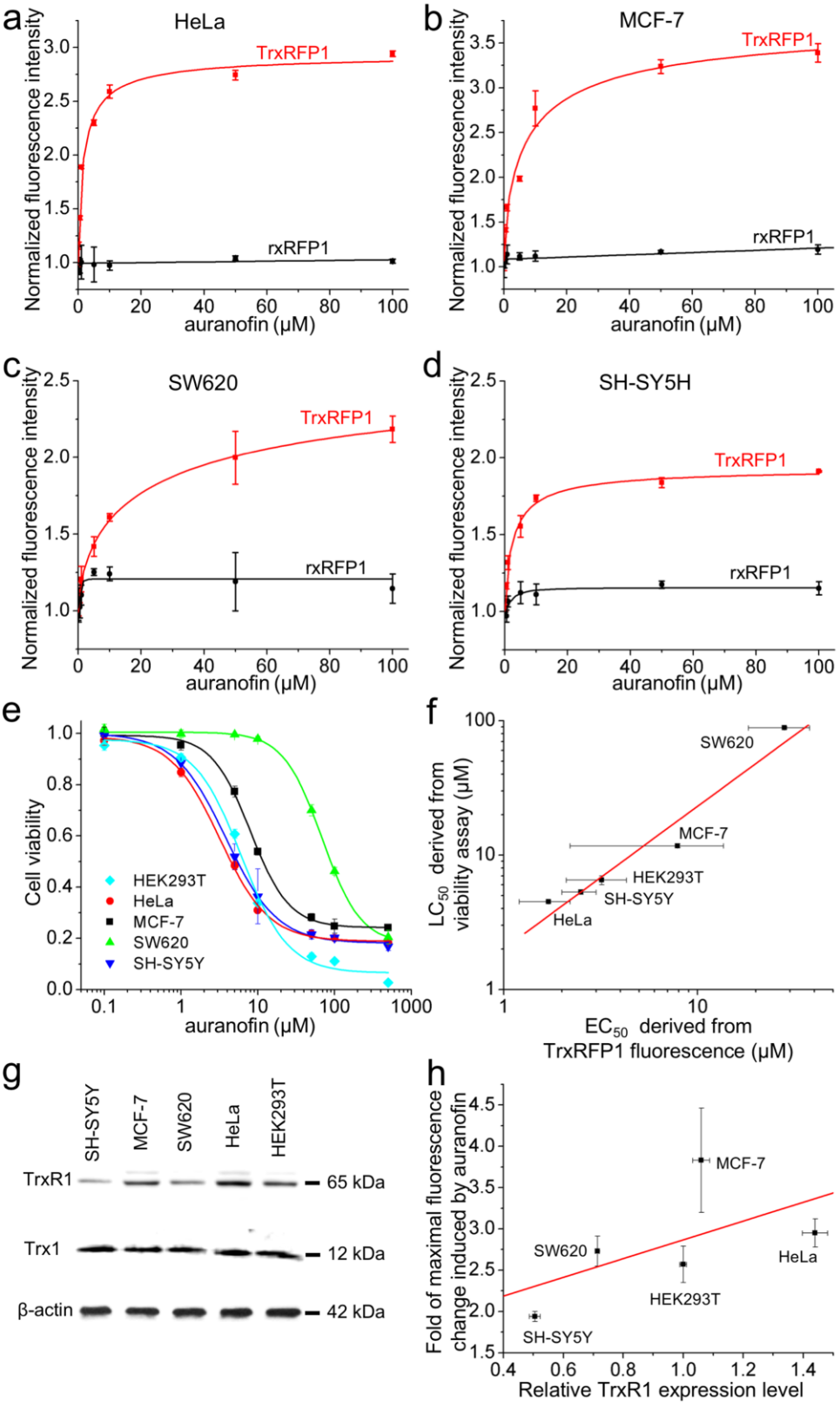
a
HeLa
TrxRFP1
rxRFP1
Normalized fluorescence intensity
auranofin (μM)
b
MCF-7
TrxRFP1
rxRFP1
Normalized fluorescence intensity
auranofin (μM)
c
SW620
TrxRFP1
rxRFP1
Normalized fluorescence intensity
auranofin (μM)
d
SH-SY5H
TrxRFP1
rxRFP1
Normalized fluorescence intensity
auranofin (μM)
e
Cell viability
HEK293T
HeLa
MCF-7
SW620
SH-SY5Y
auranofin (μM)
f
SW620
MCF-7
HEK293T
SH-SY5Y
HeLa
LC50 derived from viability assay (μM)
EC50 derived from TrxRFP1 fluorescence (μM)
g
SH-SY5Y
MCF-7
SW620
HeLa
HEK293T
TrxR1
65 kDa
Trx1
12 kDa
β-actin
42 kDa
h
MCF-7
SW620
HeLa
HEK293T
SH-SY5Y
Fold of maximal fluorescence change induced by auranofin
Relative TrxR1 expression level

Figure 4.4. Use of TrxRFP1 to monitor Trx redox dynamics in various mammalian cell lines. (**a-d**) Fluorescence responses of TrxRFP1 (red) or rxRFP1 (black) in the indicated cell lines to various concentrations of auranofin, confirming that TrxRFP1 is an effective probe for Trx redox changes under diverse conditions. (**e**) The viabilities of indicated cell lines in response to 24-h auranofin treatment. (**f**) The correlation between EC_{50} values derived from TrxRFP1 fluorescence measurements and LC_{50} values derived from viability assays of various cell lines (R^2 = 0.95). (**g**) Western blots of endogenous TrxR1, Trx1 and β-actin in various cell lines. (**h**) A plot for relative TrxR1 expression levels and the fold of fluorescence changes induced by auranofin across various cell lines (R^2 = 0.35). Data in panels **a-e** are shown as mean and s.d. of three independent experiments. Error bars in panels **f-g** are s.e.m. from curve fitting or s.d. from quantification of Western blot bands of three independent replicates.

4.3.5 Simultaneous monitoring of Trx and glutathione redox using TrxRFP1 and Grx1-roGFP2

TrxRFP1 is a red fluorescent biosensor spectrally orthogonal to common green fluorescent biosensors. A green-fluorescent excitation-ratiometric Grx1-roGFP2 biosensor was previously reported for monitoring of glutathione redox dynamics in mammalian cells.[44] Since glutathione and Trx are the two major thiol-dependent antioxidants in mammals, we next examined the use of TrxRFP1 and Grx1-roGFP2 to simultaneously monitor the two redox systems. We expressed both probes in HEK 293T cells, and treated the cells with H_2O_2. Because H_2O_2 is coupled to the redox of both glutathione and Trx (**Fig. 4.7**), we observed concurrent fluorescence changes for both biosensors in HEK 293T cells (**Fig. 4.5a,c**). We next treated cells co-expressing the two biosensors with auranofin, a small molecule preferably targeting TrxR. A prominent fluorescent change was observed for TrxRFP1, but not for Grx1-roGFP2 (**Fig. 4.5b,d**). We further examined the responses of the cells co-expressing the two biosensors to various concentrations of auranofin, arsenic trioxide, and 2-AAPA (**Fig. 4.5e-g**). No change of Grx1-roGFP2 fluorescence was observed for a wide range of auranofin concentrations (**Fig. 4.5e**), further supporting that auranofin is a selective inhibitor of TrxR over the glutathione redox system. Arsenic trioxide also preferably triggered the response of TrxRFP1, but at high concentrations (> 10 μg/ml), the fluorescence of Grx1-roGFP2, represented as fluorescence excitation ratios (F_{405nm}/F_{485nm}), also started to change (**Fig. 4.5f**). This result corroborates the previous finding that TrxR is a target for arsenic trioxide,[57] but the selectivity of arsenic trioxide is worse than that of auranofin. 2-

AAPA is a glutathione reductase inhibitor.[58] At low nanomolar concentrations, it induced the oxidation of Grx1-roGFP2, but not TrxRFP1 (**Fig. 4.5g**). When its concentration increased above 100 nM, the fluorescence of TrxRFP1 started to rise, indicating the oxidation of both Trx and glutathione induced by high concentrations of 2-AAPA. All these results collectively suggest that TrxRFP1 and Grx1-roGFP2 can be utilized simultaneously to monitor the redox dynamics of Trx and glutathione in mammalian cells, that the Trx and glutathione redox systems can be individually perturbed, and that a thermodynamic equilibrium for Trx1 and glutathione is not reached in live mammalian cells.

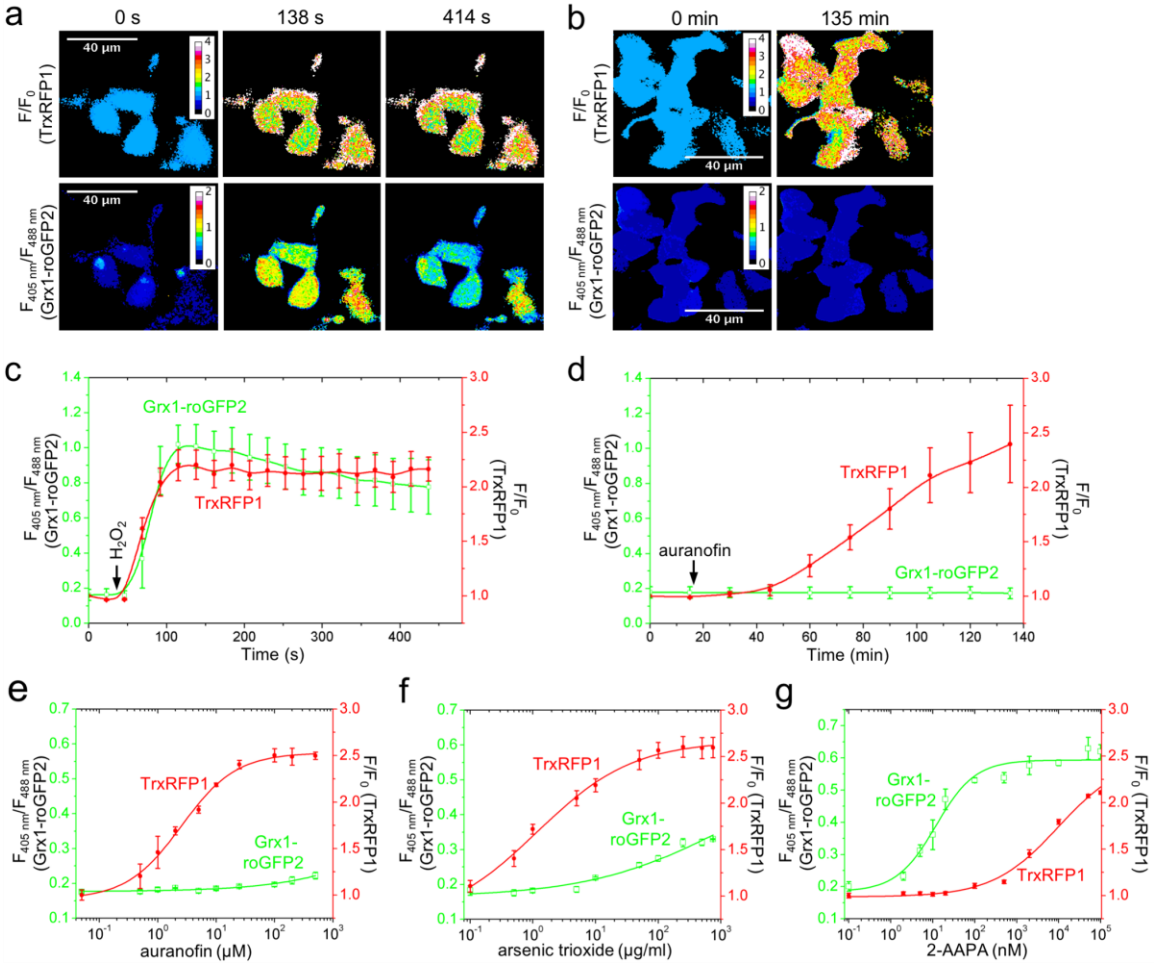

Figure 4.5. Simultaneous monitoring of thioredoxin and glutathione redox dynamics using TrxRFP1 and Grx1-roGFP2. (**a, b**) Time-lapse pseudocolored fluorescence images of HEK 293T cells expressing both TrxRFP1 and Grx1-roGFP2 treated with 13.3 μM H_2O_2 (**a**) or 15 μM auranofin (**b**), indicating that H_2O_2 induces changes in both thioredoxin and glutathione redox systems, whereas auranofin induces the oxidation of thioredoxin but not glutathione. In the top row are pseudocolored ratiometric images (F/F_0) for TrxRFP1, and in the bottom row are pseudocolored ratiometric images (405 nm excitation/488 nm excitation) for Grx1-roGFP2. H_2O_2 and auranofin were added at t = 46 s and t =16 min, respectively. (**c,d**) Ratio traces for TrxRFP1 or and Grx1-roGFP2 in HEK 293T cells in panels **a** and **b**, shown as mean and s.d. of six individual cells. The red and green lines are for TrxRFP1 and Grx1-roGFP2, respectively. The arrows indicate the time points for addition of H_2O_2 or auranofin. (**e-g**) Fluorescence responses of TrxRFP1 (red) and Grx1-roGFP2 in HEK 293T to various concentrations of auranofin (**e**), arsenic trioxide (**f**), or 2-AAPA (**g**), suggesting that the Trx redox system and the glutathione redox system can be individually perturbed. Data are shown as mean and s.d. of three independent experiments.

4.3.6 Responses of TrxRFP1 to physiological stimuli

The sensitivity of TrxRFP1 to nanomolar H2O2 in vitro suggests that the Trx system in live cells could be oxidized by low concentrations of H2O2 generated under physiologically relevant conditions. To test this, we treated HEK 293T cells co-expressing TrxRFP1 and Grx1-roGFP2 with 10% fetal bovine serum (FBS) post a 6-h serum starvation. FBS contains a mixture of growth factors and hormones, which are expected to stimulate various signaling pathways. A robust oxidation of Trx1 was observed, as the fluorescence of TrxRFP1 increased rapidly in the first 10 min post stimulation (Fig. 4.6a,b). In contrast, we only observed a very small fluorescence change for Grx1-roGFP2. We further tested the response of HEK 293T cells to epidermal growth factor (EGF), which is known to induce the biological production of H_2O_2.[46] We observed fluorescence changes for both TrxRFP1 and Grx1-roGFP2, suggesting the oxidation of both Trx1 and glutathione under this condition (Fig. 4.6c,d). In comparison to FBS stimulation after serum starvation, the EGF-induced TrxRFP1 response was relatively slow. It is not yet possible for us to fully rationalize the observations. Potentially, these different processes can activate different compartmentalized sources of H_2O_2 or induce different antioxidant systems. These results, however, at least support that TrxRFP1 could detect Trx redox changes in live cells under physiologically relevant conditions. We further repeated our serum and EGF stimulation experiments with control HEK 293T cells expressing the pH indicator pHRFP.[22] None of these conditions increased the fluorescence of pHRFP (**Fig. 4.20**), suggesting that the observed fluorescence increase of TrxRFP1 was not caused by pH changes.

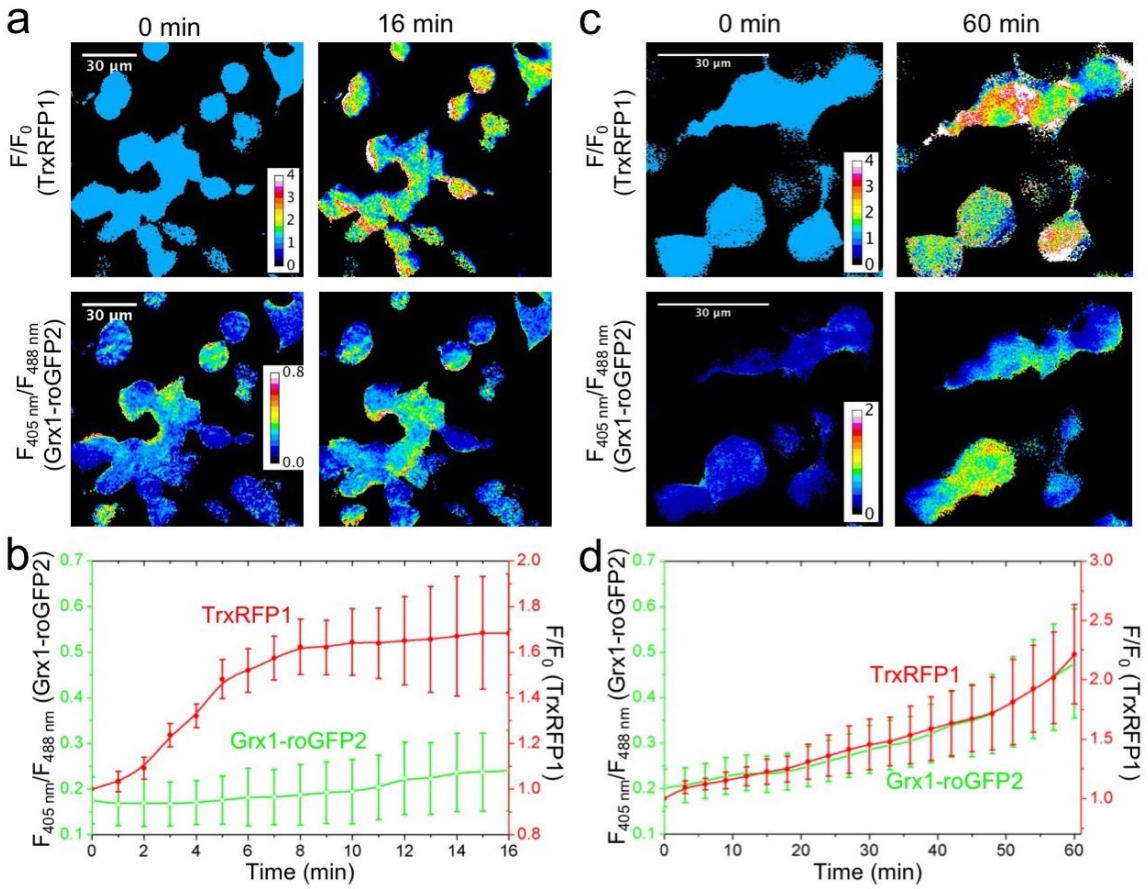

Figure 4.6. Responses of TrxRFP1 to physiological stimuli in HEK 293T cells. (**a, b**) Time-lapse responses of TrxRFP1 and Grx1-roGFP2 to serum stimulation at t = 0 min, indicating an oxidation of Trx. Prior to the 10% FBS treatment, cells were subjected to 6-h serum starvation. (**c, d**) Time-lapse responses of TrxRFP1 and Grx1-roGFP2 to epidermal growth factor (EGF, 500 ng/mL) treatment at t = 0 min, indicating the oxidation of both Trx and glutathione. Pseudocolored ratiometric images (F/F_0) for TrxRFP1 and pseudocolored ratiometric images (405 nm excitation/488 nm excitation) for Grx1-roGFP2 are shown in panels **a** and **c.** Ratio traces for TrxRFP1 or and Grx1-roGFP2 are presented in panels **b** and **d** as mean and s.d. of eight individual cells. The red and green lines are for TrxRFP1 and Grx1-roGFP2, respectively.

4.3.7 Application of TrxRFP1 in biological studies

Trx is a cellular protein containing highly reactive cysteines important for redox homeostasis and signaling. Prior to our work, there were no genetically encoded biosensors for monitoring of Trx redox in live cells. Even methods for *in vitro* analysis of Trx redox have been quite limited. To develop a selective biosensor for Trx redox, we linked a redox sensitive rxRFP1 protein with Trx1. A similar fusion strategy based on roGFPs and rxYFP has been previously utilized to create biosensors for glutathione and H_2O_2,[34,44] but it failed for Trx.[26,44,45] Different from roGFPs and rxYFP, rxRFP1 adopts a circularly permuted topology to allow a different fusion geometry. This indeed resulted in novel biosensors in which the disulfide exchange between rxRFP1 and Trx1 is possible. To develop a highly effective biosensor, we compared a few fusion strategies and performed directed evolution to improve the redox relay between rxRFP1 and Trx1. Through this directed evolution process, we improved the dynamic ranges, sensitivity, and specificity of the biosensors. The optimized TrxRFP1 biosensor responded to low nanomolar H_2O_2 in our *in vitro* TPx enzyme assay. This is well aligned with our observation on live mammalian cells, because extracellular addition of low micromolar H_2O_2 has recently been estimated to result in nanomolar intracellular H_2O_2.[59] The mechanisms for how the mutations improved the properties of TrxRFP biosensors remain to be elucidated, but likely, the three mutations (G142S/D228G/V399Q) identified from randomized libraries increased the in intrinsic dynamic range of rxRFP1. Removing nonessential cysteine residues in Trx1 and rxRFP1 only marginally changed the redox responses of TrxRFP biosensors. The remaining four cysteine residues in TrxRFP1 are

essential for the redox relay, because our effort to mutate any of these residues to serine resulted in inactive biosensors.

Trx1 is typically considered as a reductant to reduce oxidized cysteines in proteins.[5] It was unsurprising that the fluorescence of fully oxidized TrxRFP1 decreased quickly in response to TrxR/NaDPH, because the disulfide in Trx1 reduced by TrxR/NaDPH can subsequently exchange with the disulfide in rxRFP1. Furthermore, fully reduced TrxRFP1 responded to TPx/H_2O_2 whereas rxRFP1 alone was unresponsive, suggesting that Trx1 oxidized by TPx/H_2O_2 can further oxidize the two cysteine residues in reduced rxRFP1. Chemically, such reversibility is not surprising because oxidation is an exact reverse of the reduction reaction. Biologically, the result indicates that the reversibility may also be important *in vivo* and Trx may be able to modulate the redox of its interacting proteins in both directions.

We utilized TrxRFP1 to monitor Trx redox dynamics induced by H_2O_2 and auranofin in various cell lines. In particular, the fluorescence responses of TrxRFP1 to 3-h auranofin treatment were indicative of cell viabilities determined after 24-h auranofin treatment. Such correlation is due to the fact that TrxR is a major cellular target of auranofin. On the basis of this, the TrxRFP1 biosensor may be used for mechanistic studies on the interactions between interested molecules and the Trx redox systems. It may also be utilized in high-throughput screening assays to identify selective molecular modulators of the Trx redox systems. Considering the importance of the Trx system and its implications in various diseases, TrxRFP1 may open the door for a large array of exciting studies.

The red fluorescent color of TrxRFP1 makes it highly attractive. Not only because it enhances tissue penetration and minimizes phototoxicity, but also it can be paired with many existing GFP-based biosensors for monitoring more than one parameters. We have demonstrated the use of TrxRFP1 and Grx1-roGFP2 to simultaneously monitor glutathione and Trx redox dynamics in live cells. Furthermore, we show that the glutathione and Trx redox systems can be individually perturbed without shifting the other. This finding corroborates the emerging perspective that various cellular redox couples are quasi-independent from each other and a thermodynamic equilibrium is not reached in live cells.[60] At the rest condition, the glutathione redox couple and the Trx redox couple are kinetically separated, suggesting distinct biological roles of the two redox systems.

The specificity of TrxRFP1 is partially due to the low reactivity of rxRFP1 toward H_2O_2 and its slow reaction with the glutathione couple. There is essentially no response for rxRFP1 to micromolar and low millimolar H_2O_2.[31] In contrast, roGFP2 is more reactive toward H_2O_2.[34,44] Therefore, rxRFP1 is a more preferable scaffold than roGFP2 for construction of redox-relay based biosensors. The unique circularly permuted topology of rxRFP1 may also be advantageous for construction of biosensors for various cellular redox couples, as shown in this study. Moreover, despite the high specificity of TrxRFP1, rxRFP1 serves as an excellent control to further confirm the connection between the observed fluorescence changes of TrxRFP1 and the redox dynamics of Trx.

Human expresses several Trx isozymes. This work focuses on Trx1 and TrxR1, which constitute the cytosolic system. Trx1 has also been shown to enter the cell nucleus

or to be secreted in response to signals.[61] Mammalian mitochondria contain a separate Trx redox system based on Trx2 and TrxR2.[54] Due to the similarity between the two systems, there is a high probability that the strategy presented here may be extended to sense the redox dynamics of mitochondrial Trx. Furthermore, although the data presented here were mainly based on experiments in live human cell lines, TrxRFP1 or similar biosensor may be applicable in other mammalian organisms, other eukaryotic systems, or even prokaryotic cells, because of the strong homology between the Trx redox systems across species. There is significant interest to monitor Trx redox dynamics in pathogenic bacteria, because inhibition of bacterial thioredoxin reductase has been consider as a new antibiotic mechanism.[15] This work may also be applied to such studies.

4.4 Conclusion

In conclusion, by engineering a redox relay between Trx1 and rxRFP1, we developed the first genetically encoded fluorescent biosensor that allows the observation of real-time dynamics of the Trx redox system in live mammalian cells. We further combined the resultant TrxRFP1 sensor with a green fluorescent Grx1-roGFP2 biosensor to simultaneously monitor Trx and glutathione redox dynamics in live cells. With the new capability to assess the redox dynamics of Trx in live cells, a large array of new studies will be enabled to further our understanding of redox biology.

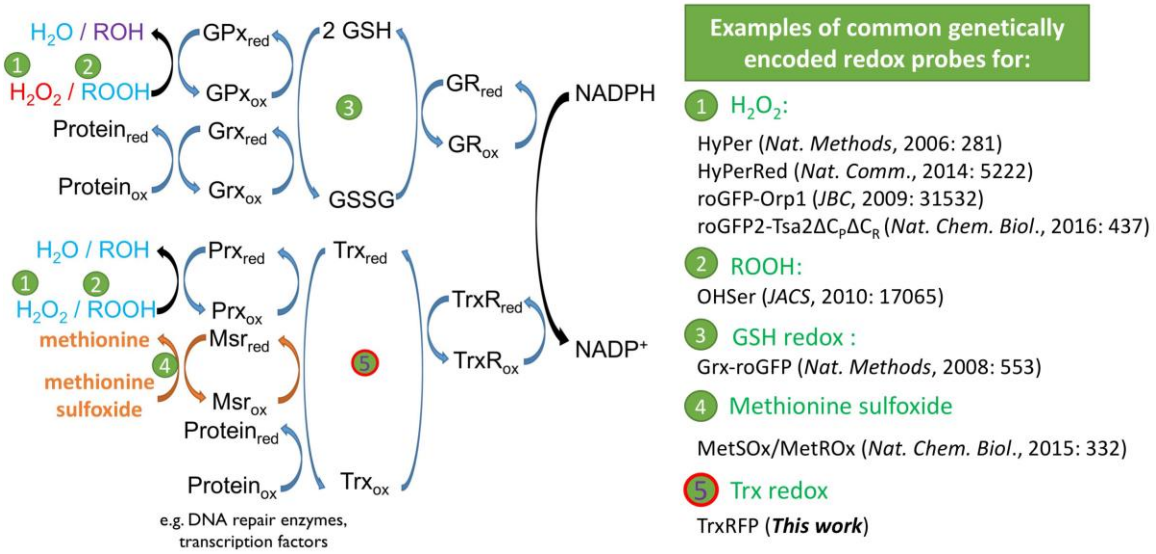

Figure 4.7. Redox reactions of the glutathione and thioredoxin (Trx) redox systems. Both systems are coupled with the oxidation of NADPH and the reduction of reactive oxygen species (ROS). Also shown are examples of some existing genetically encoded redox probes. Prior to this work, no genetically encoded biosensor had been developed for probing the redox changes of Trx.

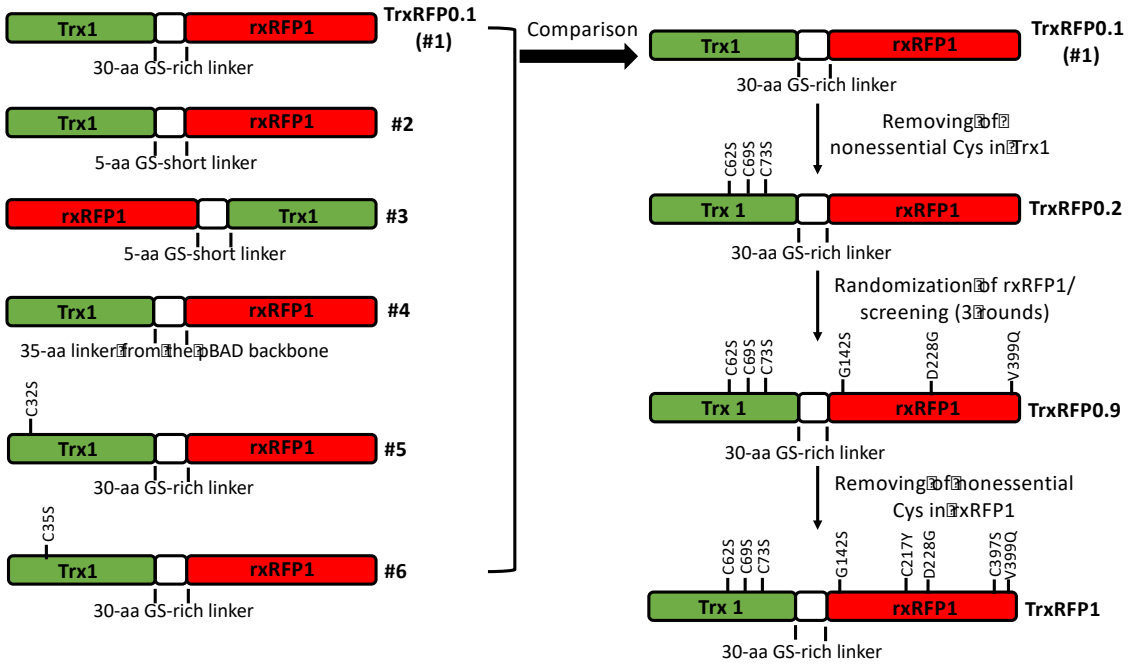

Figure 4.8. The process to engineer TrxRFP1. Also shown are topological information, linker lengths, and critical mutations introduced to each variant.

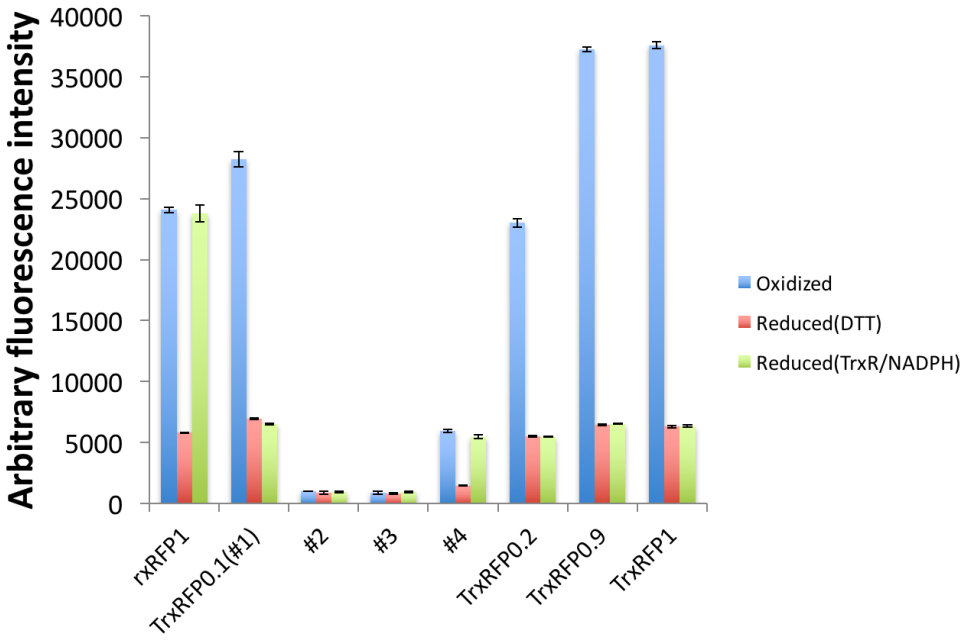

Figure 4.9. Fluorescence of the indicated proteins at the same concentration (1 µM) in their oxidized states and their reduced states maintained by DTT (10 mM) or recombinant human TrxR1 (10 µM)/NADPH (200 µM).

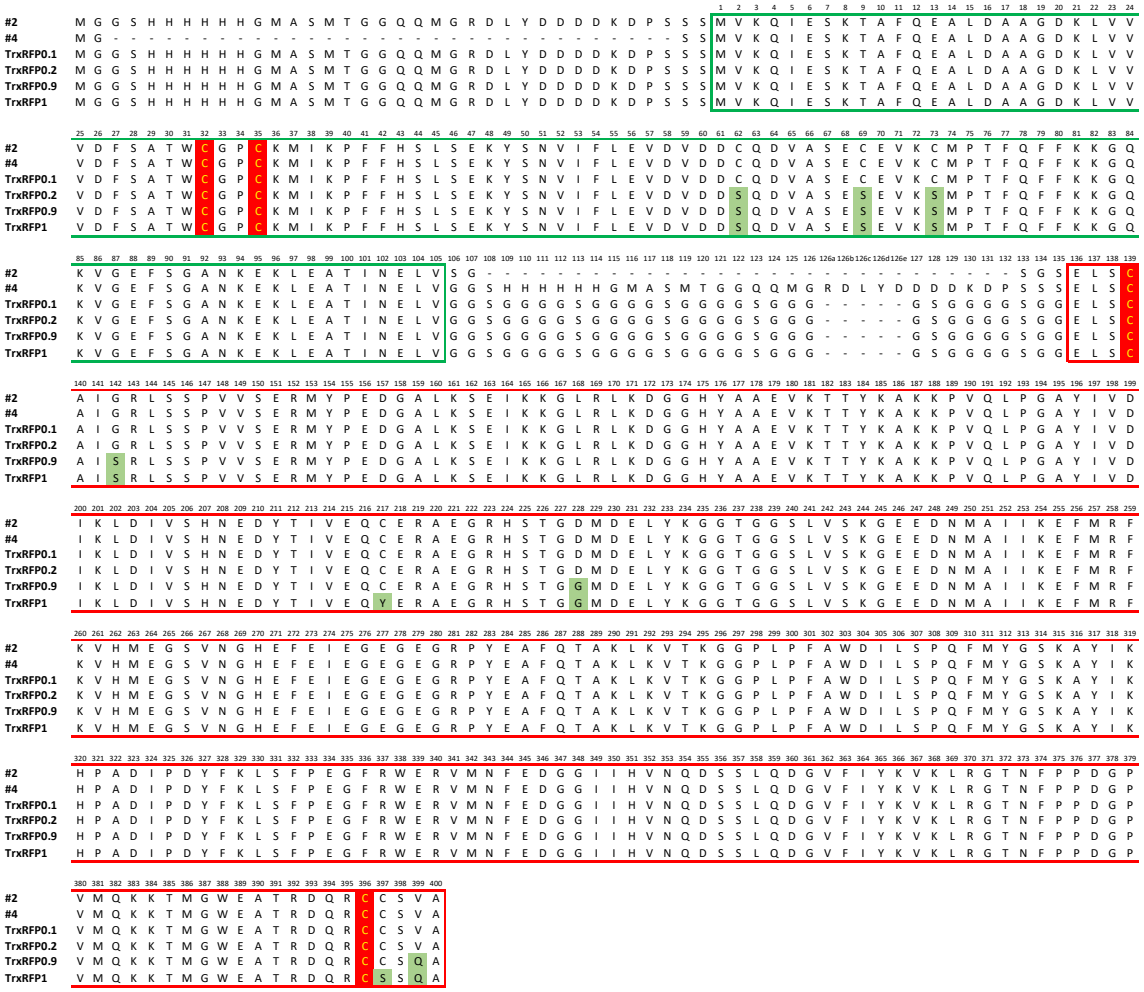

Figure 4.10. Sequence alignment of TrxRFP1 and some earlier variants described in this work. The sequences derived from Trx1 and rxRFP1 are in a green and a red box, respectively. All four critical cysteines are highlighted with yellow fonts on red background. All mutations are highlighted with green shaded background.

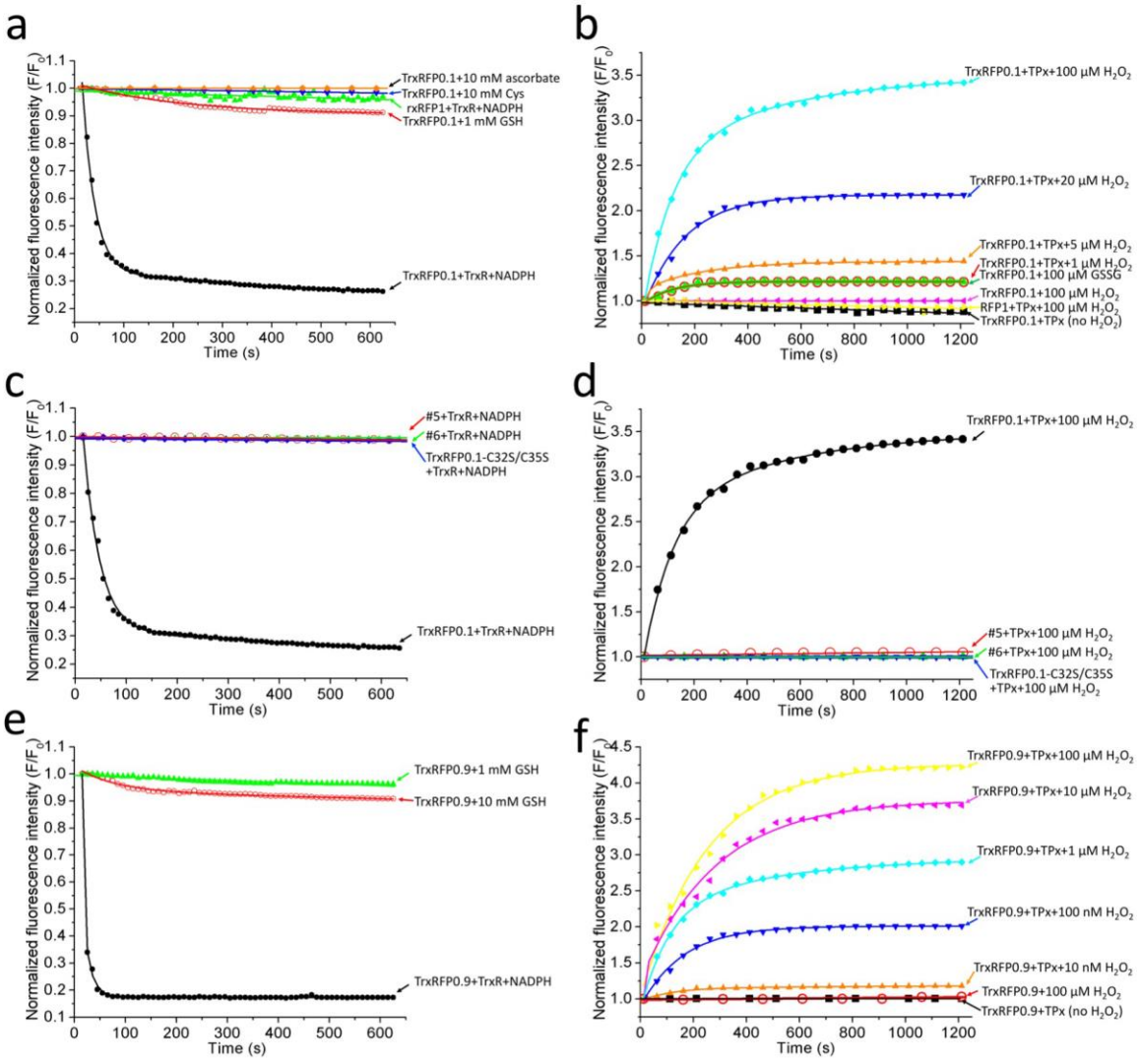

Figure 4.11. Fluorescence responses of TrxRFP mutants to indicated reducing and oxidizing enzymes and compounds. Unless otherwise specified, 1 μM each sensor protein, 10 μM recombinant human TrxR1 and 200 μM NADPH were used for enzymatic reduction reactions; 0.5 μM each sensor protein and 0.5 μM recombinant human TPx1 were used for enzymatic oxidation reactions.

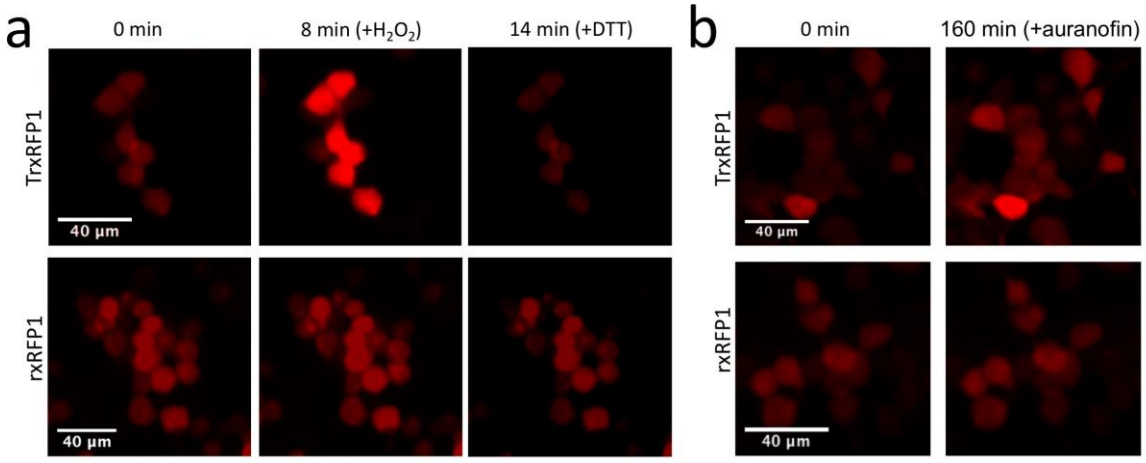

Figure 4.12. Time-lapse fluorescence images of TrxRFP1 and rxRFP1 in HEK 293T cells, sequentially treated with 16.7 µM H_2O_2 and 10 mM DTT (**a**), or treated with 10 µM auranofin (**b**), showing H_2O_2- and auranofin- induced fluorescence changes for TrxRFP1 but not for rxRFP1.

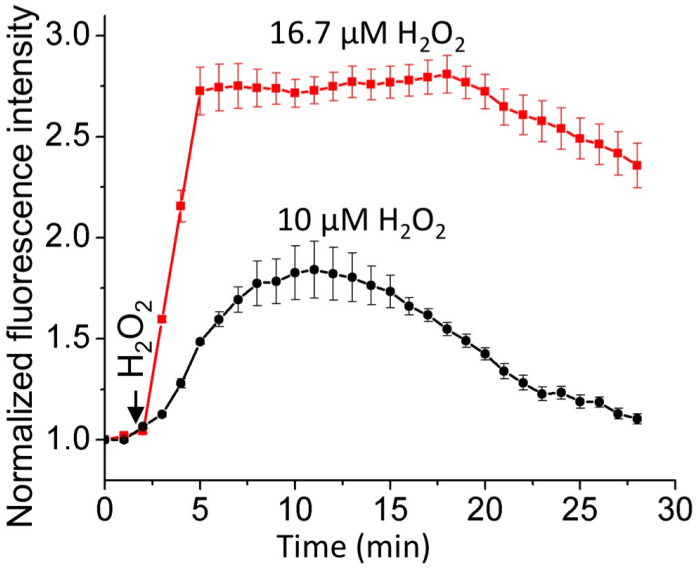

Figure 4.13. Time-lapse responses of TrxRFP1 in HEK 293T cells to two different concentrations of H_2O_2 in the imaging medium, showing that the process of Trx oxidation is reversible and Trx was reduced more quickly by intracellular systems when the lower H_2O_2 concentration was used.

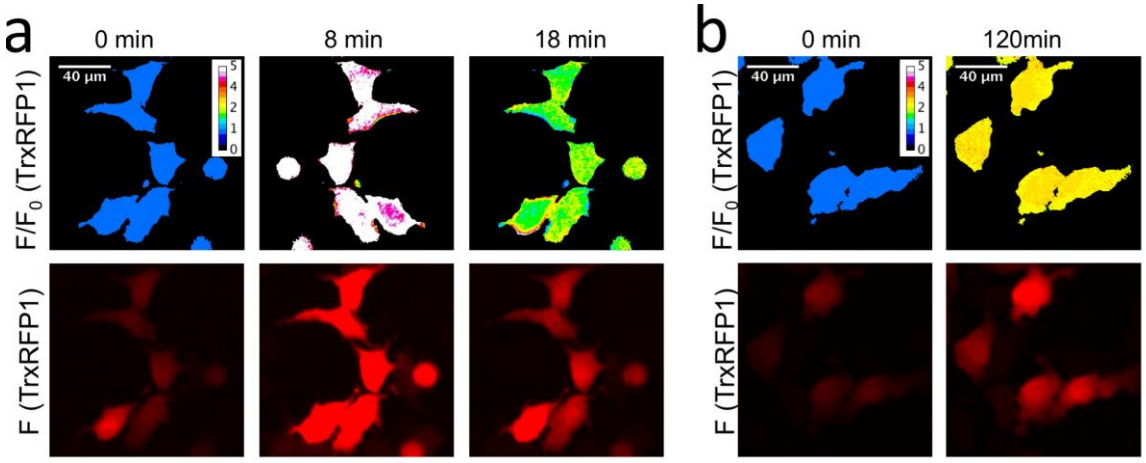

Figure 4.14. Time-lapse fluorescence images of HeLa cells expressing TrxRFP1 treated with 20 µM H_2O_2 (**a**) or 5 µM auranofin (**b**), showing H_2O_2- and auranofin- induced Trx oxidation. H_2O_2 and auranofin were added at 2 min and 10 min, respectively. In the top row are pseudocolored ratiometric images (F/F_0), and in the bottom row are fluorescence images showing relative intensities.

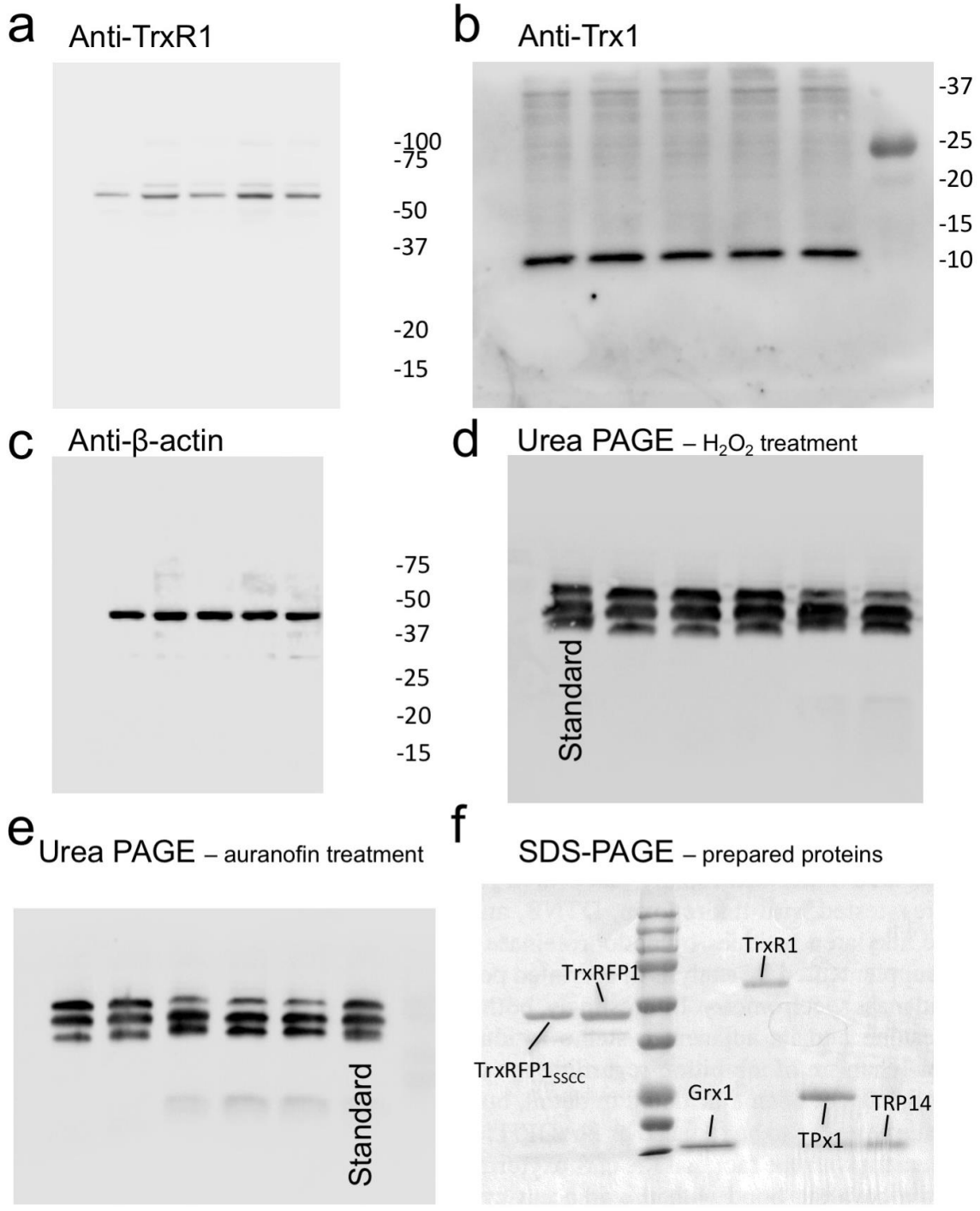

Figure 4.15. Original immunoblots presented in the manuscript and an SDS-PAGE to show the purities of our prepared proteins.

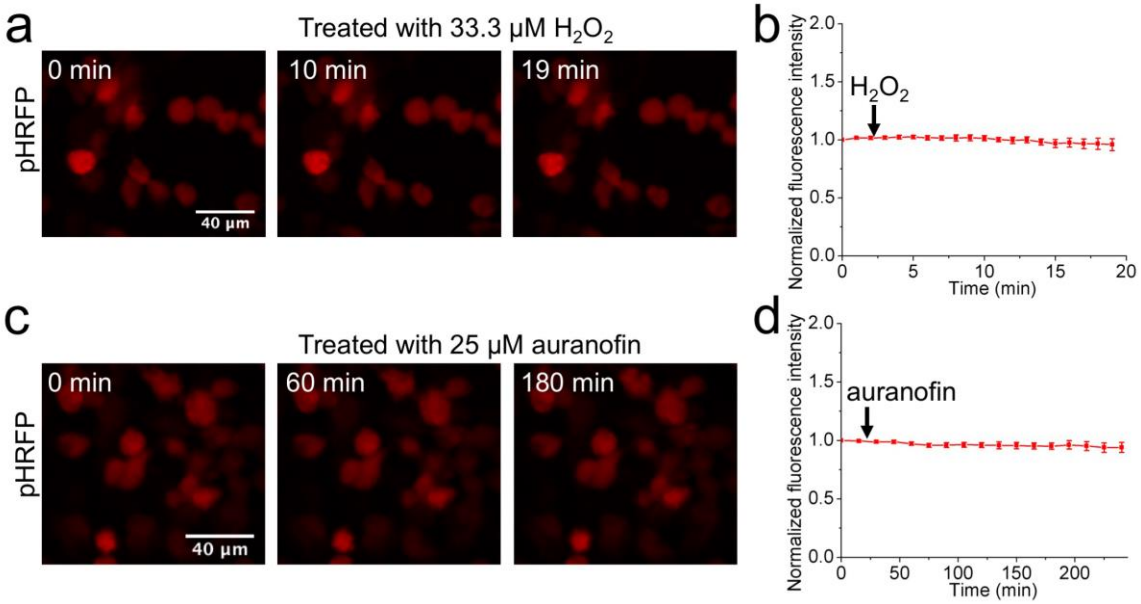

Figure 4.16. Time-lapse responses of a genetically encoded pH indicator pHRFP in HEK 293T cells to 33 μM (**a, b**) or 25 μM auranofin (**c, d**), showing no substantial pH change during there experiments (Scale bar= 40 μm). In panel **b** and **d**, the intensities were normalized to the value at t=0 min and shown as the mean and s.d. of randomly selected eight cells from three independent replicates. The arrows indicate the time points for addition of H_2O_2 or auranofin.

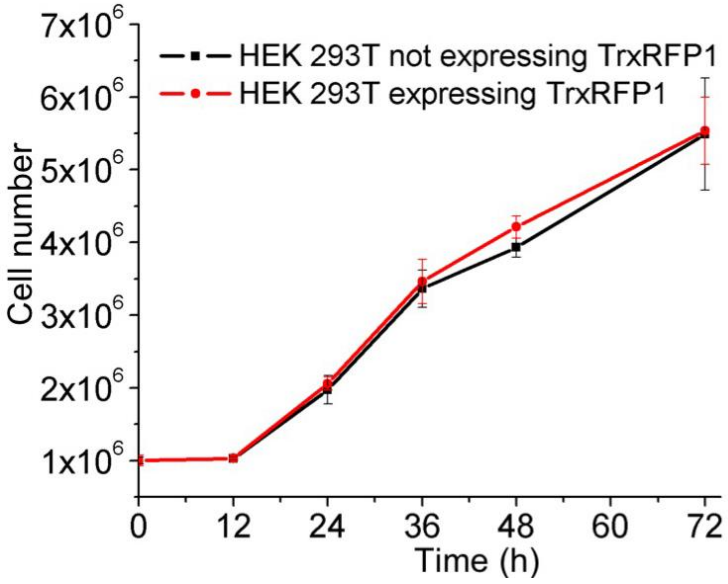

Figure 4.17. A comparison of the growth of HEK 293T cells expressing or not expressing TrxRFP1. Data are shown as mean and s.d. of three independent experiments. An unpaired Student's t-test was used to determine the significance of the differences at each time point ($p > 0.1$ for all comparisons).

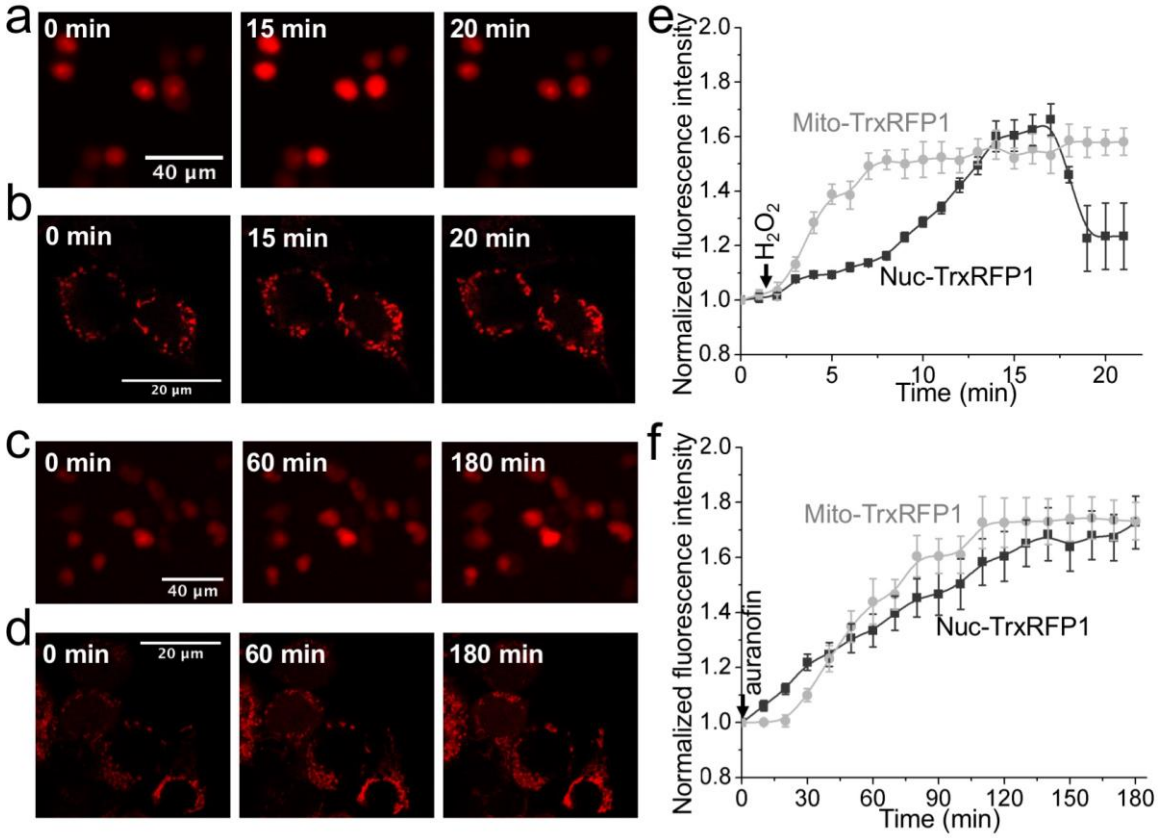

Figure 4.18. Time-lapse responses of nuclear (**a, c**) and mitochondrial (**b, d**) TrxRFP1 in HEK 293T cells to H_2O_2 (**a, b**) and auranofin (**c, d**). 66.7 μM H_2O_2 was used to treat cells at t=1.1 min in panels **a** and **b**. 10 μM and 20 μM auranofin were used to treat cells at t=0 min in panel **c** and **d**, respectively. In panels **e** and **f**, the intensities were normalized to the value at t=0 min and shown as the mean and s.d. of randomly selected eight cells from three independent replicates. The arrows indicate time points for addition of H_2O_2 or auranofin (Scale bar=40 μm for panel a and c; 20 μm for panels b and d).

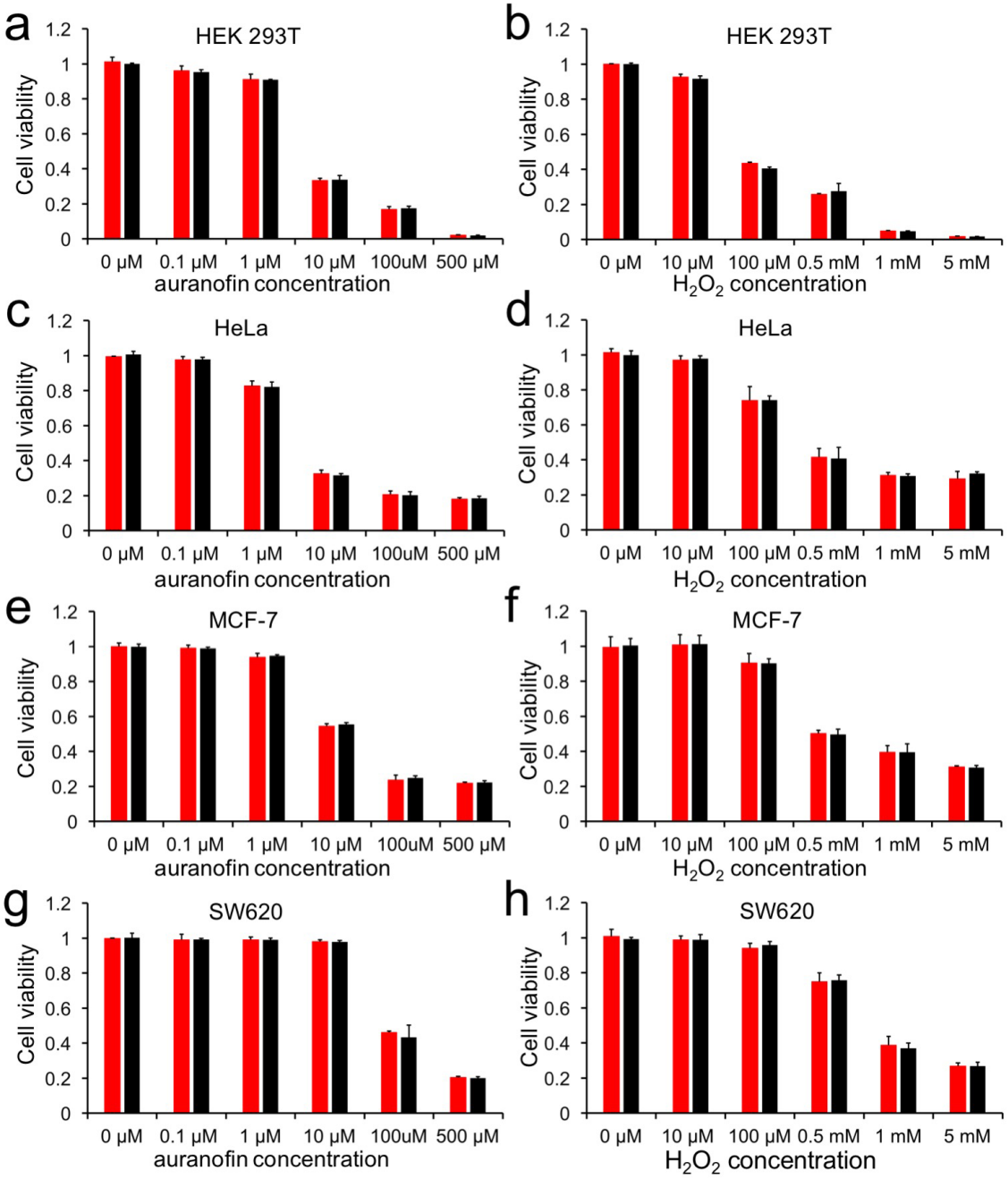

Figure 4.19. The viability of various types of cells with (red) and without (black) overexpression of TrxRFP1 in response to auranofin or H_2O_2, indicating that expression of TrxRFP1 does not affect cellular redox homeostasis. Cells were treated with the indicated concentrations of auranofin or H_2O_2 for 24 h, and cell viabilities were determined using a Promega RealTime-Glo MT cell viability assay. Data are shown as mean and s. d. of three independent experiments. The two-tailed Student's t-test was used to determine the significance of the differences at each concentration ($p > 0.1$ for all comparisons).

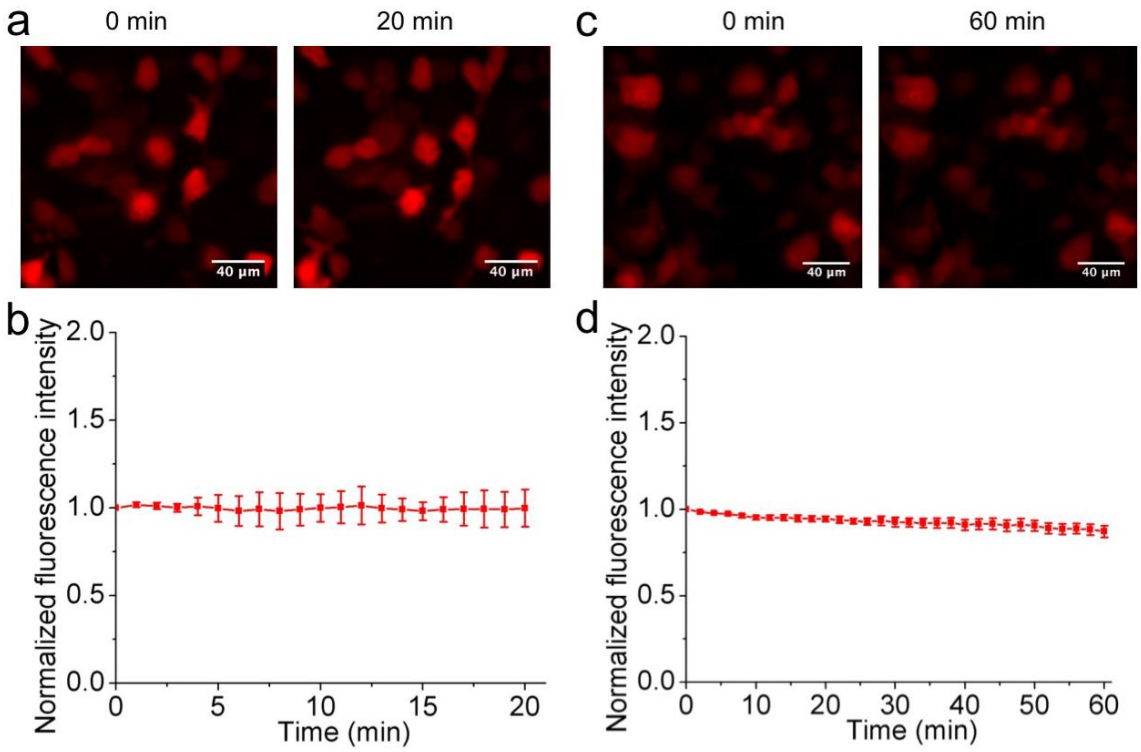

Figure 4.20. Time-lapse responses of a genetically encoded pH indicator pHRFP in HEK 293T cells to serum stimulation (**a**) and EGF (**b**), showing no pH-induced fluorescence increase (Scale bar= 40 μm). In panel **b** and **d**, the intensities were normalized to the value at t= 0 min and shown as the mean and s.d. of randomly selected six cells from three independent replicates.

Table 4.1. Oligonucleotides used in this study.

Oligo name	Nucleotide sequence
Trx-F	GTTACTCGAGCATGGTTAAACAGATC
Trx-R	GCTAAGCTTAACCAGTTCGTTGATGG
0.1-R1	GCCACCACTGCCACCAACCAGTTCGTTGATGGT
0.1-R2	CCCTCCGCTCCCTCCACCGCCACTACCGCCGCCACCACTGCCACC
0.1-R3	CCCGCCACTTCCACCTCCCCCGCTTCCCCCCCCTCCGCTCCCTCC
0.1-R4	TATAGCGCAACTAAGCTCGCCCCCACTACCTCCCCCGCCACTTCCACC
0.1-F	GGAGGTAGTGGGGGCGAGCTTAGTTGCGCTATA
2-R	AGAGCCGGAACCAGAAACCAGTTCGTTGAT
2-F	TCTGGTTCCGGCTCTGAGCTTAGTTGCGCTATA
3-R	CATAGAGCCGGAACCAGAAGCCACACTGCAGCACCT
3-F	GCTTCTGGTTCCGGCTCTATGGTTAAACAGATCGAATCT
TrxRFP3-R	GTCGATAAGCTTAAACCAGTTCGTTGATGGTCGC
4-R	ATGATGATGAGAACCCCCAACCAGTTCGTTGAT
4-F	ATCAACGAACTGGTTGGGGGTTCTCATCATCAT
32S-R	TTTGCACGGACCGCTCCAGGTCGCAGA
32S-F	TCTGCGACCTGGAGCGGTCCGTGCAAA
35S-R	TTTGATCATTTTGCTCGGACCGCACCA
35S-F	TGGTGCGGTCCGAGCAAAATGATCAAA
32/35S-R	GATCATTTTGCTCGGACCGCTCCAGGT
32/35S-F	ACCTGGAGCGGTCCGAGCAAAATGATC
62S-R	TTCAGACGCAACGTCCTGGGAGTCGTC
69/73S-F	CAGGACGTTGCGTCTGAATCCGAAGTTAAATCCATGCCG
62/69C-R	TCAGACGCAACGTCCTGGCAGTCGTCAACG
62/69-F	GACGTTGCGTCTGAATGCGAAGTTAAATCC
0.2-F	ATCAACGAACTGGTTGGTGGATCCGGTGGCGGC
0.2-R	GCCGCCACCGGATCCACCAACCAGTTCGTTGAT
C397S-R	CTGAAGCTTAAGCCTGACTGGAGCACCTTTGGTCACG
C217Y-F	CCATCGTGGAACAGTACGAACGCGCCGAGGG
C217Y-R	CCCTCGGCGCGTTCGTACTGTTCCACGATGG
TRND-F	GTTACTCGAGCATGAACGGCCCTGAAGAT
TRND-R	TAGCAAGCTTAGTAAGCGCAGCAGCCAGC
PRD-F	GTTACTCGAGCATGTCTTCAGGAAATGCT
PRD-R	TAGCAAGCTTACTACTTCTGCTTGGAGAA
Grx-F	CACTCGAGAATGGCTCAAGAGTTTGTGA
Grx-R	CTAAGCTTAAGTCTGCAGAGCTCCAATCT
pBAD-F	ATGCCATAGCATTTTTATCC
pBAD-R	GATTTAATCTGTATCAGG
CMV-F1	ATACTAAAGCTTGCCGCCACCATGGGAGGTTCTCATCATCATCAT
CMV-TrxRFP1-R	CGTCTAGATTAAGCCTGACTGGAGCACCTTTGGTCACG
Nuc-R1	CTTCTTTTTTGGATCAGCCTGACTGGAGCACCTT
Nuc-R2	TCGTTTTTTCTTCGGGTCTACCTTTCTCTTCTTTTTTGGATC
Nuc-R3	CGATTCTAGATTACTTTCTCTTCTTCTTTGGATCTACCTTTCGTTTTTTCT TCGG
Mito-F	GACCCAAGCTTGCCGCCACCATGCTAT
Mito-TrxRFP-F	AATACGATTCTTCAAGCCAGCAA

Mito-TrxRFP-R	TTGCTGGCTTGAAGAATCGTATT
NES-F1	CTTGAACGTCTTACTCTTGGAGGTTCTCATCATCAT
NES-F2	AAGAGTAAGACGTTCAAGAGGAGGAAGTTGAAGCATAAGCTTGAT
NES-R	ACTGTCTAGAAGCCTGACTGGAGCACCTTT
HyPer-F	ATCAAGCTTATGGAGATGGCAAGC
HyPer-R	CCGTCTAGATTAAACCGCCTGTTT
HyPer-NES-F	CGTAGGATCCATGGAGATGGCAAGCCAG
HyPer-NES-R	CAGTCTAGAAACCGCCTGTTTTAAAAC
HyPer-Nuc-R1	CTTCTTTTTTGGATCAACCGCCTGTTTTAAAAC

References

1. Meyer, J.N. et al. Mitochondria as a target of environmental toxicants. *Toxicol Sci* **134**, 1-17 (2013).

2. Madamanchi, N.R. & Runge, M.S. Redox signaling in cardiovascular health and disease. *Free Radic Biol Med* **61**, 473-501 (2013).

3. Sesti, F., Liu, S. & Cai, S.Q. Oxidation of potassium channels by ROS: a general mechanism of aging and neurodegeneration? *Trends Cell Biol* **20**, 45-51 (2010).

4. Finkel, T. Reactive oxygen species and signal transduction. *IUBMB Life* **52**, 3-6 (2001).

5. Lu, J. & Holmgren, A. The thioredoxin antioxidant system. *Free Radic Biol Med* **66**, 75-87 (2014).

6. Rhee, S.G. Overview on Peroxiredoxin. *Mol Cells* **39**, 1-5 (2016).

7. Sengupta, R. & Holmgren, A. Thioredoxin and glutaredoxin-mediated redox regulation of ribonucleotide reductase. *World J Biol Chem* **5**, 68-74 (2014).

8. Matthews, J.R., Wakasugi, N., Virelizier, J.L., Yodoi, J. & Hay, R.T. Thioredoxin regulates the DNA binding activity of NF-kappa B by reduction of a disulphide bond involving cysteine 62. *Nucleic Acids Res* **20**, 3821-30 (1992).

9. Wei, S.J. et al. Thioredoxin nuclear translocation and interaction with redox factor-1 activates the activator protein-1 transcription factor in response to ionizing radiation. *Cancer Res* **60**, 6688-95 (2000).

10. Saitoh, M. et al. Mammalian thioredoxin is a direct inhibitor of apoptosis signal-regulating kinase (ASK) 1. *Embo j* **17**, 2596-606 (1998).

11. Ma, X.X. et al. Structural plasticity of the thioredoxin recognition site of yeast methionine S-sulfoxide reductase Mxr1. *J Biol Chem* **286**, 13430-7 (2011).

12. Porqué, P.G., Baldesten, A. & Reichard, P. The Involvement of the Thioredoxin System in the Reduction of Methionine Sulfoxide and Sulfate. *Journal of Biological Chemistry* **245**, 2371-2374 (1970).

13. Sido, B. et al. Potential role of thioredoxin in immune responses in intestinal lamina propria T lymphocytes. *Eur J Immunol* **35**, 408-17 (2005).

14. Masutani, H., Ueda, S. & Yodoi, J. The thioredoxin system in retroviral infection and apoptosis. *Cell Death Differ* **12 Suppl 1**, 991-8 (2005).

15. Lu, J. et al. Inhibition of bacterial thioredoxin reductase: an antibiotic mechanism targeting bacteria lacking glutathione. *Faseb j* **27**, 1394-403 (2013).

16. Gallegos, A. et al. Transfection with human thioredoxin increases cell proliferation and a dominant-negative mutant thioredoxin reverses the transformed phenotype of human breast cancer cells. *Cancer Res* **56**, 5765-70 (1996).

17. Tonissen, K.F. & Di Trapani, G. Thioredoxin system inhibitors as mediators of apoptosis for cancer therapy. *Mol Nutr Food Res* **53**, 87-103 (2009).

18. Shalev, A. Minireview: Thioredoxin-interacting protein: regulation and function in the pancreatic beta-cell. *Mol Endocrinol* **28**, 1211-20 (2014).

19. Arner, E.S. & Holmgren, A. The thioredoxin system in cancer. *Semin Cancer Biol* **16**, 420-6 (2006).

20. Kim, S.J. et al. High thioredoxin expression is associated with resistance to docetaxel in primary breast cancer. *Clin Cancer Res* **11**, 8425-30 (2005).

21. Li, C. et al. Over-expression of Thioredoxin-1 mediates growth, survival, and chemoresistance and is a druggable target in diffuse large B-cell lymphoma. *Oncotarget* **3**, 314-26 (2012).

22. Yoo, M.H., Xu, X.M., Carlson, B.A., Gladyshev, V.N. & Hatfield, D.L. Thioredoxin reductase 1 deficiency reverses tumor phenotype and tumorigenicity of lung carcinoma cells. *J Biol Chem* **281**, 13005-8 (2006).

23. Bhatia, M. et al. The thioredoxin system in breast cancer cell invasion and migration. *Redox Biol* **8**, 68-78 (2016).

24. Mahmood, D.F., Abderrazak, A., El Hadri, K., Simmet, T. & Rouis, M. The thioredoxin system as a therapeutic target in human health and disease. *Antioxid Redox Signal* **19**, 1266-303 (2013).

25. Garcia-Garcia, A., Zavala-Flores, L., Rodriguez-Rocha, H. & Franco, R. Thiol-redox signaling, dopaminergic cell death, and Parkinson's disease. *Antioxid Redox Signal* **17**, 1764-84 (2012).

26. Schwarzlander, M., Dick, T.P., Meyer, A.J. & Morgan, B. Dissecting Redox Biology Using Fluorescent Protein Sensors. *Antioxid Redox Signal* **24**, 680-712 (2016).

27. Ren, W. & Ai, H.W. Genetically encoded fluorescent redox probes. *Sensors (Basel)* **13**, 15422-33 (2013).

28. Meyer, A.J. & Dick, T.P. Fluorescent protein-based redox probes. *Antioxid Redox Signal* **13**, 621-50 (2010).

29. Ostergaard, H., Henriksen, A., Hansen, F.G. & Winther, J.R. Shedding light on disulfide bond formation: engineering a redox switch in green fluorescent protein. *EMBO J* **20**, 5853-62 (2001).

30. Hanson, G.T. et al. Investigating mitochondrial redox potential with redox-sensitive green fluorescent protein indicators. *J Biol Chem* **279**, 13044-53 (2004).

31. Fan, Y., Chen, Z. & Ai, H.W. Monitoring redox dynamics in living cells with a redox-sensitive red fluorescent protein. *Anal. Chem.* **87**, 2802-2810 (2015).

32. Fan, Y. & Ai, H.W. Development of redox-sensitive red fluorescent proteins for imaging redox dynamics in cellular compartments. *Anal Bioanal Chem* **408**, 2901-11 (2016).

33. Belousov, V.V. et al. Genetically encoded fluorescent indicator for intracellular hydrogen peroxide. *Nat. Methods* **3**, 281-6 (2006).

34. Gutscher, M. et al. Proximity-based protein thiol oxidation by H2O2-scavenging peroxidases. *J Biol Chem* **284**, 31532-40 (2009).

35. Morgan, B. et al. Real-time monitoring of basal H2O2 levels with peroxiredoxin-based probes. *Nat Chem Biol* **12**, 437-43 (2016).

36. Zhao, B.S. et al. A highly selective fluorescent probe for visualization of organic hydroperoxides in living cells. *J Am Chem Soc* **132**, 17065-7 (2010).

37. Chen, Z.J., Ren, W., Wright, Q.E. & Ai, H.W. Genetically encoded fluorescent probe for the selective detection of peroxynitrite. *J Am Chem Soc* **135**, 14940-3 (2013).

38. Chen, S., Chen, Z.J., Ren, W. & Ai, H.W. Reaction-based genetically encoded fluorescent hydrogen sulfide sensors. *J Am Chem Soc* **134**, 9589-92 (2012).

39. Chen, Z.J. & Ai, H.W. A Highly Responsive and Selective Fluorescent Probe for Imaging Physiological Hydrogen Sulfide. *Biochemistry* **53**, 5966-5974 (2014).

40. Hung, Y.P., Albeck, J.G., Tantama, M. & Yellen, G. Imaging cytosolic NADH-NAD(+) redox state with a genetically encoded fluorescent biosensor. *Cell Metab* **14**, 545-54 (2011).

41. Zhao, Y. et al. Genetically encoded fluorescent sensors for intracellular NADH detection. *Cell Metab* **14**, 555-66 (2011).

42. Tarrago, L., Peterfi, Z., Lee, B.C., Michel, T. & Gladyshev, V.N. Monitoring methionine sulfoxide with stereospecific mechanism-based fluorescent sensors. *Nat Chem Biol* **11**, 332-8 (2015).

43. Bjornberg, O., Ostergaard, H. & Winther, J.R. Mechanistic insight provided by glutaredoxin within a fusion to redox-sensitive yellow fluorescent protein. *Biochemistry* **45**, 2362-71 (2006).

44. Gutscher, M. et al. Real-time imaging of the intracellular glutathione redox potential. *Nat Methods* **5**, 553-9 (2008).

45. Ostergaard, H., Tachibana, C. & Winther, J.R. Monitoring disulfide bond formation in the eukaryotic cytosol. *J Cell Biol* **166**, 337-45 (2004).

46. Ungerstedt, J., Du, Y., Zhang, H., Nair, D. & Holmgren, A. In vivo redox state of Human thioredoxin and redox shift by the histone deacetylase inhibitor suberoylanilide hydroxamic acid (SAHA). *Free Radical Biology and Medicine* **53**, 2002-2007 (2012).

47. Barglow, K.T., Knutson, C.G., Wishnok, J.S., Tannenbaum, S.R. & Marletta, M.A. Site-specific and redox-controlled S-nitrosation of thioredoxin. *Proc Natl Acad Sci U S A* **108**, E600-6 (2011).

48. Du, Y., Zhang, H., Zhang, X., Lu, J. & Holmgren, A. Thioredoxin 1 is inactivated due to oxidation induced by peroxiredoxin under oxidative stress and reactivated by the glutaredoxin system. *J Biol Chem* **288**, 32241-7 (2013).

49. Shaner, N.C. et al. Improving the photostability of bright monomeric orange and red fluorescent proteins. *Nat Methods* **5**, 545-51 (2008).

50. Giustarini, D., Dalle-Donne, I., Milzani, A., Fanti, P. & Rossi, R. Analysis of GSH and GSSG after derivatization with N-ethylmaleimide. *Nat Protoc* **8**, 1660-9 (2013).

51. Du, Y., Zhang, H., Lu, J. & Holmgren, A. Glutathione and glutaredoxin act as a backup of human thioredoxin reductase 1 to reduce thioredoxin 1 preventing cell death by aurothioglucose. *J Biol Chem* **287**, 38210-9 (2012).

52. Hill, K.E., McCollum, G.W., Boeglin, M.E. & Burk, R.F. Thioredoxin reductase activity is decreased by selenium deficiency. *Biochem Biophys Res Commun* **234**, 293-5 (1997).

53. Jurado, J., Prieto-Alamo, M.J., Madrid-Risquez, J. & Pueyo, C. Absolute gene expression patterns of thioredoxin and glutaredoxin redox systems in mouse. *J Biol Chem* **278**, 45546-54 (2003).

54. Spyrou, G., Enmark, E., Miranda-Vizuete, A. & Gustafsson, J. Cloning and expression of a novel mammalian thioredoxin. *J Biol Chem* **272**, 2936-41 (1997).

55. Rackham, O. et al. Substrate and inhibitor specificities differ between human cytosolic and mitochondrial thioredoxin reductases: Implications for development of specific inhibitors. *Free Radical Biology and Medicine* **50**, 689-699 (2011).

56. Kumar, K.K., Karnati, S., Reddy, M.B. & Chandramouli, R. Caco-2 cell lines in drug discovery- an updated perspective. *J Basic Clin Pharm* **1**, 63-9 (2010).

57. Lu, J., Chew, E.H. & Holmgren, A. Targeting thioredoxin reductase is a basis for cancer therapy by arsenic trioxide. *Proc Natl Acad Sci U S A* **104**, 12288-93 (2007).

58. Seefeldt, T. et al. Characterization of a novel dithiocarbamate glutathione reductase inhibitor and its use as a tool to modulate intracellular glutathione. *J Biol Chem* **284**, 2729-37 (2009).

59. Huang, B.K. & Sikes, H.D. Quantifying intracellular hydrogen peroxide perturbations in terms of concentration. *Redox Biol* **2**, 955-62 (2014).

60. Kemp, M., Go, Y.M. & Jones, D.P. Nonequilibrium thermodynamics of thiol/disulfide redox systems: a perspective on redox systems biology. *Free Radic Biol Med* **44**, 921-37 (2008).

61. Arner, E.S. & Holmgren, A. Physiological functions of thioredoxin and thioredoxin reductase. *Eur J Biochem* **267**, 6102-9 (2000).

Chapter 5: Summary and Future Work

In the thesis, I have successfully developed the first genetically encoded redox-sensitive red fluorescent protein (rxRFP1) and its derivatives with different basal redox potentials. They have been proven to be effective for detection of redox dynamics in various subcellular domains, such as mitochondria, the cell nucleus, and endoplasmic reticulum (ER). Not only can they respond to membrane-permeable oxidants and reductants, a mitochondrially localized rxRFP1 mutant, Mito-rxRFP1.1, has been used to detect mitochondrial oxidative stress induced by doxorubicin—a widely used cancer chemotherapy drug. Our work has expanded the fluorescent protein toolkit with new research tools for studying compartmentalized redox dynamics under various pathophysiological conditions. Moreover, I also developed the very first genetically encoded fluorescent biosensor to detect Trx dynamics in live cell. The red emission makes it compatible fluorescent other green-color biosensors and when combined together they can be utilized simultaneously to monitor Trx and GSH redox dynamics.

The successful development of these genetically encoded fluorescent sensors allow for the quantitation and experimental regulation of defined redox progresses. Emerging as one of the most innovative and promising tools, they not only provide new insights into the growing field of redox biology but can also be utilized as an excellent scaffold for the development of biosensors.

We also explored another novel strategy to develop the first genetically encoded red fluorescent peroxynitrite probe—pnRFP, by introducing *p*BoF into the scaffold of a

cpRFP. Moreover, through protein directed evolution, we were able to tune the chemoselectivity of boron, generating a sensitive probe—hpRFP, which selectively detects hydrogen peroxide. The new probe pnRFP has been successfully applied to detect physiologically relevant peroxynitrite in both live mammalian cells and mouse macrophage cells. We also report a group of genetically encoded reversible fluorescent probes by using boronic acid and short peptides as synergistic recognition motifs. We were able to engineer a series of reversible probes for nucleotides and carbohydrates showing surprisingly high specificity and large dynamic ranges. We have successfully utilized this new family of fluorescent probes to visualize various cellular activities.

To summarize, my work has greatly expanded the capabilities of current genetically encoded biosensors. With extended emission region into red color, more cellular parameters can be monitored simultaneously and more opportunities for dynamic live cell or *in vivo* imaging are allowed with minimal perturbation from outside. Together with other molecular fluorescent imaging tools, they provide us with more meaningful and interpretable quantitative information on biological cellular signaling.